

CANADIAN THESES ON MICROFICHE

I.S.B.N.

THESES CANADIENNES SUR MICROFICHE



National Library of Canada  
Collections Development Branch

Canadian Theses on  
Microfiche Service

Ottawa, Canada  
K1A 0N4

Bibliothèque nationale du Canada  
Direction du développement des collections

Service des thèses canadiennes  
sur microfiche

NOTICE

The quality of this microfiche is heavily dependent upon the quality of the original thesis submitted for microfilming. Every effort has been made to ensure the highest quality of reproduction possible.

If pages are missing, contact the university which granted the degree.

Some pages may have indistinct print especially if the original pages were typed with a poor typewriter ribbon or if the university sent us a poor photocopy.

\*Previously copyrighted materials (journal articles, published tests, etc.) are not filmed.

Reproduction in full or in part of this film is governed by the Canadian Copyright Act, R.S.C. 1970, c. C-30. Please read the authorization forms which accompany this thesis.

THIS DISSERTATION  
HAS BEEN MICROFILMED  
EXACTLY AS RECEIVED

AVIS

La qualité de cette microfiche dépend grandement de la qualité de la thèse soumise au microfilmage. Nous avons tout fait pour assurer une qualité supérieure de reproduction.

S'il manque des pages, veuillez communiquer avec l'université qui a conféré le grade.

La qualité d'impression de certaines pages peut laisser à désirer, surtout si les pages originales ont été dactylographiées à l'aide d'un ruban usé ou si l'université nous a fait parvenir une photocopie de mauvaise qualité.

Les documents qui font déjà l'objet d'un droit d'auteur (articles de revue, examens publiés, etc.) ne sont pas microfilmés.

La reproduction, même partielle, de ce microfilm est soumise à la Loi canadienne sur le droit d'auteur, SRC 1970, c. C-30. Veuillez prendre connaissance des formules d'autorisation qui accompagnent cette thèse.

LA THÈSE A ÉTÉ  
MICROFILMÉE TELLE QUE  
NOUS L'AVONS REÇUE

56



National Library of Canada

Bibliothèque nationale du Canada

0-315-07774-3

Canadian Theses Division

Division des thèses canadiennes

Ottawa, Canada  
K1A 0N4

55694

**PERMISSION TO MICROFILM — AUTORISATION DE MICROFILMER**

• Please print or type — Écrire en lettres moulées ou dactylographier

Full Name of Author — Nom complet de l'auteur

ANAND MOHAN SHARAN

Date of Birth — Date de naissance

MAY 7, 1945

Country of Birth — Lieu de naissance

INDIA

Permanent Address — Résidence fixe

29 TRILLIUM RD, D.D.O. P.O. H9B, 1T3

Title of Thesis — Titre de la thèse

DYNAMIC RESPONSE AND OPTIMAL DESIGN OF A LATHE  
SPINDLE UNDER EXPERIMENTALLY MEASURED RANDOM CUTTING  
FORCE EXCITATIONS

University — Université

CONCORDIA UNIVERSITY, MONTREAL

Degree for which thesis was presented — Grade pour lequel cette thèse fut présentée

PH. D. (MECHANICAL ENGINEERING)

Year this degree conferred — Année d'obtention de ce grade

1982

Name of Supervisor — Nom du directeur de thèse

DR. S. SANKAR & DR. T. S. SANKAR

Permission is hereby granted to the NATIONAL LIBRARY OF CANADA to microfilm this thesis and to lend or sell copies of the film.

The author reserves other publication rights, and neither the thesis nor extensive extracts from it may be printed or otherwise reproduced without the author's written permission.

L'autorisation est, par la présente, accordée à la BIBLIOTHÈQUE NATIONALE DU CANADA de microfilmer cette thèse et de prêter ou de vendre des exemplaires du film.

L'auteur se réserve les autres droits de publication; ni la thèse ni de longs extraits de celle-ci ne doivent être imprimés ou autrement reproduits sans l'autorisation écrite de l'auteur.

Date

March 22, 1982

Signature

Anand Mohan Sharan

DYNAMIC RESPONSE AND OPTIMAL DESIGN OF A LATHE SPINDLE UNDER  
EXPERIMENTALLY MEASURED RANDOM CUTTING FORCE EXCITATIONS

Anand Mohan Sharan

A Thesis  
in  
The Faculty  
of  
Engineering  
and  
Computer Science

Presented in Partial Fulfillment of the Requirements  
for the degree of Doctor of Philosophy at  
Concordia University  
Montreal, Quebec, Canada

March 1982

© Anand Mohan Sharan, 1982

CONCORDIA UNIVERSITY  
Graduate Studies

This is to certify that the thesis prepared

By Anand Mohan Sharan

Entitled Dynamic Response and Optimal Design of a Lathe Spindle

Under Experimentally Measured Random Cutting Force Excitations.

and submitted in partial fulfillment of the requirements for the degree  
of

Doctor of Philosophy

complies with the regulations of this University and meets the accepted  
standards with respect to originality and quality.

Signed by the final examining committee:

M.N.S. Swamy M.N.S. Swamy, Chair

S. Sankar S. Sankar, Supervisor

T.S. Sankar T.S. Sankar, Supervisor

M.O.M. Osman M.O.M. Osman, Examiner

C. Marsh C. Marsh, Examiner

R.B. Bhat R.B. Bhat, Examiner

M.F. Massoud M.F. Massoud, External Examiner

Approved by S. Sankar  
Chair of Department or Graduate  
Program Director

April 19, 19 82.

M.N.S. Swamy  
Dean of Faculty or Division

DEDICATION

Dedicated to my parents who instilled in me a deep appreciation  
for the virtues of life.

## ABSTRACT

### DYNAMIC RESPONSE AND OPTIMAL DESIGN OF A LATHE SPINDLE UNDER EXPERIMENTALLY MEASURED RANDOM CUTTING FORCE EXCITATIONS

A.M. Sharan, Ph.D.  
Concordia University, 1982

This thesis presents the dynamic response and optimal design of a lathe spindle under experimentally measured random cutting force excitations. The optimal design is based on minimizing the maximum mean square displacement response of the workpiece under the action of random cutting forces.

The stochastic partial differential equation of motion characterizing the behavior of a lathe spindle-workpiece system is formulated based on the Euler-Bernoulli equation. A finite element method using beam elements is used for free vibration analysis to compute the undamped mode shapes and the natural frequencies of the spindle-workpiece system. The workpiece support at the running center has been modelled as hinged or fixed support and the theoretical results are compared with the laboratory experiments to classify the nature of the support condition. Based on the results, the end condition at the running center is classified as hinged. The effect of varying the spindle-bearing stiffness on the natural frequencies and mode shapes are also presented.

The forced vibration of the spindle-workpiece system is studied by first investigating the nonstationary random response of a workpiece subjected to a constantly varying cutting tool contact in a turning

operation. The results indicate that the workpiece response at the cutting tool is not significantly influenced by the tool feed rate for normal turning operations. A modal analysis in conjunction with the finite element technique is then used to calculate the mean square displacement of the workpiece. The experimentally calculated power spectral density of the cutting forces is used as the input excitation to the mathematical model. A parametric study on the effect of bearing stiffness and damping, bearing spacing, sectional rigidity, and external damper on the mean square displacement is presented.

An optimal design of a lathe spindle using a direct search optimization technique with bearing stiffness and spacing, and spindle cross-sectional diameter as design variables, has been carried out. The effect of chuck diameter and workpiece slenderness ratio on the dynamic response of an optimized spindle is also studied. Finally, the influence of a third bearing in the spindle on an optimized system and the design of an external damper are also discussed.

### ACKNOWLEDGEMENTS

The author is deeply indebted to his supervisors, Drs. S. Sankar and T.S. Sankar, for their continued guidance and encouragement during the course of this investigation. The author also wishes to thank Dr. R.B. Bhat for his valuable suggestions and Mrs. I. Crawford for typing this thesis.

The author would like to express his appreciation to his wife Veena; son, Rajat; and daughter, Swati for their understanding and patience during the course of this work.

Finally, the author wishes to acknowledge the support of the National Science and Engineering Research Council of Canada (NSERC), grant numbers A3685 and A7104, as well as La Formation de Chercheurs et d'Action Concertee (FCAC), grant number G12 during the course of this research.



## TABLE OF CONTENTS

|  | <u>Page</u> |
|--|-------------|
| ABSTRACT   | i           |
| ACKNOWLEDGEMENTS   | iii         |
| LIST OF FIGURES  | ix          |
| LIST OF TABLES   | xii         |
| NOMENCLATURE   | xiv         |
| CHAPTER 1  |             |
| INTRODUCTION AND LITERATURE SURVEY   |             |
| 1.1 Machining Processes  | 1           |
| 1.2 Various Considerations in Machine-Tool Design                          | 2           |
| 1.2.1 Stability of the Machine Tool Structure                              | 2           |
| 1.2.2 The Cutting Forces (Deterministic Model)                             | 4           |
| 1.2.3 The Cutting Forces (Random Model)                                    | 5           |
| 1.2.4 Damping in Machine Tools   | 5           |
| 1.2.5 Flexural Vibration of Rotating Shafts                                | 6           |
| 1.2.6 The Dynamic Response of Machine Tools                                | 7           |
| 1.3 Scope of the Investigation   | 9           |
| CHAPTER 2  |             |
| DESCRIPTION OF A LATHE SPINDLE-WORKPIECE SYSTEM AND ITS MATHEMATICAL MODEL |             |
| 2.1 Introduction.  | 13          |
| 2.2 Components of a Spindle-Workpiece System                               | 13          |
| 2.2.1 The Spindle  | 13          |
| 2.2.2 Bearings   | 18          |
| 2.2.3 Damping in a Spindle-Workpiece System                                | 19          |
| 2.3 External Forces Acting on the Spindle Workpiece System                 | 20          |
| 2.4 Objectives of the Mathematical Analysis                                | 20          |
| 2.5 Assumptions and Justifications   | 24          |
| 2.6 Formulation of the Mathematical Model                                  | 26          |

|  | <u>Page</u> |
|--|-------------|
| 2.7 Method of Solution                                       | 28          |
| 2.7.1 The Finite Difference Approach                         | 28          |
| 2.7.2 The Finite Element Method                              | 29          |
| 2.8 The Finite Element Model of the Spindle Workpiece System | 30          |
| 2.8.1 Element Equation of Motion                             | 30          |
| 2.8.2 The Equations of Motion for the Complete System        | 34          |
| 2.8.3 The Boundary Conditions                                | 37          |
| 2.9 Conclusions  | 38          |

### CHAPTER 3

#### THEORETICAL AND EXPERIMENTAL INVESTIGATION OF THE FREE VIBRATION OF THE SPINDLE-WORKPIECE SYSTEM

|   |    |
|---|----|
| 3.1 Introduction  | 39 |
| 3.2 Selection of the System Parameters  | 39 |
| 3.3 The Experimental Investigation  | 42 |
| 3.3.1 The Experimental Set-Up   | 42 |
| 3.3.2 Experimental Results  | 47 |
| 3.4 Results of the Analytical Investigation   | 47 |
| 3.5 Comparison and Discussion of the Theoretical and the Experimental Results                         | 49 |
| 3.6 The Effect of the Variation of the Bearing Stiffness on the Free Vibration Behavior of the System | 49 |
| 3.6.1 Effect of Variation in Bearing Stiffness  | 52 |
| 3.7 Conclusions   | 60 |

### CHAPTER 4

#### DYNAMIC RESPONSE OF A LATHE SPINDLE-WORKPIECE SYSTEM UNDER RANDOM CUTTING FORCES

|   |    |
|---|----|
| 4.1 Introduction  | 62 |
| 4.2 Workpiece Response Under Spatially Moving Random Cutting Forces | 63 |
| 4.2.1 The Mathematical Model and Analysis                           | 65 |

|  | <u>Page</u> |
|--|-------------|
| 4.2.2 Response Under Non-Stationary Random Cutting Forces  | 68          |
| 4.2.3 Characterization of the Moving Cutting Force   | 70          |
| 4.2.4 The Mean and the Variance Response of the Workpiece at the Tool Location                                   | 71          |
| 4.2.5 Results and Discussion   | 76          |
| 4.3 Spindle Workpiece System Under Random Cutting Forces   | 80          |
| 4.3.1 The Dynamometer  | 82          |
| 4.3.2 Static Calibration of the Dynamometer  | 84          |
| 4.3.3 The Dynamic Calibration of the Dynamometer   | 87          |
| 4.4 Cutting Force Measurements   | 87          |
| 4.5 Power Spectral Density (PSD) of the Cutting Force  | 88          |
| 4.6 The Mean Square Response of the Spindle-Workpiece System   | 94          |
| 4.7 The Parameters of the Spindle-Workpiece System   | 98          |
| 4.7.1 The Bearing Stiffness  | 98          |
| 4.7.2 Bearing Location   | 98          |
| 4.7.3 Cross-Sectional Area of the Spindle  | 99          |
| 4.7.4 Damping  | 100         |
| 4.8 Results and Discussion   | 101         |
| 4.8.1 The Effect of Tool Location on the Mean Square Displacement (MSD) of the Workpiece                         | 101         |
| 4.8.2 The Effect of the Bearing Stiffness on the MSD of the Workpiece  | 103         |
| 4.8.3 The Effect of the Bearing Spacing on the Workpiece MSD   | 103         |
| 4.8.4 The Effect of the Sectional Rigidity of the Spindle on the Mean Square Displacement (MSD) of the Workpiece | 106         |
| 4.8.5 Effect of Damping on the MSD of the Workpiece  | 109         |
| 4.9 Conclusions  | 111         |

## CHAPTER 5

### OPTIMIZATION OF THE LATHE SPINDLE-WORKPIECE SYSTEM UNDER STOCHASTIC CUTTING FORCES

|                                  |     |
|----------------------------------|-----|
| 5.1 Introduction                 | 117 |
| 5.2 Formulation of the Problem   |     |
| 5.2.1 First Optimization Scheme  | 119 |
| 5.2.2 Second Optimization Scheme | 120 |

|   | <u>Page</u> |
|---|-------------|
| 5.3 The Optimization Algorithm  | 120         |
| 5.4 Results and Discussion on the Optimized System                                    | 125         |
| 5.5 Effect of Chuck Diameter on the Mean Square Response of the Optimized System      | 128         |
| 5.6 Effect of the Size of Workpiece on the Mean Square Response of the Optimal System | 128         |
| 5.7 Conclusions   | 130         |

## CHAPTER 6

### EFFECT OF ADDITIONAL BEARING AND EXTERNAL DAMPER ON THE RESPONSE OF A SPINDLE-WORKPIECE SYSTEM

|  |     |
|--|-----|
| 6.1 Introduction   | 133 |
| 6.2 Effect of Introducing a Third Bearing in the System                | 133 |
| 6.3 External Damping in the Spindle-Workpiece System                   | 135 |
| 6.3.1 Introduction   | 135 |
| 6.3.2 Dynamic Damped Vibration Absorbers                               | 137 |
| 6.3.3 Fluid Damper   | 141 |
| 6.3.4 Theoretical Formulation of a Damper                              | 145 |
| 6.3.5 Location of the Fluid Damper                                     | 151 |
| 6.3.6 Design of a Squeeze Film Damper for the Spindle-Workpiece System | 153 |
| 6.4 Conclusions  | 156 |

## CHAPTER 7

### CONCLUSIONS AND RECOMMENDATIONS

|  |     |
|--|-----|
| 7.1 Major Highlights   | 160 |
| 7.1.1 The Mathematical Model of the System Response Acted Upon by Random Excitations of Arbitrarily Varying Power Spectral Density | 160 |
| 7.1.2 Workpiece Response due to Spatially Moving Random Cutting Forces   | 160 |
| 7.1.3 Dynamic Behavior of Lathe Spindles with Elastic Supports Including Damping   | 161 |
| 7.1.4 Dynamic Analysis and Optimal Selection of Parameters of a Lathe Spindle Under Random Cutting Forces                          | 161 |
| 7.1.5 Other Applications   | 162 |

|                                      | <u>Page</u> |
|--------------------------------------|-------------|
| 7.2 Limitations of the Investigation | 164         |
| 7.3 Recommendations for Future Work  | 164         |
| REFERENCES                           | 166         |

#### APPENDIX A

|   |     |
|---|-----|
| MASS AND STIFFNESS MATRICES OF AN ELEMENT | A.1 |
|---|-----|

#### APPENDIX B

|   |     |
|---|-----|
| B.1 Introduction  | B.1 |
| B.2 Mathematical Formulation  | B.2 |
| B.3 Step-by-Step Procedure of the New Method  | B.4 |
| B.4 Numerical Examples  |     |
| B.4.1 The Inertia Matrix Diagonal, and the Stiffness<br>and the Damping Matrices, Nondiagonal | B.5 |
| B.4.2 The Inertia Matrix Nondiagonal, and the Stiffness<br>and the Damping Matrices, Diagonal | B.9 |
| B.5 Results and Discussion  | B.9 |

## LIST OF FIGURES

| <u>Figure</u> |  | <u>Page</u> |
|---------------|--|-------------|
| 2.1           | A Typical Lathe.   | 14          |
| 2.2a          | Lathe Spindle-Workpiece System.  | 16          |
| 2.2b          | Schematic Model of a Spindle-Workpiece System.                         | 16          |
| 2.3           | A Typical Cutting Force in a Turning Operation.                        | 21          |
| 2.4           | Finite Element Model of One of the Elements of the System.             | 31          |
| 3.1           | The Variation of Mass Along the System.                                | 40          |
| 3.2           | The Variation of Stiffness Along the System.                           | 41          |
| 3.3           | A Schematic Diagram of the Experimental Set Up.                        | 44          |
| 3.4           | A Pictorial View of the Instrumentation for the Frequency Analysis.    | 45          |
| 3.5           | The Pictorial View of the Shaker and Workpiece for Frequency Analysis. | 46          |
| 3.6           | Acceleration Response Versus Frequency.                                | 48          |
| 3.7           | Hinged, Clamped and Experimental Frequencies Versus Frequency Number.  | 51          |
| 3.8           | The First Five Natural Frequencies Versus Front Bearing Stiffness.     | 53          |
| 3.9           | The First Undamped Mode Shape Versus Front Bearing Shaft.              | 54          |
| 3.10          | The Second Undamped Mode Shape Versus Front-Bearing Shaft.             | 55          |
| 3.11          | The Third Undamped Mode Shape Versus Front Bearing Shaft.              | 56          |
| 3.12          | The Fourth Undamped Mode Shape Versus Front Bearing Shaft.             | 57          |
| 3.13          | The Fifth Undamped Mode Shape Versus Front Bearing Shaft.              | 58          |
| 4.1           | The Representation of a Chuck-Workpiece-Running Center System.         | 64          |

| <u>Figure</u>   | <u>Page</u> |
|---|-------------|
| 4.2 Normalized Mean Displacement Response of the Workpiece Versus Tool Location.  | 78          |
| 4.3 Normalized Centered-Mean Square Displacement of Workpiece Against Tool Location.  | 79          |
| 4.4 The Schematic of the Instrumentation Used for the Cutting Force Measurement.  | 81          |
| 4.5 A Cross-Section of the Dynamometer (after Rakhit [41]).   | 83          |
| 4.6 A Schematic Diagram of the Set Up for Static Calibration of the Dynamometer.  | 85          |
| 4.7 Static Calibration Chart of the Dynamometer (after Rakhit [41]).  | 86          |
| 4.8 A Typical Record of Cutting Forces (after Maragos [48]).  | 89          |
| 4.9 Typical Spectral Density Plot of the Cutting Forces (after Rakhit [41]).  | 90          |
| 4.10 The Schematic of the Instrumentation Used for the Frequency Analysis.  | 93          |
| 4.11 The Experimental Power Spectral Density of the Cutting Forces Versus Frequency.  | 95          |
| 4.12 The Effect of Tool Location on the MSD of the Spindle-Workpiece System.  | 104         |
| 5.1 Two-Dimensional Complex.  | 122         |
| 5.2 Flow Chart of the Complex Optimization Method.  | 123         |
| 6.1 Decrease of the Resonance Amplitude by Means of an Absorber in Relation to its Frequency and Damping (after Umback [70]). | 139         |
| 6.2 Two-Dimensional Absorber for a Milling Machine (after Stone and Andrew [72]).   | 140         |
| 6.3 Chatter Receptance of Machine Without Absorber (after Stone and Andrew [72]).   | 142         |
| 6.4 Predicted and Measured Optimized Chatter Receptance With Two-Dimensional Absorber Added (after Stone and Andrew [72]).    | 143         |
| 6.5 Amplitude of Forced Vibration Receptance With and Without Absorber (after Stone and Andrew [72]).                         | 144         |

| <u>Figure</u>  | <u>Page</u> |
|--|-------------|
| 6.6 Relative Viscous Damper of Spindle of a Lathe<br>(after Peters [74]).  | 146         |
| 6.7 Flat Liquid Film Damper.   | 147         |
| 6.8 Influence of Location of Damper (after Peters [74]).                   | 152         |
| 6.9 Designed Fluid Damper.   | 154         |
| B.1 Three-Degrees of-Freedom System.                                       | B.6         |
| B.2 Geometric Representation of the Four Degrees of<br>Freedom Cab System. | B.10        |



LIST OF TABLES

| <u>Table</u> |   | <u>Page</u> |
|--------------|---|-------------|
| 3.1          | Parameter Values of Spindle-Workpiece System.   | 43          |
| 3.2          | Undamped Natural Frequencies of the System.   | 50          |
| 4.1          | The Effect of Tool Location on the MSD Response of the System.  | 102         |
| 4.2          | The Effect of the Bearing Stiffness on the MSD Response of the Workpiece.   | 105         |
| 4.3          | The Effect of Bearing Spacing on the Maximum MSD Response of the Workpiece.   | 107         |
| 4.4          | The Effect of the Variation of the Spindle Diameter on the MSD Response.  | 108         |
| 4.5          | The Effect of Groupwise Variation of Diameter of Various Elements on the MSD Response.                                | 110         |
| 4.6          | Additional Damping at the Front Bearing Location Versus MSD of the Workpiece.   | 112         |
| 4.7          | The Effect of Additional Damping Applied at the Rear Bearing Location on the Maximum MSD Response of the Workpiece.   | 113         |
| 4.8          | The Effect of Damping Location on the MSD Response of the Workpiece.  | 114         |
| 5.1          | Optimal Values for Two Parameter Optimization.  | 126         |
| 5.2          | Optimal Values for Three Parameter Optimization.  | 127         |
| 5.3          | The Effect of the Diameter of the Chuck on Workpiece Response.  | 129         |
| 5.4          | The Effect of Workpiece Slenderness Ratio on the Workpiece Response.  | 131         |
| 6.1          | Parametric Variations for the Third Bearing.  | 134         |
| 6.2          | Optimal Values for the Third Bearing.   | 136         |
| 6.3          | The Effect of Additional Damping Applied at the Free-End on the MSD Response of the Three Parameter Optimized System. | 157         |

| <u>Table</u> |  | <u>Page</u> |
|--------------|--|-------------|
| B.1          | Various Matrices of the Mechanical System.   | B.7         |
| B.2          | Computational Time for the Response Power Spectral Density Matrix of the 3 Degrees of Freedom Mechanical System. | B.8         |
| B.3          | Various Matrices of the Tractor Cab Suspension System [76].  | B.11        |
| B.4          | The Computation Time for the Response Power Spectral Density of the Cab Suspension System.                       | B.12        |

## NOMENCLATURE

|                                    |   |
|------------------------------------|---|
| [ ]                                | matrix  |
| $\dot{\phantom{x}}$                | differentiation with respect to time                          |
| $c(x)$                             | damping coefficient   |
| $d_0$                              | diameter of the element number 8                              |
| $e$                                | gap in the damper   |
| $f^1(x,t)$                         | centered random part of cutting force                         |
| $f(x,t)$                           | externally impressed force                                    |
| $h_m(t)$                           | impulse response function for m-th mode                       |
| $k$                                | stiffness   |
| $k_f$                              | front bearing stiffness                                       |
| $k(x)$                             | stiffness coefficient   |
| $l$                                | length of an element  |
| $m(x)$                             | mass per unit length  |
| $q_m(t)$                           | generalized modal coordinate for m-th mode                    |
| $t$                                | time variable   |
| $v$                                | tool feed rate  |
| $\bar{w}(t)$                       | joint displacement vector in global coordinate                |
| $w_i(t)$                           | joint displacement in local coordinate system                 |
| $x$                                | global displacement coordinate along spindle-workpiece system |
| $x_1$                              | local position coordinate                                     |
| $z$                                | normalized space coordinate along the workpiece               |
| $C_d$                              | the damping coefficient of the designed damper                |
| $C_{W,W'}(x_1, x_2, t_1, t_2)$     | covariance of displacement                                    |
| $C_{F^1, F^1}(x_1, x_2, t_1, t_2)$ | covariance of the random force                                |
| $C_{Q_m^1, Q_m^1}(t_1, t_2)$       | covariance of the generalized force                           |

|                           |  |
|---------------------------|--|
| $C_{q_m' q_m'}(t_1, t_2)$ | covariance of the generalized displacement                   |
| $E$                       | modulus of elasticity  |
| $E[\bar{W}]^2$            | mean square displacement                                     |
| $F$                       | force  |
| $\bar{F}(x, t)$           | mean value of cutting force                                  |
| $F(\bar{x})$              | objective function   |
| $G_{f_1}(\cdot)$          | power spectral density of a sample of a cutting force signal |
| $H(j\omega)$              | transfer function  |
| $H_d$                     | a constant in the design of a damper                         |
| $I(x)$                    | diametral moment of inertia                                  |
| $L^*$                     | Lagrangian   |
| $L_d$                     | length of the damper   |
| $L$                       | total length of the spindle-workpiece system                 |
| $L_B$                     | spacing between the front and the rear bearings              |
| $M_m$                     | generalized mass of m-th mode                                |
| $R_d$                     | radius of the circular plate damper                          |
| $R_w(\cdot)$              | autocorrelation function of the displacement                 |
| $R_f(\cdot)$              | autocorrelation function of the force                        |
| $Q_m$                     | generalized force for m-th mode                              |
| $S_f$                     | power spectral density of cutting force                      |
| $T^*(t)$                  | kinetic energy   |
| $V^*(t)$                  | potential energy   |
| $W(x, t)$                 | deflection   |
| $W_j$                     | joint displacement in global coordinate system               |
| $W'(x, t)$                | centered random part of displacement                         |
| $W_0$                     | static displacement at the mid-point of the workpiece        |
| $W_0^*$                   | normalized mean square displacement response                 |

|                   |  |
|-------------------|--|
| $[m]$             | mass matrix  |
| $[k]$             | stiffness matrix   |
| $[c]$             | damping matrix   |
| $\{f\}$           | force vector in local coordinate system                      |
| $[A(j\omega)]$    | matrix of transfer functions                                 |
| $[\bar{C}]$       | global damping matrix  |
| $\{\bar{F}\}$     | force vector in global coordinate system                     |
| $[G]$             | transformation matrix relating local vector to global vector |
| $[H]$             | a rectangular constant matrix                                |
| $[\bar{K}]$       | global stiffness matrix                                      |
| $[S_F(\omega)]$   | power spectral density matrix of excitation                  |
| $[S_W(\omega)]$   | power spectral density matrix of displacement response       |
| $[V]$             | matrix of eigen vectors                                      |
| $\rho_d$          | specific mass of the fluid in the damper                     |
| $\eta_d$          | dynamic viscosity of the fluid in the damper                 |
| $\phi_m(x)$       | normal mode shape function                                   |
| $\phi_j(x)$       | shape function   |
| $\beta$           | the equivalent viscous damping                               |
| $\omega_m$        | natural frequency of $m^{\text{th}}$ mode                    |
| $\sigma_W^2(x,t)$ | variance of displacement response                            |
| $\delta(\ )$      | dirac delta function   |
| $\omega$          | frequency  |
| $\epsilon$        | a convergence factor   |
| $[\phi]$          | matrix eigen vectors of the modified system                  |
| $\psi$            | experimental power spectral density                          |
| $\tau_1$          | dummy variable   |
| $\tau_2$          | dummy variable   |

## CHAPTER 1

### INTRODUCTION AND LITERATURE SURVEY

#### 1.1 Machining Processes

In manufacturing any product, there are usually a number of machining operations performed on a raw workpiece. These machining processes can be classified into two categories, which are: (1) traditional chip removal processes, and (2) non-traditional machining processes. Operations such as turning, shaping, drilling, etc., belong to the first category, whereas operations such as ultrasonic machining, electro-discharge machining (EDM), electro-chemical machining (ECM), belong to the second category.

In all these processes, which are necessary for products requiring close dimensional accuracy, metal is removed from the raw material in the form of metal chips. Such operations are performed on machine tools which operate on either a reciprocating or a rotary type principle. That is, either the tool or the workpiece reciprocates or rotates. For example, in a lathe, the workpiece rotates and the tool is stationary. Hence in a machine tool, a finished product is obtained by removing metal chips due to a relative motion between the tool and the workpiece.

A finished product should meet the specifications which are in terms of good surface finish as well as close dimensional tolerance. Finishing operations are performed to ensure a smooth surface finish, high accuracy, esthetic appearance, etc. In order to achieve good surface finish, the vibration levels in the tools or workpiece should be as low as possible. The vibration can be controlled by proper design of machine tools.

## 1.2 Various Considerations in Machine-Tool Design

Since a machine tool is an assembly of several machine components, a good design of a machine tool requires that all of its components be designed with utmost care and precision. This can only be possible if a detailed static and dynamic analysis of each of the components is carried out. The present investigation, which is, a study of the dynamic behavior of lathe spindles, is a step in that direction.

In designing a machine tool, there are several important considerations, such as:

- (i) the stability of the structure,
- (ii) nature of cutting forces,
- (iii) the type of damping,
- (iv) dynamic response of workpiece under cutting force excitation, and
- (v) selection of optimal design parameters.

In the next section, a literature survey on all the topics mentioned above are presented.

### 1.2.1 Stability of the Machine Tool Structure

A machine tool will deflect from its equilibrium position if a force is applied between the workpiece and the cutting tool. If the spectrum of these forces contain higher frequencies then not only static but dynamic stiffness also has to be considered. Since the machine tool has distributed mass, it will have a number of resonant frequencies. These may be excited due to the cutting forces.

The machine tool structures are usually made of cast iron or mild steel. For the same weight, a mild steel fabrication may be expected to be about twice as stiff as a similar design in cast iron. In designing the machine tool frame, which requires quite complex mathematical analysis, analog and digital computers are often used. Several researchers [ 1-3 ] analyzed the machine tool response by representing the structure by a number of lumped masses which are joined together by elastic and weightless beams. The response calculation is based upon the fact that, under steady state conditions, the deflected shape of a structure excited by a set of oscillating forces may be expressed as the sum of the factored mode shapes. That is, the response of each mode is computed separately as a single-degree-of-freedom system and then they are added vertically in the complex plane. The response calculation is carried out over the range of frequencies of interest. Each single degree-of-freedom mode in the complex plane gives a circular locus.

The most suitable design for any structure may be found by analyzing each of the possible designs and comparing the important criterion such as flexibilities, chatter, stabilities, etc.

The effect of torsional vibrations on the machine tool stability was studied by Knight [4]. In his study the torsional oscillations of the drive system were also included. It was concluded that the vibrations suppress the built up edge on the tool, which in turn, directly affects the change in force with the speed, under steady state conditions.

A study of a machine tool drive and structure was carried out on an analog computer by Cuppan and Bollinger [5]. The machine tool structure was represented by a system of differential equations and these equations



were solved for various values of system parameters. The theoretical results were then experimentally verified. Tlusty [6] studied the machine tool frame by organizing several tests on a prototype and outlined a procedure for machine tool frame calculations.

### 1.2.2 The Cutting Forces (Deterministic Model)

For more than a century, researchers in the field of manufacturing have been attempting to understand the nature of the cutting forces during a machining operation. Several researchers [7-9] considered metal cutting operation as a steady state process. Merchant [8,9], in order to study the mechanics of the cutting process, divided it into two parts; an orthogonal cutting, and an oblique cutting, depending on the orientation of the cutting edge to the relative motion of the tool and the workpiece. The theory and equations of the cutting process were developed, by which, with little approximation, any orthogonal cutting process could be analyzed.

Lee [10] studied the machining as a plastic flow of an ideal plastic material and thereby obtained the stress and strain distribution in the system. Sabberwall [11,12] studied the cutting process in milling operation and through these studies, an optimum configuration of the milling cutter and the workpiece was proposed. The frictional characteristics of the tool-chip interface was studied by Wallace [13]. An excellent treatment of the mechanics of the cutting process is given in [14].

In all of these studies [7-13], however, the mathematical models consider deterministic equations of motion of the system with a harmonic cutting force excitation. With these models, one can explain the chatter

instability during a roughing operation.

### 1.2.3 The Cutting Forces (Random Model)

In the area of machine-tool dynamics, the stochastic approach is fairly new. Some of the researchers [15 - 19] recognized the random nature of cutting forces in a machining operation. Kwiatkowski and Bennet [16] determined receptances of machine tools acted upon by random forces (using random generator) using correlation technique. Peklenik [17] derived the fundamental relationship of linear time invariant systems using spectral density measurements. It was shown [18] that the dynamic parameters measured during the standstill condition are different from those at working condition. The importance of system analysis by means of spectral density measurement compared with the conventional deterministic procedures was also demonstrated.

Field [19] obtained the resonant frequencies of a vertical milling machine by using the cutting force as a source of random excitation, and employing the cross-correlation technique. The cutting forces were measured by a dynamometer.

### 1.2.4 Damping in Machine Tools

The effect of vibration on a machine tool and its effect on the quality of the workpiece produced was studied by several authors [20-25]. The overall quality of a machine tool is determined by many different factors, one of them is the dynamic stability. Dynamic stability relates to the maximum material removal rate that can be achieved without chatter. This is further related to the dynamic stiffness of the machine tool. The chatter problem can be solved in part by stiffening the machine tool structure. This approach is effective up to a point only and further

stiffening leads to excessive weight. The dynamic stiffness depends both on the static stiffness and on damping of the machine tool structure.

In general, the damping in a machine tool can be due to, (a) structural damping, and (b) frictional damping. The energy dissipation due to structural damping for a cyclic stress-strain process, is proportional to the strain amplitude. This dissipation of energy takes place due to internal friction. For any solid, the structural damping coefficient is a function of temperature [26]. The frictional damping is the main source of energy dissipation in a machine tool. The energy dissipation due to friction damping takes place at guideways, joints, etc. An excellent treatment of damping can be found in the references [27-34].

#### 1.2.5 Flexural Vibration of Rotating Shafts

There has been a reasonable amount of literature published in the area of stability of symmetrical and unsymmetrical rotating shafts [35,36]. However, very little work has been carried out on the stability of machine tool spindles. The information available from the area of stability of rotating shafts, therefore, can be utilized in assessing the response of machine tool spindles.

It has been reported that the instability of transverse motion of a symmetrical shaft can occur, in the absence of internal damping, only at certain critical speeds of rotation, whereas instability can occur, in the case of unsymmetrical shafts for a whole range of speeds. It was suggested by Kimball [37] that the internal friction might be caused by elastic hysteresis which acts as a damping force rotating with the shaft. Robertson [38] summarized the causes of vibration in rotating

shafts through several theoretical and experimental investigations. He challenged the concept of viscous law of internal friction, and favored a law by which damping forces were a function of change of strain. Neither of the theories such as those put forward by Robertson nor the rotating viscous medium have been found to be exact, even though such exactness in the mathematical model is not always essential. The rotating viscous medium theory has been utilized in the present investigation.

The coupling of the transverse and the torsional modes of vibration was studied by Bagci [39] and the natural frequencies of the system were obtained by using lumped mass parametric techniques.

#### 1.2.6 The Dynamic Response of Machine Tools

The performance of a given machine tool can be estimated by studying the dynamic response under actual operating conditions. The dynamic response of machine tools should include a) spindle, b) drive system, and c) structure. Since it is very tedious to have an investigation of machine tools that include all the three aforementioned subsystems, a practical alternate solution would be to consider each system individually and to carry out the dynamic response study.

In the case of machine structural response, the fundamental criterion for the performance of a machine tool structure lies in its static and dynamic stiffness. To improve the performance of the machine tool, the response at various points on the structure has to be known. The literature survey, on the analysis of the dynamic response and stability of the machine tool structures by various authors [1-6], has been carried out in section 1.2.1.

In this section, a literature survey on the dynamic analysis of

machine tool spindles is presented. Sankar and Osman [40] studied the spindle-dynamics using 2 degree-of-freedom (translation and rotation) under stochastic excitation. These equations were solved by Fokker-Plank technique under the assumption that (a) the power spectral density of the excitation could be represented by a white noise excitation, and (b) there was no cross coupling in these two equations. Thus the two equations were solved independently.

Rakhit [41] analyzed a lathe spindle-workpiece system by representing the system by two-degree-of-freedom system. In this work, the actual cutting force was measured and its power spectral density was experimentally obtained by using a frequency analyzer. The power spectral density thus obtained was replaced by that of an equivalent white noise process. His mathematical model did not include the running center and the workpiece was held only at the chuck. It was concluded (a) that the cutting forces in a finish turning operation, are basically random in nature, and they are of wide band nature, and (b) that the probabilistic parameters which characterize the cutting forces and the surface roughness of the workpiece indicate approximate linear mutual relationships.

The multi-degree-of-freedom analysis of a lathe spindle was carried out by Bollinger [42]. The spindle was represented by seven degrees-of-freedom and the harmonic force was assumed to be acting on the chuck. In this analysis, neither the random cutting forces nor the boundary condition at the workpiece-running center interface, were included in the mathematical model. It was concluded that the approach using finite difference technique to formulate the model of the spindle, and the solution of the equations using the analog computer, is an

efficient and useful method for analyzing the variables involved in the optimal design of the spindle. It was also concluded that the external damper should be located at the free-end of the spindle

The dynamic characteristics such as dynamic response and the phase angle as a function of rotational speed of the spindle were experimentally studied by Morse [43], and Allemang [44].

Design of lathe spindles based on optimal location of bearings was carried out by Chomjakow [45]. In this analysis, the harmonic excitation was assumed to be acting on the chuck, and the optimization was based on the minimum response at the chuck. The workpiece was not included in the mathematical model.

Based on a review of the existing literature, it is found that a comprehensive analysis on the dynamic flexural response of a lathe spindle-workpiece system that includes realistic end supports and actual random cutting forces is lacking. In this thesis, a methodology for analyzing lathe spindles is developed that includes optimal design schemes for minimum mean square displacement response of the workpiece. The details of this investigation are discussed in the next section.

### 1.3 Scope of the Investigation

The objective of this thesis is to study the flexural response of the spindle-workpiece system under the action of random cutting forces. The investigation has been divided into the following sections.

- 1) Analyze the free vibration characteristics of the system and experimentally verify the mathematical model.
- 2) To investigate the nature of boundary condition at the running center that supports the workpiece.

3) To study the effect of bearing stiffness on the natural frequencies and the corresponding mode shapes of the spindle-workpiece system.

4) To study the nonstationary random response of a workpiece subjected to spatially varying cutting forces and to investigate the effect of tool feed rate on the dynamic response of the workpiece.

5) To measure the actual random cutting forces while machining a workpiece on a lathe and to calculate the PSD of the cutting forces.

6) To calculate the mean square response of the spindle-workpiece system under the random cutting forces by using a new method that is developed for this purpose.

7) To carry out a parametric study of parameters such as bearing stiffness, bearing spacing, spindle sectional rigidity, and damping on the forced response of the spindle-workpiece system.

8) To optimally select the system parameters that minimize the maximum workpiece response.

9) To investigate other design considerations such as stiffening of the spindle due to a third bearing and the design of a squeeze film damper on the system response.

In chapter 2, a mathematical model of a lathe spindle-workpiece system has been formulated. The bearings are represented by a linear spring and a viscous damper. The merits of the finite element and the finite difference methods to solve the mathematical model and the representation of the workpiece-running center as hinged or clamped boundary condition has been discussed.

In chapter 3, the free vibration behavior of the system is discussed. The nature of the end condition at the workpiece-running

center interface is established. The end condition of the workpiece supported by the running center can be better represented by a hinged condition rather than a clamped condition. The effect of the variation of the bearing stiffness on the undamped natural frequencies and the corresponding mode shapes is explained.

In chapter 4, to study the random response of the workpiece acted upon by a spatially varying random cutting force, the workpiece has been modeled as Euler-Bernoulli beam. The cutting force has been modeled as a white noise excitation and the mean and the variance response of the workpiece is calculated as a function of varying feed rates of the tool and for different values of the structural damping of the workpiece. It is established that for the range of feed rates normally used in the turning operation, the response does not depend upon feed rate of the tool. The cutting force is measured experimentally and its power spectral density (PSD) is obtained using a Fast Fourier Transform analyzer. The PSD of the cutting forces were used to calculate the mean square response of the workpiece. For this purpose a new technique for the calculation of response spectral density for linear stationary random multi-degree-of-freedom system was developed. The method is based on modifying the stochastic dynamic equations of the system by using a set of auxiliary variables. The response spectral density matrix obtained by using this new approach contains the spectral densities and cross-spectral densities of the system generalized displacements and velocities. The new technique requires significantly less computation time as compared to the conventional method for calculating the response spectral densities. A parametric study on the effect of bearing stiffness, bearing spacing, spindle sectional rigidity and damping on the mean square displacement



of the workpiece is also carried out.

Chapter 5 describes the optimum selection of parameters and the optimization technique used for the system under consideration. The system is optimized using a direct search method known as complex method. Besides optimization, the effect of the variation of the diameter of the chuck and the slenderness ratio of the workpiece have also been studied.

In chapter 6, possibility of using a third bearing, and a design of squeeze film damper is discussed. In designing a damper, considerations, such as other methods of vibration control and location of such controlling mechanism, are also discussed.

Finally, conclusions and recommendations for future work are presented in chapter 7.

## CHAPTER 2

### DESCRIPTION OF A LATHE SPINDLE-WORKPIECE

#### SYSTEM AND ITS MATHEMATICAL MODEL

##### 2.1 Introduction

Dimensional accuracy and surface finish of a machined workpiece depend upon dynamic characteristics of the machine tool spindle-workpiece system. Since the surface finish of a machined workpiece is directly related to the dynamic flexural response influenced by the nature of the metal cutting forces, the objective of the present work therefore is to select parameters such as bearing locations and spacing, bearing stiffness etc. to control this flexural response.

In other words, the stiffness and the location of each of the bearings should be such that required surface finish can be achieved during a machining process. A first step in achieving this objective would be to formulate an accurate mathematical model of a machine tool spindle-workpiece system.

##### 2.2 Components of a Spindle-Workpiece System

###### 2.2.1 The Spindle

Essentially, a lathe is a power tool which causes a workpiece to revolve so that a cutting tool in contact moves laterally and removes the metal in the form of chips. A typical lathe is shown in Fig. 2.1. It is a Model No. 821A, 12 hp. Demoor type lathe. All lathes are equipped with a motor and the power from the motor is transmitted to the spindle of the headstock through belts or gears. This power also controls the lateral movement or the feed rate of the cutting tools.

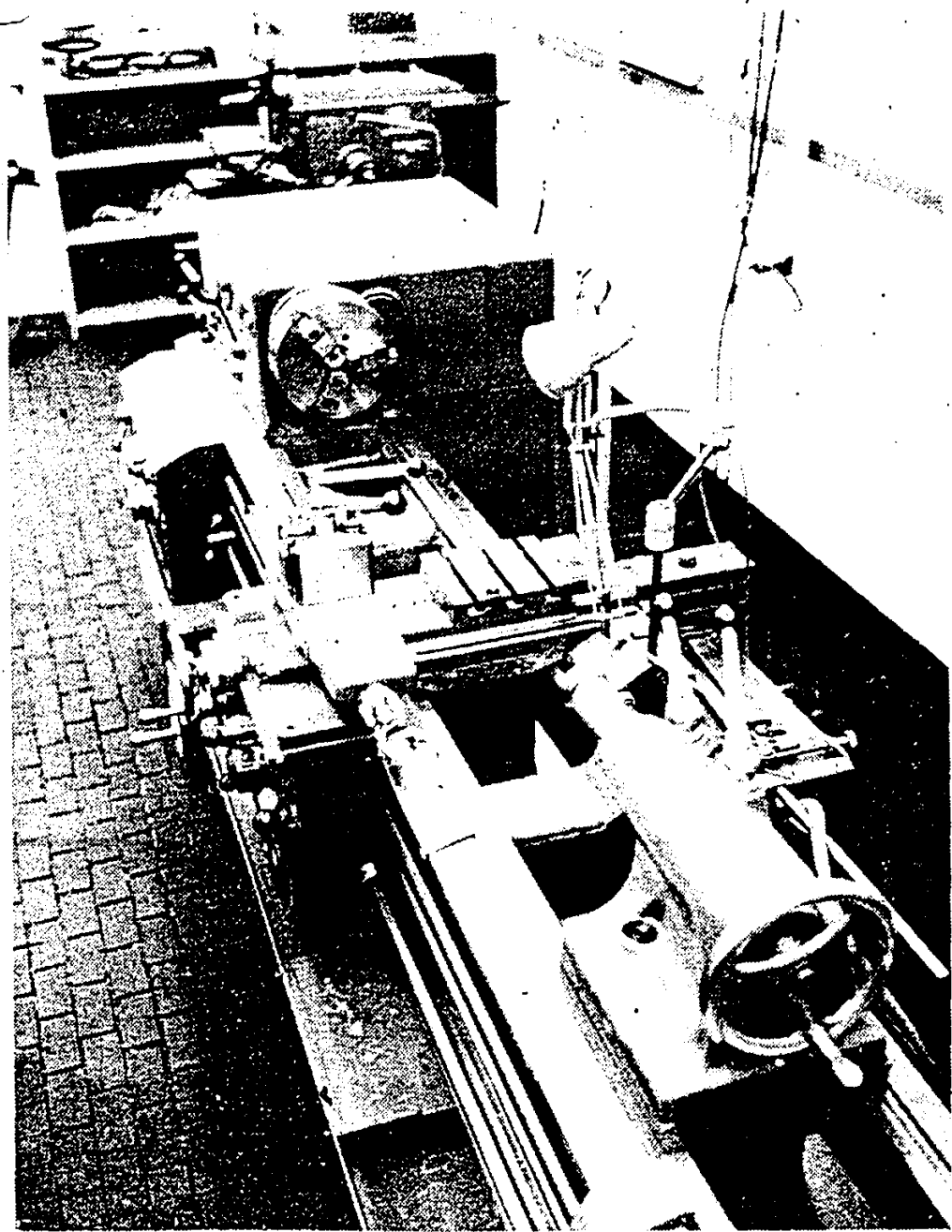


Fig. 2.1: A Typical Lathe.

The spindle-workpiece system is shown in Fig. 2.2a and its schematic model is shown in Fig. 2.2b. Referring to Fig. 2.2a, the spindle is hollow so that slender and long bars, can be fed for machining, through the rear of the spindle. The mass and the stiffness are nonuniformly distributed along the axis of the spindle. Figure 2.2b shows the schematic of the spindle-workpiece system supported by bearings which are represented by a spring and a damper. In Figs. 2.2a and 2.2b the workpiece is shown as held by the chuck on one end and supported by a running center on the other end. The chuck is normally considered as an integral part of the spindle and therefore is to be included in any mathematical model. During the machining process the tool is fed from the right to the left. The spindle is supported by two bearings and several gears are mounted on the spindle. The rotational speed of the spindle is controlled by engaging one of these gears with another gear mounted on another shaft which is not included in the above mentioned figures.

The metal cutting is performed using a cutting tool which is usually made of high speed steel or a carbide tip brazed or clamped to a solid piece. In the turning operation, the metal from the workpiece is removed in the form of metal-chips thereby continuously reducing its diameter. In general, there are two groups of machine tool-workpiece systems that can be classified on the basis of the type of relative motion between the tool and the workpiece.

(i) In the first group, the workpiece is attached to the machine spindle and has a rotary motion, whereas the tool is fixed on the machine bed and has a translatory motion. The present system (lathe) belongs

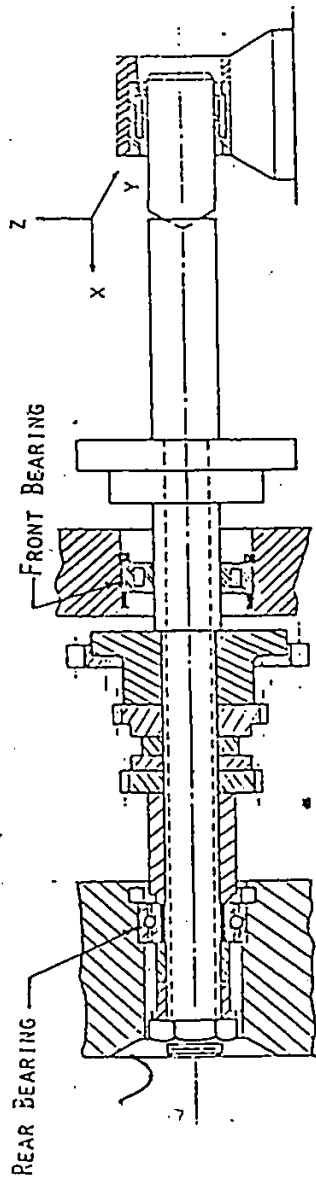


Fig. 2.2a: Lathe Spindle-Workpiece System.

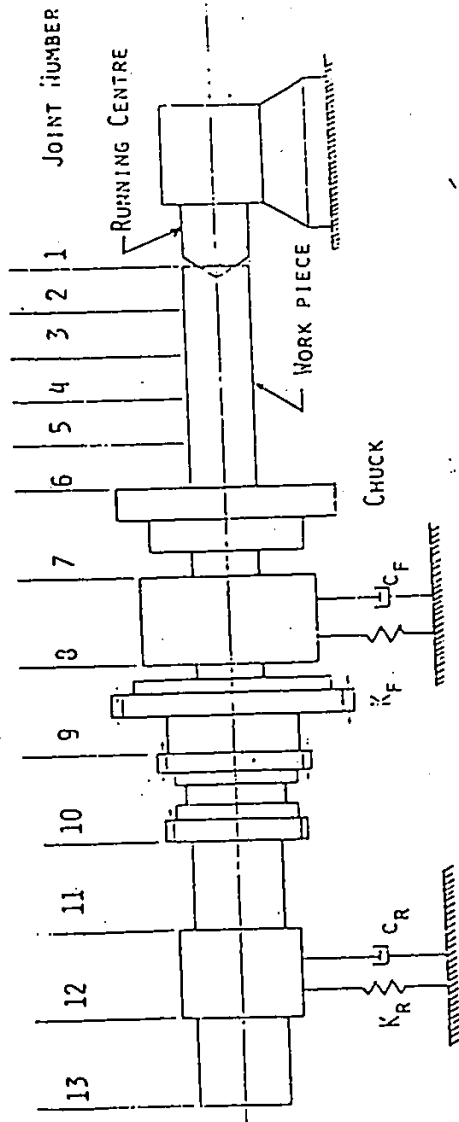


Fig. 2.2b: Schematic Model of a Spindle-Workpiece System.

to this group.

(ii) In the second group, the tool is attached to the machine spindle and has a rotary motion, whereas the workpiece is fixed on the machine bed and has a translatory motion. Milling machines and drilling machines belong to this second group.

As far as the metal removal is concerned, these two groups of machine tool-workpiece systems are similar since both involve relative motion between tool and workpiece. In general, the tool is fed from right to left and the machining of a workpiece is normally carried out in two stages. In the first stages, large amounts of material are removed in the form of metal chips and this operation is called a "roughing operation". In the second stage, known as "finishing operation" very small amounts of material are removed but great care is taken to achieve acceptable surface finish, dimensional accuracy and surface integrity.

The surface integrity is controlled by the flaws in the material of the workpiece and since it depends mainly upon the speed, feed, amount of coolant, etc. but not on the system itself, this aspect does not enter into the subject of the present investigation. It should also be noted that in a finishing operation, in order to achieve a good surface finish, the depth of cut is small compared to a roughing operation but the feed rate and rotational speed of the spindle are very high.

In this thesis, the dynamic behavior, such as the mode shapes, the natural frequencies and the flexural response, of the spindle-workpiece system is studied in detail first and then appropriate measures such as selection of the stiffness of the bearings, location of the bearings, location and geometry of an external damper, for controlling

vibrations are recommended.

### 2.2.2 Bearings

There are several factors which should be considered in the selection of bearings that support the lathe spindle. Some of these factors are: (i) clearance, (ii) stiffness and elasticity, (iii) long service life, (iv) small overall size, (v) simple and convenient assembly, and (vi) availability of higher damping. The factors (i), (ii), and (vi) are described briefly here, whereas factors (iii), (iv), and (v) are self explanatory.

The clearance determines the accuracy of guidance in the radial as well as in the axial direction. The smaller the clearance, the more accurate the performance would be. Therefore to overcome the problem due to clearance, the bearings are normally preloaded.

Secondly, the bearings should have sufficient stiffness to withstand the forces transmitted through the spindle. Since a lathe once designed is used, in addition to turning, for other types of machining processes such as drilling, reaming etc., it is desirable to select an optimum bearing stiffness by analyzing the spindle-bearing system under all these different machining operations. However, since the lathe is mainly used for turning operation, it is justifiable to select the bearing stiffness based on turning operation as presented in this thesis.

Finally, there are very small amounts of damping in the form of friction damping present in the roller or ball bearings. These damping losses increase as the loads on the bearings are increased. This is caused by the deformation of the rollers or balls. Increased number of

rollers, and sufficient preloading reduce the detrimental effects of clearances by increasing the rigidity.

### 2.2.3 Damping in a Spindle-Workpiece System

When a machine tool system is subjected to dynamic cutting forces, it exhibits external and internal dissipative forces. The source of external damping exists at the bearing location and at the workpiece tool interface. The internal damping, arising due to dissipation within the material, is in the form of hysteretic damping. These two damping effects can be combined without any significant loss of accuracy by introducing the concept of equivalent viscous damping. The external damping can represent the effects of a stationary viscous environment, while the internal can be thought of as being caused by a viscous medium which rotates with the spindle.

The major part of the damping arising in a machine tool structure is generated at the interfaces such as bolted connections, slides, etc. Lowenfield [46] showed that in the course of building up a lathe from its elements, starting with the bed, then successively adding the slides, the headstock, and finally the tailstock, the damping increased in steps to about eight times its original value (i.e. that of the lathe bed above). Peters [47] found that the damping ratio of a lathe spindle made of steel can be as small as 0.0001, and that made of cast iron between 0.0004-0.0001. When the cast iron spindle was mounted in its headstock the damping increased from 0.0001 to 0.05. In general, overall damping ratio of machine tools lie between 0.02 and 0.05.



### 2.3 External Forces Acting on the Spindle Workpiece System

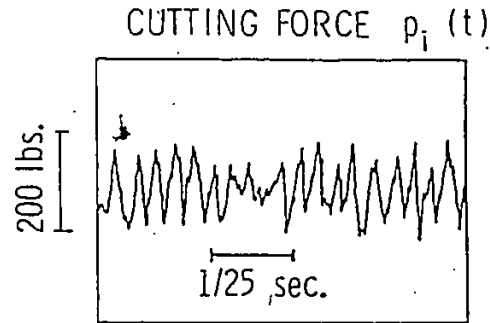
The dynamic forces present in a machine tool during metal cutting operation are generated from two sources. The first kind are the forces which are purely externally impressed due to the metal cutting actions. The second type are the self generated forces which arise due to any unbalance in the rotating machinery or due to inherent system dynamic characteristics. Spindle-workpiece system is normally balanced properly for both static and dynamic conditions and the disturbances arising from such dynamic effects of the machine tool can be usually corrected and therefore neglected in analysis. Hence, the predominant forces acting on the system are the external metal cutting forces. These forces are generally made up of a combination of harmonic and random forces [48].

A recorded plot of a typical cutting force variation is shown in Fig. 2.3. These cutting forces have a static as well as a dynamic component. The main cutting force is in the z direction (refer to Fig. 2.2a). There is a very large fluctuation in the magnitude of these cutting forces in all the three orthogonal directions. The dynamic forces are much smaller in magnitude as compared to the mean static forces. In this thesis, the flexural response due to the dynamic forces in the z direction would be investigated because it has been well established [41] that the dynamic response due to these cutting forces directly control the surface finish of the machined workpiece.

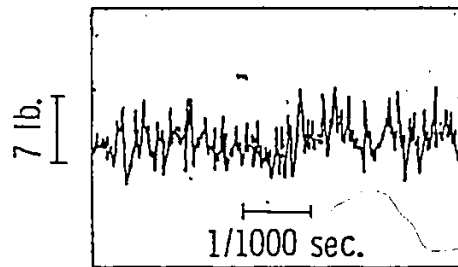
### 2.4 Objectives of the Mathematical Analysis

In a lathe spindle, the equivalent stiffness of the spindle-workpiece system is usually considerably less than that of the other parts of the machine [49]. Several authors [20-24] have developed

S - feed rate  
v - surface velocity of  
the workpiece  
s - depth of cut



S = 0.027 in/rev.  
v = 60 ft/min.  
s = 0.075 in.



S = 0.002 in/rev.  
v = 375 ft/min.  
s = 0.010 in.

MATERIAL : AISI 1015 STEEL

Fig. 2.3: A Typical Cutting Force in a Turning Operation.

mathematical models of the machine tool under self excited and forced vibrations, and have established stability criterion in terms of the rotational frequency of the system.

The dynamic characteristics of the lathe spindle were studied by Allemang [44] and Bollinger [42]. Allemang used the method of pulse testing in which the spindle at different rotational speed is excited by a deadblow hammer and the frequency response curve is obtained by using an FFT analyzer. Bollinger formulated the mathematical model of the spindle representing it by the Euler-Bernoulli flexural equation of motion and used a finite difference approach. In this model the spindle was divided into equal segments and each of these segments were assigned certain values of cross sectional moments of inertia and mass. The workpiece was held by chuck on one end and the other end of the workpiece was free. The system natural frequencies and the response due to harmonic excitation applied at the chuck were obtained using an analog technique. The effect of bearing stiffness, bearing location, damping location on the system natural frequencies as well as response under harmonic excitation were studied. An optimization scheme was employed and was based on two criteria which were: (a) the minimum response at the chuck, and (b) the minimum of the average response at several selected locations along the spindle. The effect of a third bearing on the rigidity of the spindle was also studied.

This mathematical model has several shortcomings which are explained below:

(i) An actual spindle has nonuniform distribution of mass and stiffness along the spindle axis therefore the assumption of uniform

variation of these two parameters at equal intervals would lead to inaccurate results.

(ii) In actual practice the workpiece is held by a running center on the free end and also the spindle-workpiece system is acted upon by rapidly fluctuating cutting forces. Since these effects have not been included in the mathematical model, any design based on such a model would be unrealistic.

Rakhit [41] studied the spindle dynamics under the action of the actual random cutting forces. The dynamics of the system was based on a two-degrees of freedom mathematical model. Actually the entire spindle was represented as a single degree-of-freedom system, and in the same way, the workpiece was also modeled by a single vibratory mass spring system. The actual cutting forces were measured using a special dynamometer. The power spectral density (PSD) of these cutting forces were replaced by an approximate equivalent white noise power spectral density (PSD). With this, the mean square response of the workpiece was calculated and a linear relationship between surface roughness and workpiece mean square response was established. Some of the deficiencies of this mathematical model are:

(i) It does not take into account the boundary conditions at the workpiece-running center interface as a consequence, the computed mean square response would be much higher than the actual mean square response.

(ii) The deflections at all the points along the workpiece or the spindle are assumed to be equal. In actual practice the deflection of the workpiece at the tool location is a maximum and there is large

variation in the deflection and its pattern at various points along the spindle-workpiece system.

(iii) The mass and the stiffness along the spindle are taken to be uniformly distributed which is not true in the actual case and therefore there would be a significant discrepancy between the computed and the actual deflections.

(iv) The power spectral density of the machining excitation has been approximated by a theoretical wideband process or an equivalent-white noise excitation. Such an approximation cannot yield the system behavior on a frequency by frequency basis. Therefore, there can be significant errors in the computation of the mean square response.

Hence in this chapter a comprehensive mathematical model of the tool-spindle-workpiece system is formulated to meet the following objectives:

(i) to investigate the nature of the end conditions of the workpiece supported at the running center. That is to determine whether the end condition can be identified as hinged or clamped support.

(ii) to calculate all the important undamped natural frequencies, and the mode shapes of the system. These are needed in the computation of the mean square response using a modal analysis.

(iii) to study the effect of the bearing stiffness on the undamped natural frequencies and the corresponding undamped mode shapes of the spindle-workpiece system.

## 2.5 Assumptions and Justifications

Several assumptions are made in the formulation of the mathematical

model of the system. They are:

1) The workpiece is considered to be rigidly attached to the chuck and forms an integral part of the spindle. This assumption can be justified by the fact that there is no relative translation or rotation between the chuck and the workpiece at the jaws.

2) The bearings which support the spindle-workpiece system, are assumed to be rigidly mounted in the housing. This assumption is valid because there is an interference fit between the bearing and the housing.

3) The inner races of the bearings are considered to exhibit some viscous damping and stiffness properties and could be represented by a viscous damper and a linear spring in the mathematical model.

4) The spindle-workpiece system is taken to be statically and dynamically balanced and to be operating at a constant speed.

5) The change in the diameter of the workpiece during the cutting operation is assumed to be negligible. This is because the depth of cut in a finishing operation is very small compared to dimensions of the workpiece.

6) The flexural vibration of the spindle-workpiece system is considered to be the dominant mode of vibration during a turning operation. The torsional oscillations of the system due to the combined flexural-torsional action of the metal cutting forces are assumed to be insignificant, and therefore neglected in the mathematical model.

7) The effects of shear deformation and rotary inertia have been assumed to be negligible.

## 2.6 Formulation of the Mathematical Model

The equation of motion of the spindle-workpiece, as shown in Figs. 2.2a and 2.2b, using the Euler-Bernoulli formulation can be written as [50]

$$\frac{\partial^2}{\partial x^2} \left[ EI(x) \frac{\partial^2 W(x,t)}{\partial t^2} \right] = -m(x) \frac{\partial^2 W(x,t)}{\partial t^2} \quad (2.1)$$

$$-K(x) W(x,t) - c(x) \frac{\partial W(x,t)}{\partial t} + f_{\text{ext}}(x,t)$$

where:

- E = modulus of elasticity,
- I(x) = diametral moment of inertia,
- m(x) = mass per unit length,
- W(x,t) = deflection along the system,
- K(x) = stiffness coefficient,
- c(x) = damping coefficient
- f<sub>ext</sub>(x,t) = externally impressed force, and
- t = time

The solution of the equation (2.1) must also satisfy the associated boundary conditions, which are:

(i) the bending moment and the shear force must vanish at the free end of the system;

(ii) if the workpiece-running center connection is assumed as hinged then the bending moment and the deflection must be zero at the connecting point; or,

(iii) if the above mentioned connection is assumed as clamped then the slope of the deflection curve and the deflection must be zero

at the connecting point.

In equation (2.1) the effects of the rotary inertia and shear deformation are neglected as indicated earlier. The terms on the right hand side of equation (2.1) represent the inertia forces, the spring forces at the bearings, the damping forces, and the externally applied forces. The system may now be divided into 12 lumped elements as described in Fig. 2.2. To investigate the dynamic behavior of the lathe spindle-workpiece system, the fourth order partial differential equation (2.1) has to be solved by representing in an appropriate fashion the random cutting forces  $f_{ext}(x,t)$  and with proper boundary conditions.

The nature of the boundary condition at the running center is unknown. That is, the end condition can be classified either as hinged or clamped. If a hinged condition is assumed, then the boundary condition at the running center would be [51]

$$W(x,t) \Big|_{x=0} = 0, \text{ and } EI(x) \frac{\partial^2 W(x,t)}{\partial x^2} \Big|_{x=0} = 0 \quad (2.2)$$

If the workpiece is assumed to be clamped instead of being hinged at the running center, then the corresponding set of boundary conditions are to be represented by

$$W(x,t) \Big|_{x=0} = 0, \text{ and } \frac{\partial W(x,t)}{\partial x} \Big|_{x=0} = 0 \quad (2.3)$$

The boundary condition for the free end of the spindle in either of the above mentioned cases would be



$$EI(x) \frac{\partial^2 W(x,t)}{\partial x^2} \Big|_{x=L} = 0 ,$$
$$\text{and } \frac{\partial}{\partial x} \left[ EI(x) \frac{\partial^2 W(x,t)}{\partial x^2} \right]_{x=L} = 0$$

(2.4)

where  $L$  is the total length of the combined spindle-workpiece system. It should be noted that in equations (2.2) to (2.4), the variable  $x$  is measured from the running center towards the free end of the spindle.

## 2.7 Method of Solution

The fourth order partial differential equation (2.1) and the associated boundary conditions represented by equations (2.2) or (2.3), and (2.4) can be solved by finite difference method as used by Bollinger [42] or it can be solved by finite element method [51].

### 2.7.1 The Finite Difference Approach

In the finite difference method, the partial differential equation is transformed into a total differential equation. This could be done in two ways. In the first method, the integration is performed along the spindle by keeping time  $t$  at some constant value. All the derivatives of  $W(x,t)$  are expressed as the differences of displacement at each section. The system is solved starting from the section at one of the boundaries once the displacements of each section are known then these values are used as initial condition for the next step. In the second method, time  $t$  is considered as an independent variable at various sections along the spindle-workpiece system. The latter method is preferred because in many vibration problems often the displacement-time relationships are needed. However, to solve equation (2.1), the fourth

derivative of  $W(x,t)$  as a function of  $x$  should exist. Secondly, if the second method is used, then the various sections need to be located at equal spacing. If the spacing between the sections are not equal then this approach becomes computationally tedious.

### 2.7.2 The Finite Element Method

In classical continuum mechanics a problem is usually described by a set of differential equations with appropriate boundary conditions or by the extremum of a variational principle, if it exists, or by some form of variational statement (incomplete variational principle).

The solution sought for such continuum problems usually possesses high order differentiability, satisfies the differential equation everywhere, and satisfies all the boundary conditions exactly. This situation is different in finite element approach. The solutions are defined exclusively in terms of a finite number of degrees-of-freedom and are only piecewise-smooth functions. The differentiability of these functions is usually lower than the highest order of derivatives in the field equations. The advantage of the finite element method over the finite-difference methods is the relative ease with which the boundary conditions of the problem can be handled. An excellent discussion about this particular topic is given by Burden [52].

As an example, it was suggested earlier that the boundary condition at the workpiece-running center can be assumed as hinged or clamped. To test the boundary condition for the clamped condition, it is required that the deflection and the slope of the deflection curve of the spindle-workpiece should be zero. Since deflection and slope both are formulated as the coordinates in the finite element

analysis, this boundary condition is easily accommodated in the finite element model. In the finite difference method, the condition that the slope equal to zero requires that the displacement of a point spaced  $\Delta x$  (refer to Fig. 2.2) to the left of the running center support, also be zero. Secondly, even if the various element lengths are unequal, this is easily dealt with in the finite element model because the element length is explicitly represented in the element stiffness and inertia matrices. On the other hand, this condition imposes considerable difficulties in the finite difference technique.

In view of these reasons, finite element technique is preferable in dynamic analysis as the present case and therefore employed as the method for obtaining the dynamic response of the machine tool-spindle-workpiece system.

## 2.8 The Finite Element Model of the Spindle Workpiece System

### 2.8.1 Element Equation of Motion

The finite element model of a shaft in bending is shown in Fig. 2.4. In this figure  $w_1(t)$ ,  $w_2(t)$  are the joint translational and rotational coordinates respectively, whereas, the generalized forces along these coordinates are represented by  $f_1(t)$  and  $f_2(t)$ . Thus, a joint can undergo both translational and rotational displacements. Correspondingly, there are not only joint forces to consider, but also bending moments. Expressing the displacements at any point in the system as

$$w(x_1, t) = \sum_{i=1}^4 \phi_i(x_1) w_i(t) \quad (2.5)$$

where,  $\phi_i(x)$  is the shape function,  $x$  is local position coordinate, and  $w_i(t)$  is the joint displacement function. Assuming the

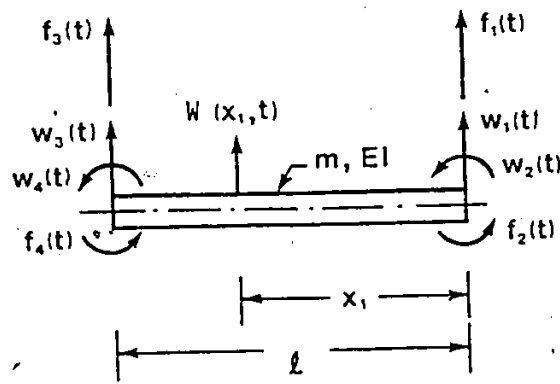


Fig. 2.4: Finite Element Model of One of the Elements of the System.

7

shape functions are given by the static displacement patterns, that is, the differential equation governing the static bending of a uniform bar with the inertia term set to zero, the generalized displacement at any point on the bar is expressed as [51]

$$W(x_1, t) = \left(1 - \frac{3x_1^2}{\ell^2} + \frac{2x_1^3}{\ell^3}\right) w_1(t) + \left(\frac{x_1}{\ell} - \frac{2x_1^2}{\ell^2} + \frac{x_1^3}{\ell^3}\right) \ell w_2(t) \\ + \left(\frac{3x_1^2}{\ell^2} - \frac{2x_1^3}{\ell^3}\right) w_3(t) - \left(\frac{x_1^2}{\ell^2} + \frac{x_1^3}{\ell^3}\right) \ell w_4(t) \quad (2.6)$$

where  $\ell$  is the length of an element. The equations of motion for the element can be derived by writing the expressions for the kinetic energy,

$$T^*(t) = \frac{1}{2} \int_0^{\ell} m \left[ \frac{\partial W(x_1, t)}{\partial t} \right]^2 dx_1 \quad (2.7a)$$

the potential energy,

$$V^*(t) = \frac{1}{2} \int_0^{\ell} EI \left[ \frac{\partial^2 W(x_1, t)}{\partial x^2} \right]^2 dx_1 \quad (2.7b)$$

and the virtual work

$$\delta W = \sum_{j=1}^4 f_j(t) \delta w_j(t) \quad (2.7c)$$

The details of the derivation of the equation of motion of an element are given in the Appendix A, and the expressions for the inertia and the stiffness matrix as obtained in Appendix A are:

$$[m] = \frac{m\ell}{420} \begin{bmatrix} 156 & 22\ell & 54 & -13\ell \\ 22\ell & 4\ell^2 & 13\ell & -3\ell^2 \\ 54 & 13\ell & 156 & -22\ell \\ -13\ell & -3\ell^2 & -22\ell & 4\ell^2 \end{bmatrix} \quad (2.8a)$$

and

$$[k] = \frac{EI}{\ell^3} \begin{bmatrix} 12 & 6\ell & -12 & 6\ell \\ 6\ell & 4\ell^2 & -6\ell & 2\ell^2 \\ -12 & -6\ell & 12 & -6\ell \\ 6\ell & 2\ell^2 & -6\ell & 4\ell^2 \end{bmatrix} \quad (2.8b)$$

The inertia and stiffness matrices for elements 7 and 11 (refer to Fig. 2.2), where the boundary conditions are different due to the presence of the bearings, are slightly different. For these elements the stiffness matrix is given by:

$$[k] = \frac{EI}{\ell^3} \begin{bmatrix} 12 + k_f & 6\ell & -12 & 6\ell \\ 6\ell & 4\ell^2 & -6\ell & 2\ell^2 \\ -12 & -6\ell & 12 + k_f & -6\ell \\ 6\ell & 2\ell^2 & -6\ell & 4\ell^2 \end{bmatrix} \quad (2.9)$$

where  $2k_f$  is the bearing stiffness at the element in consideration. In addition, a damping matrix will be present and is given by

$$[c] = \begin{bmatrix} c & 0 & 0 & 0 \\ 0 & 0 & 0 & 0 \\ 0 & 0 & c & 0 \\ 0 & 0 & 0 & 0 \end{bmatrix} \quad (2.10)$$

where  $2c$  is the damping value at the element in consideration.

### 2.8.2 The Equations of Motion for the Complete System

In the finite element method a continuous structure is regarded as an assemblage of individual discrete elements. By requiring that the displacement be compatible and the internal forces be in balance at the joints, the entire structure is compelled to act as one entity. The displacement components at the joints of any individual element are chosen in a direction which depends upon the nature of the element considered. For example, in the case of a slender bar, it is convenient to choose the displacement components of one end so that one of the components is in the axial direction and the other two in the orthogonal transverse direction. But the individual elements can have different orientation in space. This coordinate system is known as the local coordinate system.

These coordinates are related to the global coordinate system by a matrix of direction cosines, which plays a role of a transformation matrix. In general

$$\{w\} = [G] \{\bar{w}\} \quad (2.11)$$

where  $[G]$  is the transformation matrix relating the local displacement vector,  $\{w\}$  to the global displacement vector,  $\{\bar{w}\}$  respectively.

In the previous section, the equations of motion of an element was derived in terms of the local coordinate system. The remaining task is to extend these results to obtain the equation of motion of the complete structure.

Let a new set of displacements  $\bar{w}_j$  ( $j = 1, 2, \dots, N$ ) represent the

joint displacements of the complete structure in terms of components along the global system of coordinates. Then,  $\bar{w}_j$  ( $j=1, 2, \dots, N$ ) can be represented by a column matrix  $\{\bar{w}\}$ . Suppose, the structure consists of  $p$  elements, and denoting quantities pertaining to the  $s^{\text{th}}$  element by the subscript  $s$ , the relationship between the vectors  $\{\bar{w}\}$  and  $\{\bar{w}\}_s$  can be written as

$$\{\bar{w}\}_s = [H]_s \{\bar{w}\}, \quad s = 1, 2, \dots, p \quad (2.12)$$

where  $[H]_s$  is a rectangular transformation matrix. The matrix  $[H]_s$  has as many rows as  $\{\bar{w}\}_s$  and as many columns as  $\{\bar{w}\}$  has rows. The elements of every row of  $[H]_s$  are all zero, with the exception of one element in each row which is equal to unity. The position of the unit element in every row of  $[H]_s$  is such that equation (2.2) is an identity. It should be noted that a given joint displacement can occur in several of the vectors  $\{\bar{w}\}_s$ . In fact, it appears in those vectors sharing corresponding joints. Therefore, the elements of the matrix  $\{\bar{w}\}$  can be regarded as a set of generalized coordinates for the complete system.

Representing the kinetic energy of the complete structure by  $T^*$  and adding the contribution of each of the elements, one can write

$$T^* = \frac{1}{2} \sum_{s=1}^p \{\dot{\bar{w}}\}_s^T [\bar{m}]_s \{\dot{\bar{w}}\}_s \quad (2.13)$$

where  $[\bar{m}]_s$  is the inertia matrix of the element in terms of the global coordinates;

$$[\bar{m}]_s = [G]^T [m] [G] \quad (2.14)$$

Differentiation of equation (2.12) gives

$$\{\dot{\bar{w}}\}_s = [H]_s \{\dot{\bar{w}}\} \quad s = 1, 2, \dots, p \quad (2.15)$$



combining equations (2.15) and (2.13) one obtains

$$T^* = \frac{1}{2} \sum_{s=1}^p \{\dot{\bar{w}}\}^T [H]_s^T [m]_s [H]_s \{\dot{\bar{w}}\} \quad (2.16)$$

$$= \frac{1}{2} \{\dot{\bar{w}}\}^T [\bar{M}] \{\dot{\bar{w}}\} \quad (2.17)$$

where

$$[\bar{M}] = \sum_{s=1}^p [H]_s^T [m]_s [H]_s \quad (2.18)$$

represents the inertia matrix of the system.

The potential energy  $V$ , of the complete system can be obtained by adding the contributions from each of the element and mathematically it can be written as

$$V^* = \frac{1}{2} \sum_{s=1}^p \{\bar{w}\}^T [H]_s^T [k]_s [H]_s \{\bar{w}\} \quad (2.19)$$

$$= \frac{1}{2} \{\bar{w}\}^T [\bar{K}] \{\bar{w}\} \quad (2.20)$$

where,

$$[\bar{K}] = \sum_{s=1}^p [H]_s^T [k]_s [H]_s \quad (2.21)$$

is the stiffness matrix of the complete structure. Similarly  $[\bar{C}]$ , the damping matrix of the complete structure can be represented in the form

$$[\bar{C}] = \sum_{s=1}^p [H]_s^T [c]_s [H]_s \quad (2.22)$$

where,  $[c]_s$  is a matrix of damping coefficients associated with  $s^{\text{th}}$  discrete element in the global coordinates.

By using the formulation of virtual work, the vector of the joint

non-conservative forces for the complete structure, corresponding to the displacement vector  $\{\bar{W}\}$ , can be expressed as

$$\{\bar{F}\} = \sum_{s=1}^p [H]_s \{f\}_s \quad (2.23)$$

where  $\{f\}_s$  is a vector representing the forces interacting between elements associated with the  $s^{\text{th}}$  element in global coordinates.

Using the formulation of Lagrange's equations of motion in conjunction with the above set of equations, the matrix differential equation of the complete spindle-workpiece system is derived in the form

$$[\bar{M}] \{\ddot{W}\} + [\bar{C}] \{\dot{W}\} + [\bar{K}] \{W\} = \{\bar{F}\} \quad (2.24)$$

where  $[\bar{M}]$ ,  $[\bar{C}]$ , and  $[\bar{K}]$  are the global mass, damping and stiffness matrices respectively having a size of (26 x 26) obtained by assembling the elemental matrices.

### 2.8.3 The Boundary Conditions

Referring to Fig. 2.2, the boundary conditions at the running center have to be applied in order to remove the rigid body mode, and also to determine the nature of the workpiece connection at this end. If this connection is to be assumed as hinged then the first component of the displacement vector  $\{\bar{W}\}$  would vanish. Similarly, if the connection is assumed to be rigid then the first two components of the displacement vector  $\{\bar{W}\}$  would be zero. As a consequence of this, the size of the stiffness and the damping matrices would be 25 x 25 in the first case and 24 x 24 in the second case.

## 2.9 Conclusions

In this chapter, a lathe spindle-workpiece system supported by elastic bearings with damping and acted upon by random cutting forces is described and based on this an appropriate mathematical model of the system is formulated. A short review of the different methods of solution for the governing equations such as the finite difference method and the finite element method are presented. The finite element method is chosen as the better approach for obtaining a solution to the present study. Using the finite element analysis, the complete system is represented by a system of matrix differential equation of motion with stochastic excitation. The boundary conditions existing at the workpiece-running center are also explained. In the next chapter the free vibration behavior of the system will be presented, and an appropriate model of the workpiece-running center boundary will be established.

## CHAPTER 3

### THEORETICAL AND EXPERIMENTAL INVESTIGATION OF THE FREE VIBRATION OF THE SPINDLE-WORKPIECE SYSTEM

#### 3.1 Introduction

In Chapter 2, a lathe spindle-workpiece system was mathematically modelled and the equations of motion of the complete system were presented in the form of a matrix differential equation using a finite element formulation. It was also mentioned that the nature of the boundary condition at the running center is unknown and that it can be considered either as hinged or clamped support. In order to establish accurately the mathematical model of the system, the first step is to evaluate the nature of the end condition at the running center. This can be achieved only by carrying out an independent theoretical analysis of the spindle-workpiece system using hinged and clamped conditions respectively and comparing both the results with those obtained from an experimental investigation on a test model [53].

#### 3.2 Selection of the System Parameters

In order to carry out both theoretical and experimental investigations, the spindle of a 12 hp Demoor type lathe, Model No. 821A as shown previously in Fig. 2.2 was considered. A workpiece of material AISI 1020 steel with a diameter of 0.051m (2 in.) and a length of 0.302m (13 in.) was selected and held between the chuck and a running center. The variations in the mass and the stiffness along the spindle-workpiece system used in this investigation are shown in Figs. 3.1 and 3.2 respectively. It should be noted that in these two figures, both mass and stiffness of all sections have been normalized with respect to

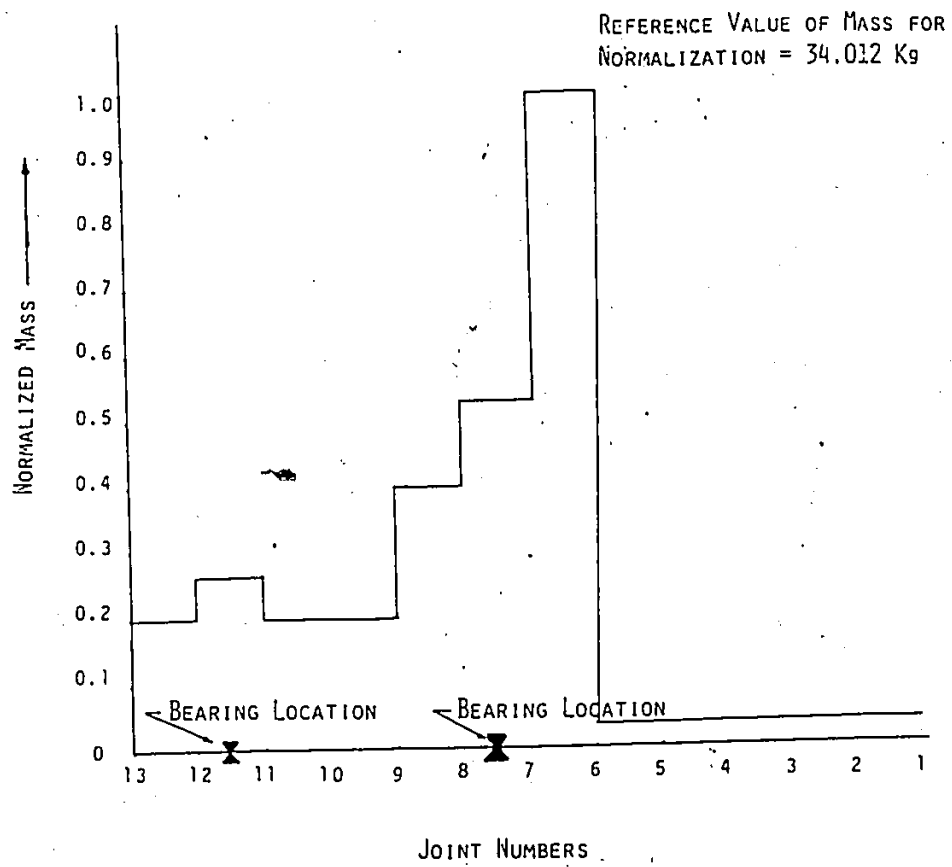


Fig. 3.1: The Variation of Mass Along the System.

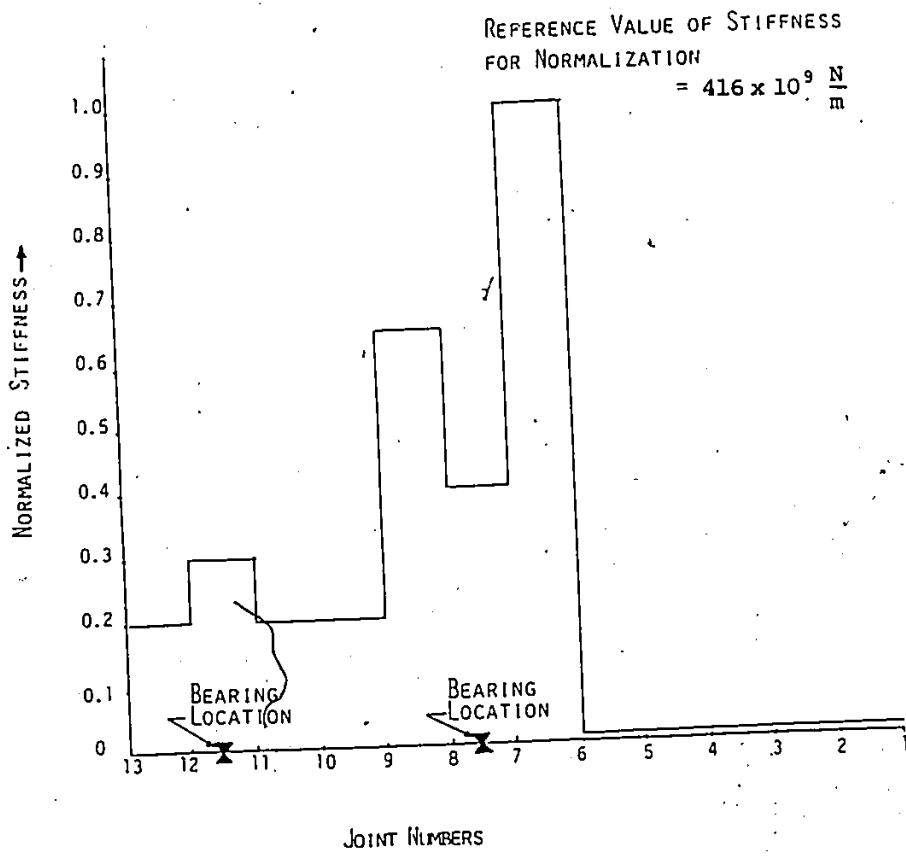


Fig. 3.2: The Variation of Stiffness Along the System.

the mass and the stiffness of the chuck. Also, the front bearing stiffness has been taken as 3.19 times the rear bearing stiffness. Other parameters used in this investigation are listed in Table 3.1.

### 3.3 The Experimental Investigation

#### 3.3.1 The Experimental Set-Up

In order to estimate the nature of the boundary conditions at the workpiece-running center interface, an experiment on a 12 hp Demoor type lathe was carried out. The object of this experiment was to estimate the natural frequencies of the spindle-workpiece system and compare these natural frequencies with the theoretically computed natural frequencies for both types of end conditions, that is, the hinged end condition, and the clamped end condition. This way an appropriate model to represent the system at the workpiece-running center interface can be established.

The experimentation was carried out by holding an AISI 1020 steel workpiece, 0.051m (2 in.) in diameter, and 0.302m (13 in.) in length, between the chuck and the running center. An electromagnetic shaker type B&K-4812 having a specification of maximum force of 445N (100 lb<sub>f</sub>) and a displacement limit of 0.013m (0.5 in.), was employed to provide a sinusoidal force excitation to the spindle-workpiece system, using a push rod. One end of the push rod was connected to the shaker, and the other end to the workpiece. A schematic diagram of the experimental set up is presented in Fig. 3.3 and the pictorial views of the set up are shown in Figs. 3.4 and 3.5.

An accelerometer, B&K model 8302, having sensitivity of 10 pc/g was mounted on the chuck. The output signal of the accelerometer was

TABLE 3.1

Parameter Values of Spindle-Workpiece System

| PARAMETERS                     | VALUES OF THE PARAMETERS   |
|--------------------------------|--|
| Modulus of Elasticity          | $206.456 \times 10^9 \text{ N/m}^2$<br>( $30 \times 10^6 \text{ lbs/inch}^2$ ) |
| Mass of the Chuck              | 34.012 kg (75 lbs)   |
| Diameter of the Chuck          | 0.254 m (10 inches)  |
| Stiffness of the Front Bearing | $1530.1 \times 10^6 \text{ N/m}$<br>( $8.74 \times 10^6 \text{ lbs/inch}$ )    |
| Stiffness of the Rear Bearing  | $479.84 \times 10^6 \text{ N/m}$<br>( $2.741 \times 10^6 \text{ lbs/inch}$ )   |



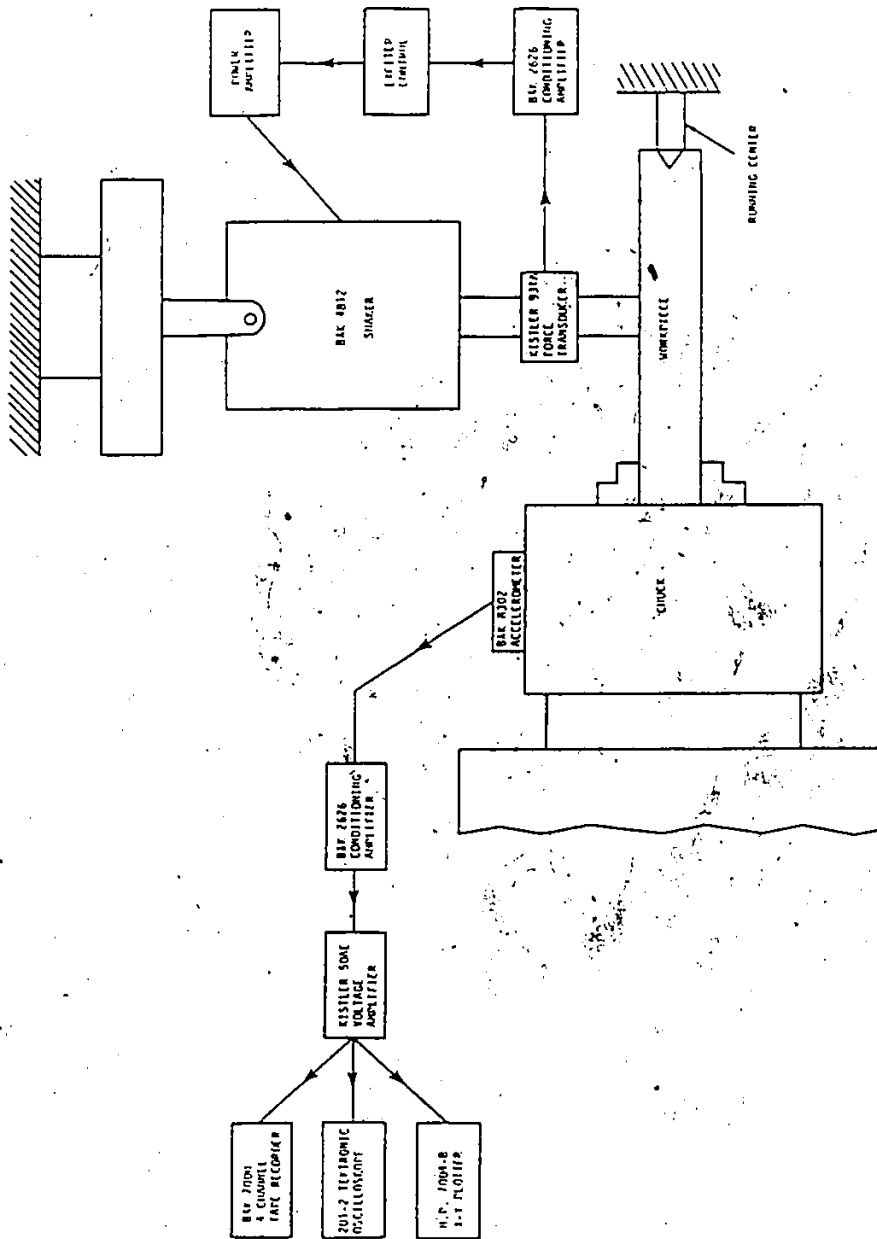


Fig. 3.3: A Schematic Diagram of the Experimental Set Up.

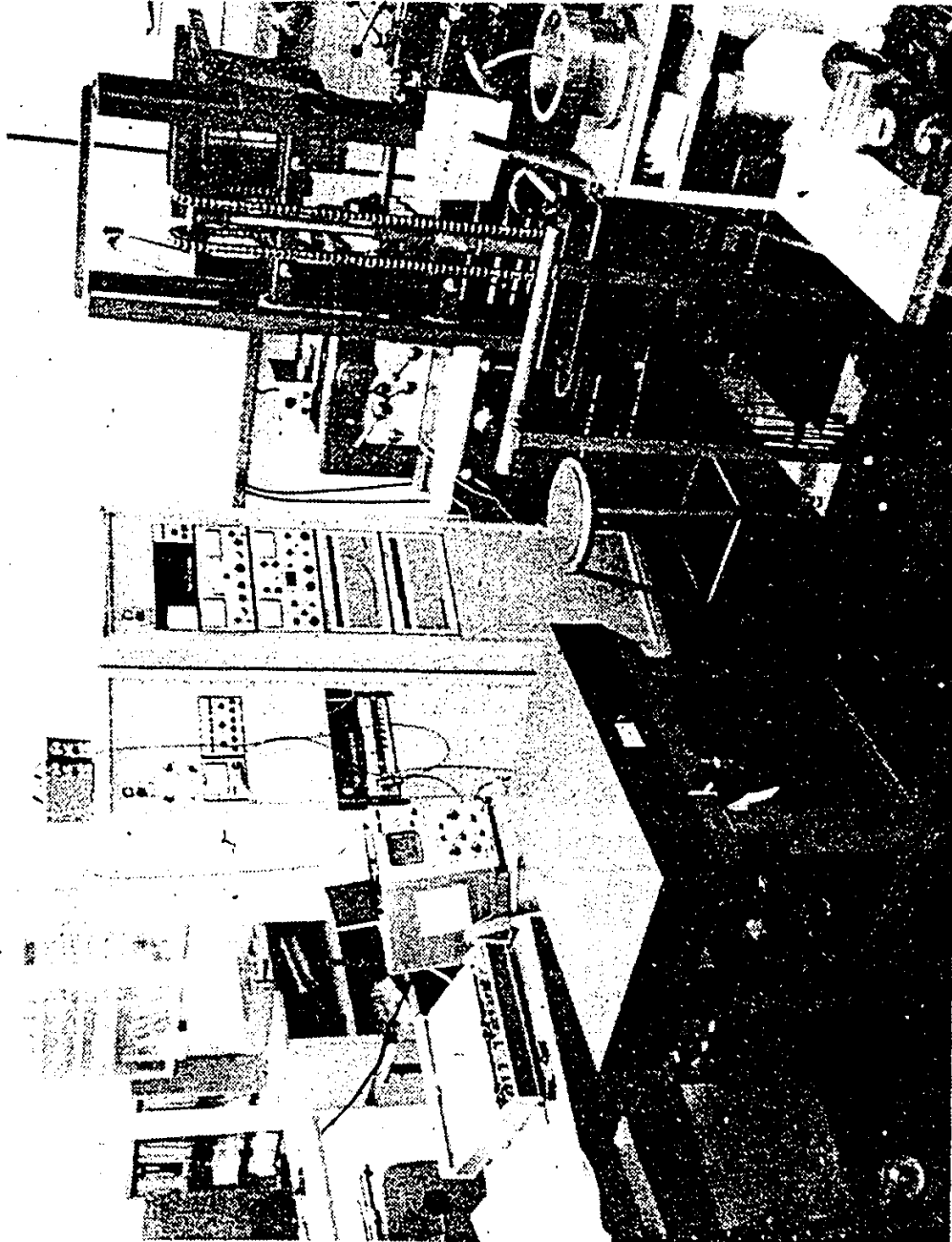


Fig. 3.4: A Pictorial View of the Instrumentation for the Frequency Analysis.

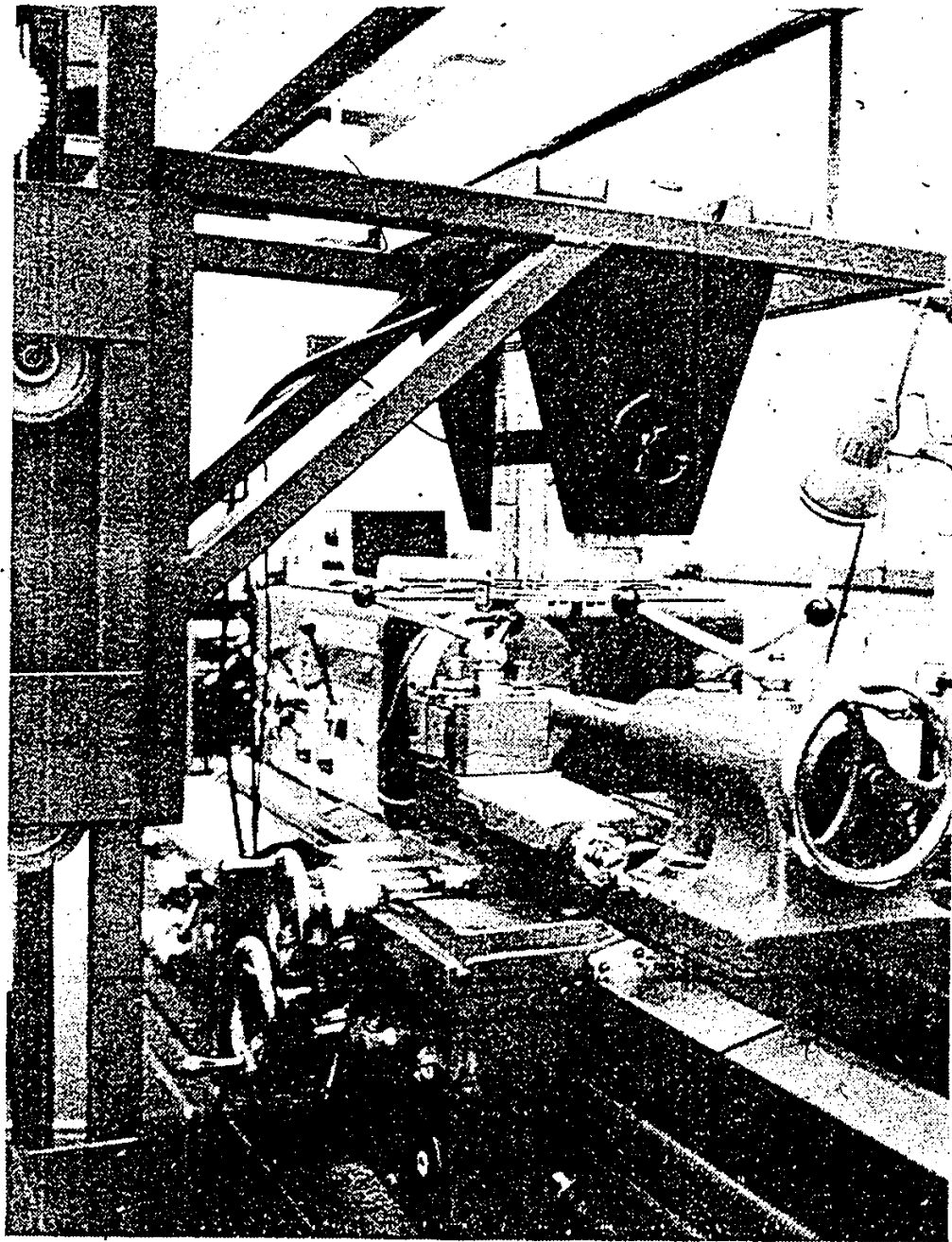


Fig. 3.5: The Pictorial View of the Shaker and Workpiece for Frequency Analysis.

conditioned using a B&K model 2626 charge amplifier, and then amplified by a Kistler 504E voltage amplifier. The amplified signal was plotted on a H.P. 7004-B x-y plotter, and at the same time it was recorded on B&K 7000, 4 channel tape recorder. An oscilloscope, Tektronix model 201-2 was used to observe the generated response signal which was being recorded. One end of the force transducer was screwed on to the push rod of the exciter and the other end was screwed on to the workpiece. The output signal from the force transducer was conditioned and fed to the shaker exciter control so as to maintain a constant excitation force. The exciter was statically loaded at first, and then the spindle-workpiece system was excited within the range of 25 Hz to 1500 Hz with a constant dynamic force of 44.5 N (10 lb<sub>f</sub>) and at a sweep rate of 1000 Hz/min.

### 3.3.2 Experimental Results

A typical experimental record of the acceleration versus frequency is shown in Fig. 3.6. The peaks in the output response were identified to be the natural frequencies of the spindle-workpiece system. In this figure, the output of the accelerometer below 25 Hz is not shown. This is due to the low frequency limitation of the electro-dynamic shaker. That is, to maintain the constant force, the exciter displacement was exceeding the designed displacement limit.

### 3.4 Results of the Analytical Investigation

For the free vibration analysis of the spindle-workpiece system, the homogeneous part of the equation (2.1) was solved numerically on a CDC Cyber 174 digital computer using the properties given in the previous section. The undamped natural frequencies and the matrix of the eigen-

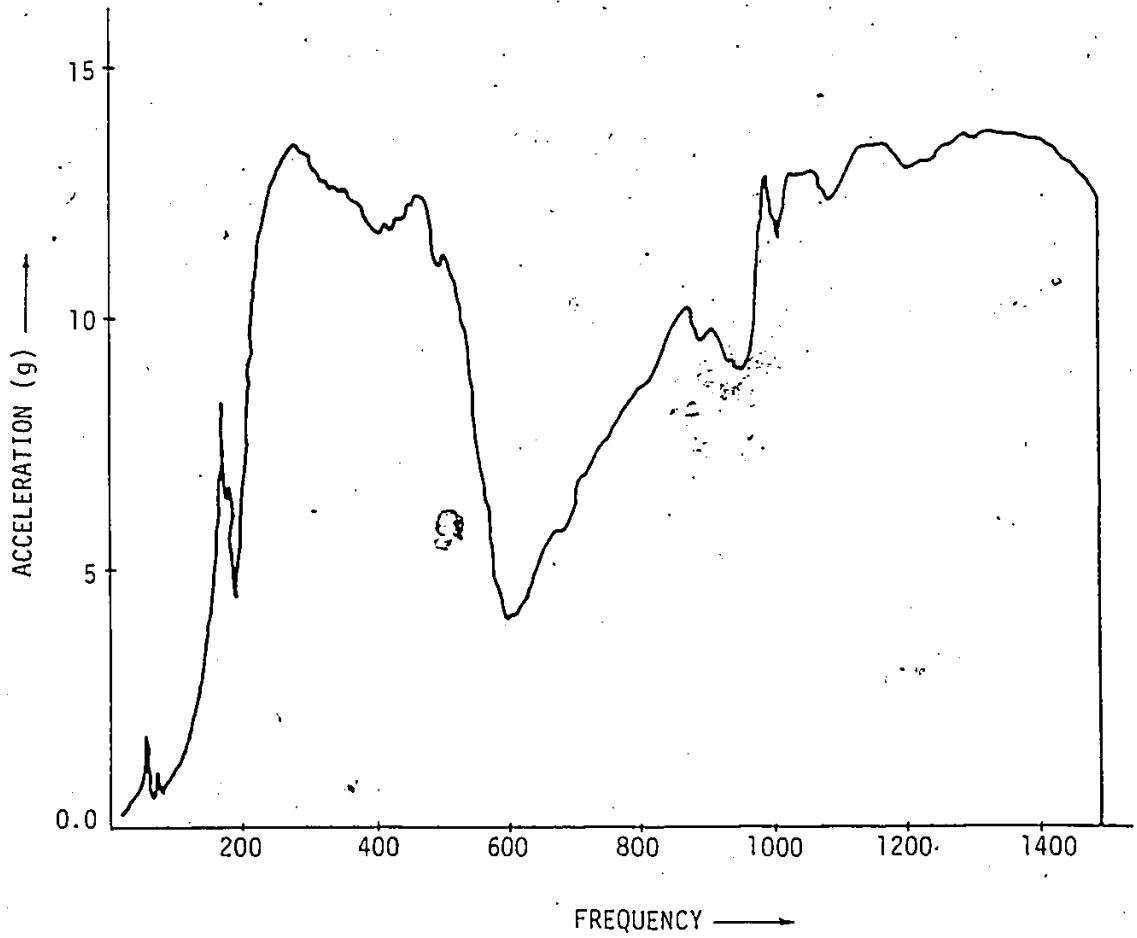


Fig. 3.6: Acceleration Response Versus Frequency.

vectors [53] were obtained. Table 3.2 shows the analytically obtained undamped natural frequencies for both hinged and clamped end conditions at the running center, along with the experimentally obtained natural frequencies. These results are also plotted as shown in Fig. 3.7.

### 3.5 Comparison and Discussion of the Theoretical and the Experimental Results

The experimentally obtained natural frequencies as well as the theoretically computed natural frequencies are shown in Table 3.2 and Fig. 3.7. It can be seen that, the theoretically computed values of the natural frequencies lie in close proximity of the experimentally obtained values. Based on a comparison of the percentage error in the first five natural frequencies, the hinged end condition for the workpiece has an error of less than 8% in comparison to the clamped end condition which exhibits a maximum error of 20%. Considering the twelve theoretically calculated natural frequencies, the computation of the root sum squared (RSS) error for hinged and clamped conditions also show that the hinged condition has an error of 3.3% less than the clamped condition.

Based on these comparative analyses mentioned above, one can conclude that the hinged support at the running center for a spindle-workpiece system, is a better representation of the actual system and is considered in the mathematical model in all further computations.

### 3.6 The Effect of the Variation of the Bearing Stiffness on the Free Vibration Behavior of the System

After the identification of the proper end condition at the workpiece-running center connection, the homogeneous part of the equation (2.10) was solved for several values of the front bearing

TABLE 3.2  
Undamped Natural Frequencies of the System

| Frequency Number | Finite-Element Analysis |                     | Experimental Hz | % Error = $\frac{(F.E. Analysis - Exp) \times 100}{Exp}$ |                 |
|------------------|-------------------------|---------------------|-----------------|--|-----------------|
|                  | Hinged Support, Hz      | Clamped Support, Hz |                 | Hinged Support   | Clamped Support |
| 1                | 20                      | 28                  | —               | —  | —               |
| 2                | 30                      | 31                  | —               | —  | —               |
| 3                | 55                      | 72                  | 58              | 5.2  | 17.2            |
| 4                | 83                      | 91                  | 77              | 7.8  | 15.4            |
| 5                | 178                     | 210                 | 175             | 1.7  | 20.0            |
| 6                | 234                     | 246                 | 275             | 14.9   | 10.5            |
| 7                | 377                     | 424                 | 425             | 11.2   | 0.23            |
| 8                | 455                     | 471                 | 465             | 2.1  | 1.3             |
| 9                | 659                     | 726                 | 545             | 20.9   | 33.2            |
| 10               | 772                     | 780                 | 985             | 21.6   | 20.8            |
| 11               | 1082                    | 1150                | 1075            | 0.3  | 7.0             |
| 12               | 1178                    | 1352                | 1295            | 9.03   | 3.3             |

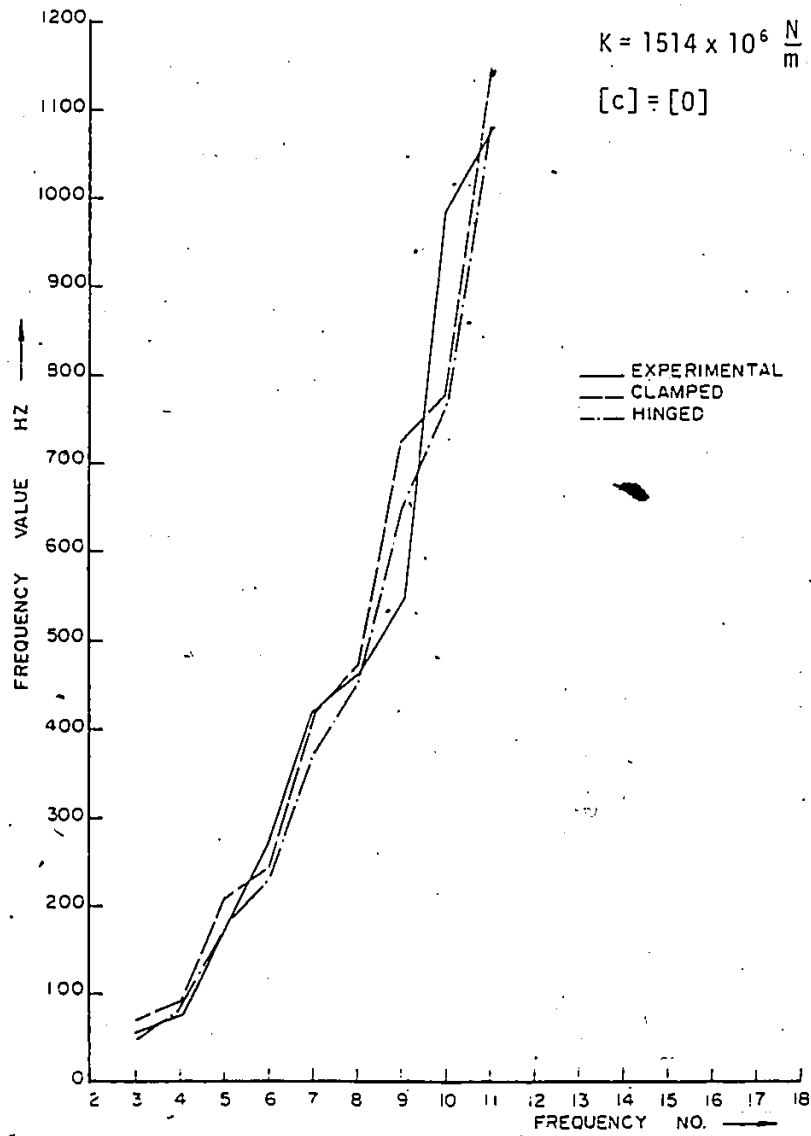


Fig. 3.7: Hinged, Clamped and Experimental Frequencies Versus Frequency Number.



stiffness. These variations ranged from, the existing design value which is represented by  $K$  in Figs. 3.8 through 3.13, to eight times this value. In all of these computations, the ratio of the front bearing stiffness and the rear bearing stiffness was held constant and equal to 3.19.

The free vibration behavior of this system is due to the interaction between the inertia forces, the spring forces, and the flexural rigidity of the system. In other words, the deflection of any point along the spindle-workpiece system depends upon the above mentioned factors. The effect of the variation of the stiffness of the bearings on the natural frequencies and the mode shapes is discussed in the next section.

### 3.6.1 Effect of Variation in Bearing Stiffness

In order to study the influence of bearing stiffness on the free vibration of the spindle-workpiece system, the finite element analysis was repeated considering the variations in the front end bearing stiffness but keeping the stiffness ratio of the two bearings a constant. The variation of the natural frequencies as a function of the bearing stiffness is shown in Fig. 3.8. The results indicate that the first natural frequency increases rapidly at first, that is, when the bearing stiffness is in the range of  $K$  to  $4K$ , but there is very little increase in its value for bearing stiffness values between  $4K$  and  $8K$ . It may be seen that the second, the third, and the fourth natural frequencies show very large increase, if the bearing stiffness is varied between  $K$  and  $8K$ . The effect of bearing stiffness variation on the fifth natural frequency as shown in this figure, clearly indicates that there is a very little

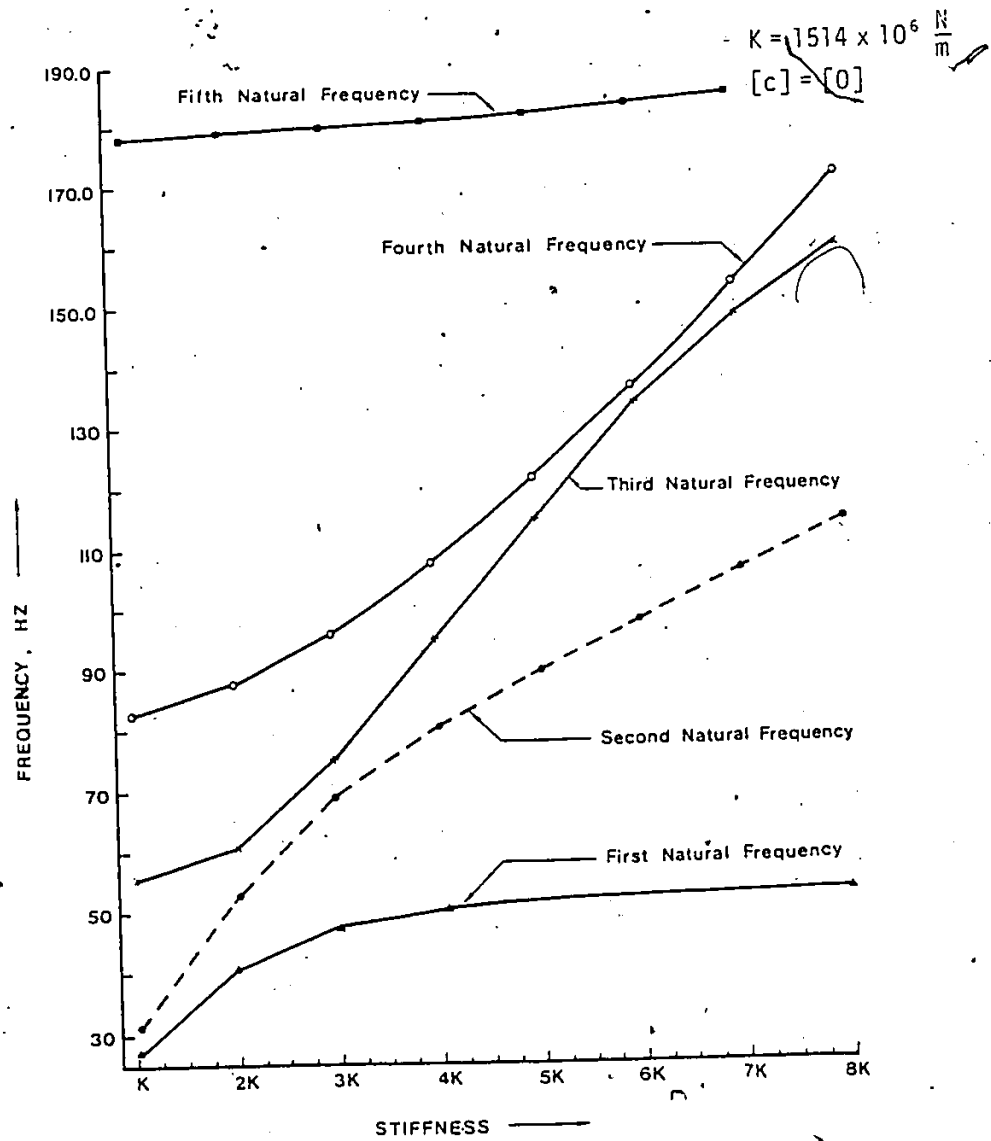


Fig. 3.8: The First Five Natural Frequencies Versus Front Bearing Stiffness.

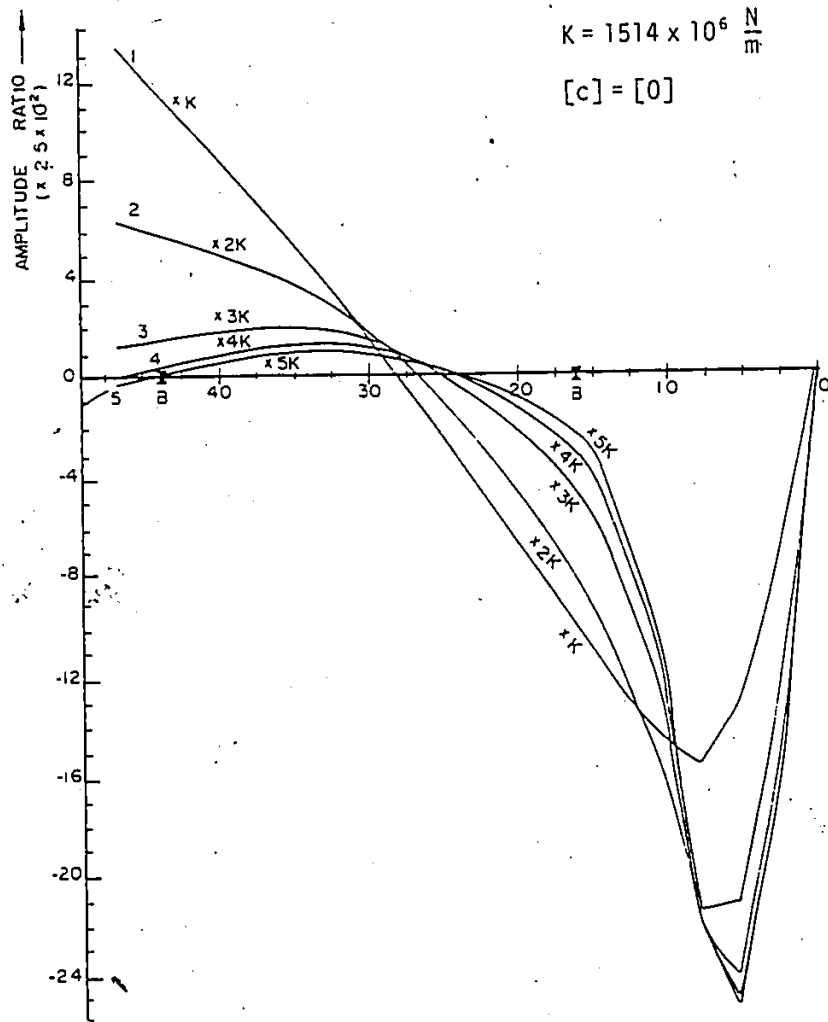


Fig. 3.9: The First Undamped Mode Shape Versus Front Bearing Stiffness.

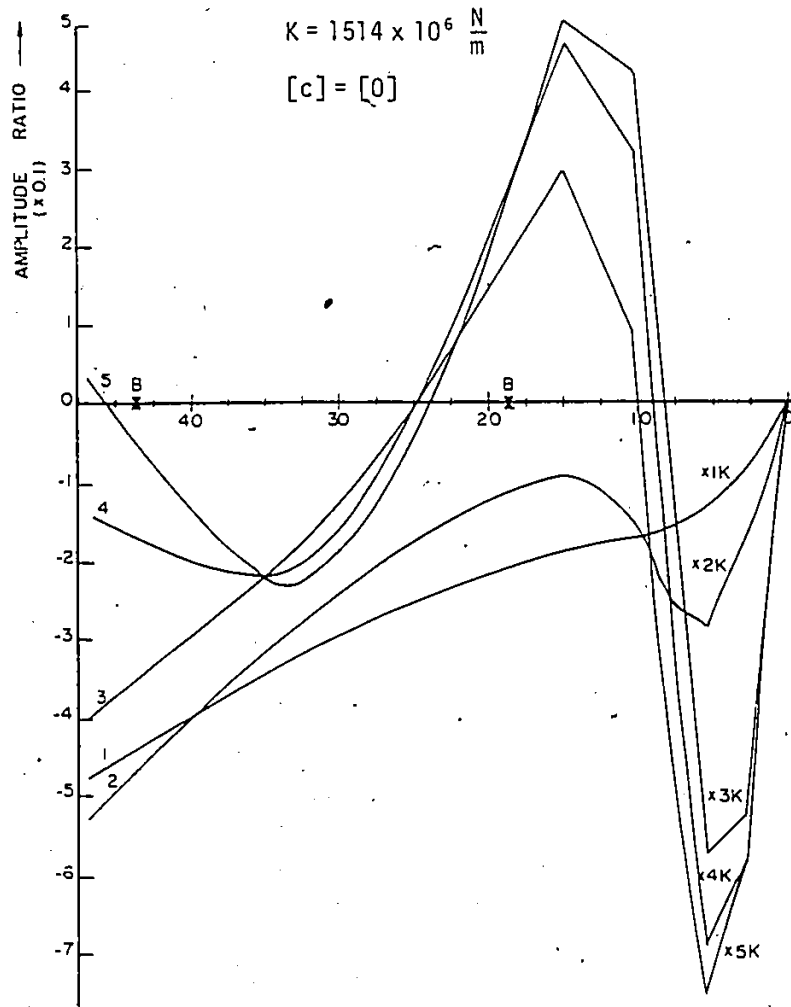


Fig. 3.10: The Second Undamped Mode Shape Versus Front Bearing Stiffness.

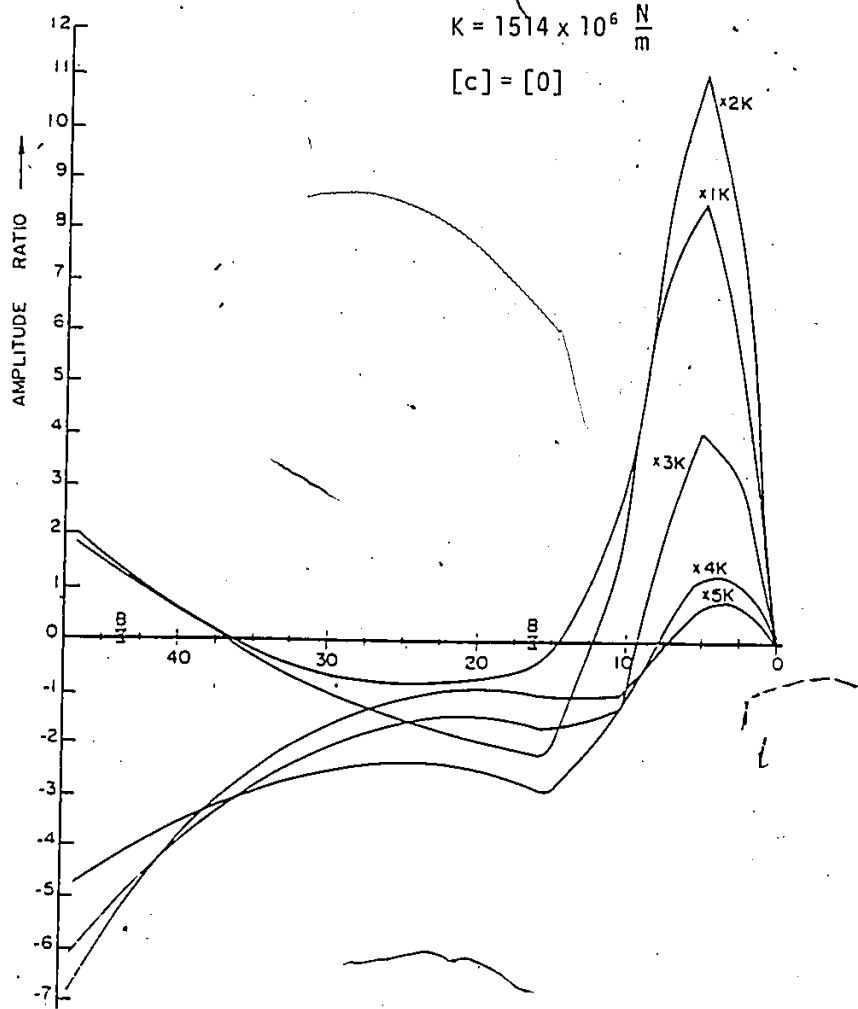


Fig. 3.11: The Third Undamped Mode Shape Versus Front Bearing Stiffness.

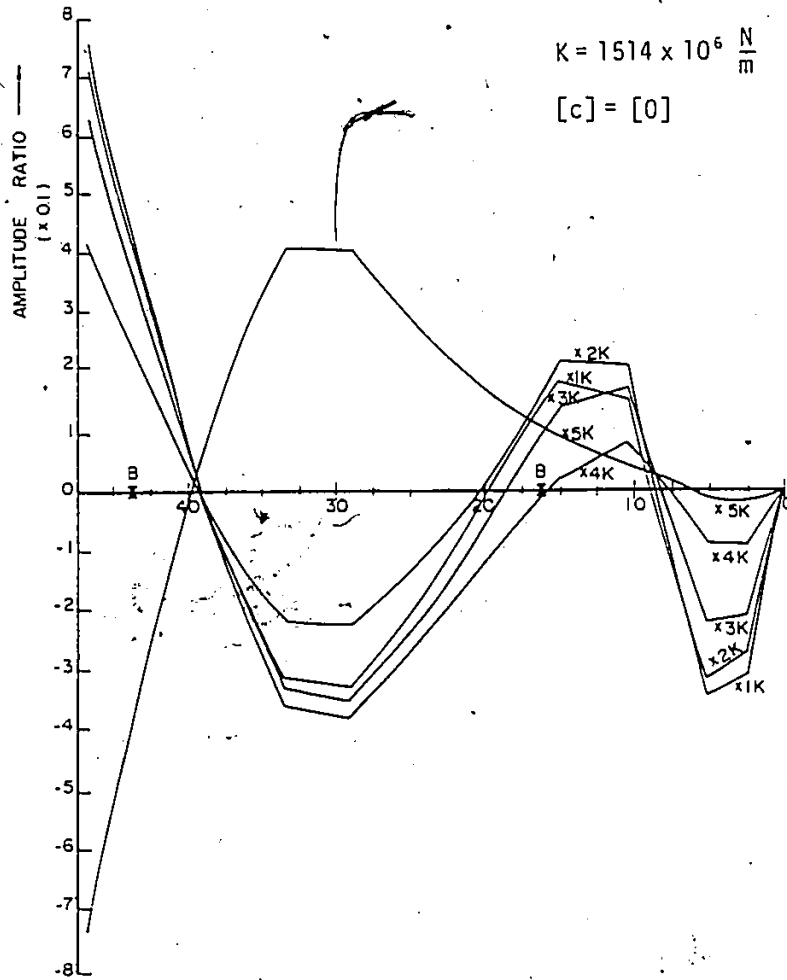


Fig. 3.12: The Fourth Undamped Mode Shape Versus Front Bearing Stiffness.

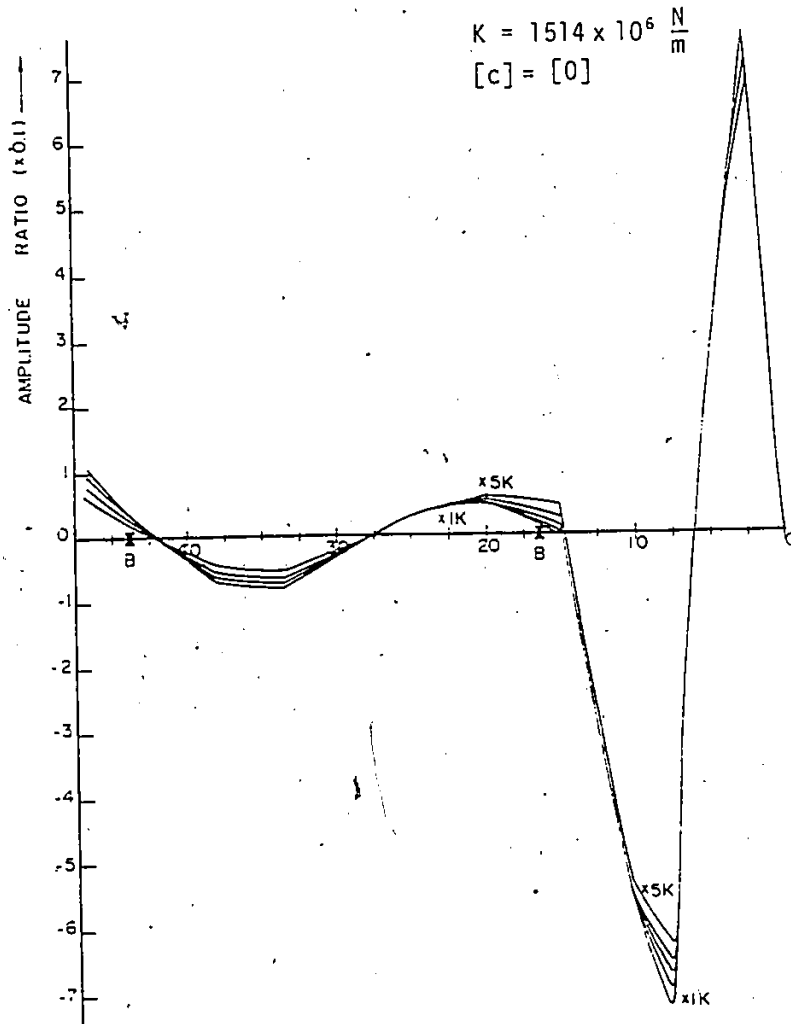


Fig. 3.13: The Fifth Undamped Mode Shape Versus Front Bearing Stiffness.

increase in its value.

The effects of varying the bearing stiffness on the undamped mode shapes of the system are shown in Figs. 3.9 to 3.13. Figure 3.9 presents the variation of the first mode shape with respect to the variation of the front bearing stiffness. In the first mode, for low values of the bearing stiffness, there is a considerable variation in the deflection along the workpiece due to its slenderness and at the same time the deflection curve of the spindle is linear owing to its high flexural rigidity. However, as the bearing stiffness is increased, the deflection at the bearing location decreases, and as a consequence, there is a significant curvature in the deflection curve of the spindle. These results are due to the fact that the natural frequency increases as the bearing stiffness increases. Also, in the first mode, due to the large inertia forces of the chuck, the deflection of the front bearing is larger as compared to the rear bearing even though the front bearing stiffness is 3.19 times greater than the rear bearing stiffness. Referring to the first mode, it can also be seen that increasing the stiffness of the bearings increases the deflection in the workpiece and has little variation in the mode shape for large stiffness values. Based on these results, it should be noted that the selection of bearing stiffness based simply on the first mode alone is not sufficient.

Figures 3.10, 3.11 and 3.12 show that the second, the third and the fourth mode shapes undergo considerable changes as the bearing stiffness is increased. This can be explained by referring to Fig. 3.8, where the corresponding natural frequencies undergo large variation as the bearing stiffness is increased. As a consequence, there would be large variation in the inertia forces. Since the system has irregular



distribution of the stiffness along its length, the interacting forces result in the complicated mode shapes which are quite sensitive to any change in the bearing stiffness.

It can be seen that for the second, the third and the fourth mode as the front bearing stiffness increases, the maximum deflection of the workpiece increases initially and then decreases with the minimum of the maxima occurring in the fourth mode. Comparing the deflection at the bearing locations, the amplitude increases and then decreases in the third and in the fourth bearing location while for the second mode, the deflection increases initially and then decreases.

The fifth mode, as shown in Fig. 3.13, is almost insensitive to changes in the bearing stiffness. This is due to the fact that the fifth and the higher natural frequencies change very little, due to increase in the bearing stiffness in the given range. As a consequence of this, the inertia forces do not change, therefore the corresponding modes are not affected.

### 3.7 Conclusions

In order to identify the proper end condition at the running-center, estimates of the undamped natural frequencies were made from the experimental acceleration response versus frequency curve. In this experiment, the spindle-workpiece system was acted upon by a force of constant amplitude but variable frequency between the range of 25 Hz to 2500 Hz, and the acceleration response signal was plotted on a x-y plotter. The experimentally obtained natural frequencies were compared with the theoretically computed natural frequencies, and using minimum root sum squared error criterion, it was inferred that the hinged end

condition is a better representation of the actual behavior of the system. After arriving at a suitable model of the spindle-workpiece system, the effect of the variation of the bearing stiffness on the natural frequencies and the mode shapes were studied.

In summary, the following conclusions are drawn:

- 1) The end condition of the workpiece supported by the running center can be better represented by a hinged condition rather than a clamped condition.
- 2) The first natural frequency increases rapidly if the bearing stiffness increases between  $K$  and  $4K$  but the increase is very little for higher than this range of stiffness values.
- 3) There is considerable increase in the values of the second, the ~~third~~ and the fourth natural frequencies if the bearing stiffness is increased from  $K$  to  $8K$ .
- 4) There is very little increase in the fifth natural frequency values corresponding to the changes in the bearing stiffness values.

## CHAPTER 4

### DYNAMIC RESPONSE OF A LATHE SPINDLE-WORKPIECE SYSTEM UNDER RANDOM CUTTING FORCES

#### 4.1 Introduction

The workpiece experiences vibratory motions during any turning operation because of the dynamic action of the cutting forces. The dimensional accuracy and the surface finish of a machined workpiece is influenced considerably by the vibratory response of the spindle-workpiece system under the direct action of the cutting forces. During the actual machining process, the cutting forces are essentially a random process and such a random phenomenon, as stated earlier, has been observed clearly in many experimental investigations such as those by Bickel [18] and Field [19]. Hence it is essential to carry out a complete dynamic analysis of the spindle-workpiece system under the actual stochastic force excitation so that results or conclusions can be drawn and can be applied to the design of the spindle to achieve a better performance including a better surface finish of the machined workpiece.

For an analytical investigation of the dynamic response of the spindle-workpiece system, the matrix differential equations formulated in chapter 2 have to be solved with the random cutting forces as the forcing function. For this purpose, the main cutting force fluctuations along the z direction was actually measured in the laboratory using a piezoelectric dynamometer and used as an excitation input to the matrix differential equation of motion of the system. In this chapter, the experimental procedure for the cutting force measurement, calculation of the Power Spectral Density (PSD), descriptions of the cutting force

variations, and the procedure for the computation of the mean square response of the workpiece are outlined.

Since the cutting tool continually moves along the workpiece during machining, the excitation and hence the response of the workpiece are to be characterized as a non-stationary random process. In any general dynamic problem dealing with non-stationary random processes, analytically determining the response of the system is highly complex and sometimes not possible without introducing certain approximations compared to a corresponding case of stationary random processes, only. In the present case of the spindle-workpiece system, the dynamic response under the random cutting forces can be evaluated in a simpler manner if the cutting forces are approximated by a stationary random process if the workpiece response at the cutting tool contact can be assumed to have negligible influence on the variation of the tool feed rate. In order to justify this approach, an independent analysis on the dynamic response of the given system in turning under the action of spatially moving random metal cutting forces, resulting in a non-stationary type of random cutting forces, is carried out [54] and presented in the following section.

#### 4.2 Workpiece Response Under Spatially Moving Random Cutting Forces

The system under consideration is the chuck-workpiece-running center system as shown in Fig. 4.1. The workpiece is supported by the heavy chuck on one end and the running center at the tailstock end. The cutting tool is fed from right to left at a constant feed rate. Usually this feed rate is much higher for a finish turning than for a

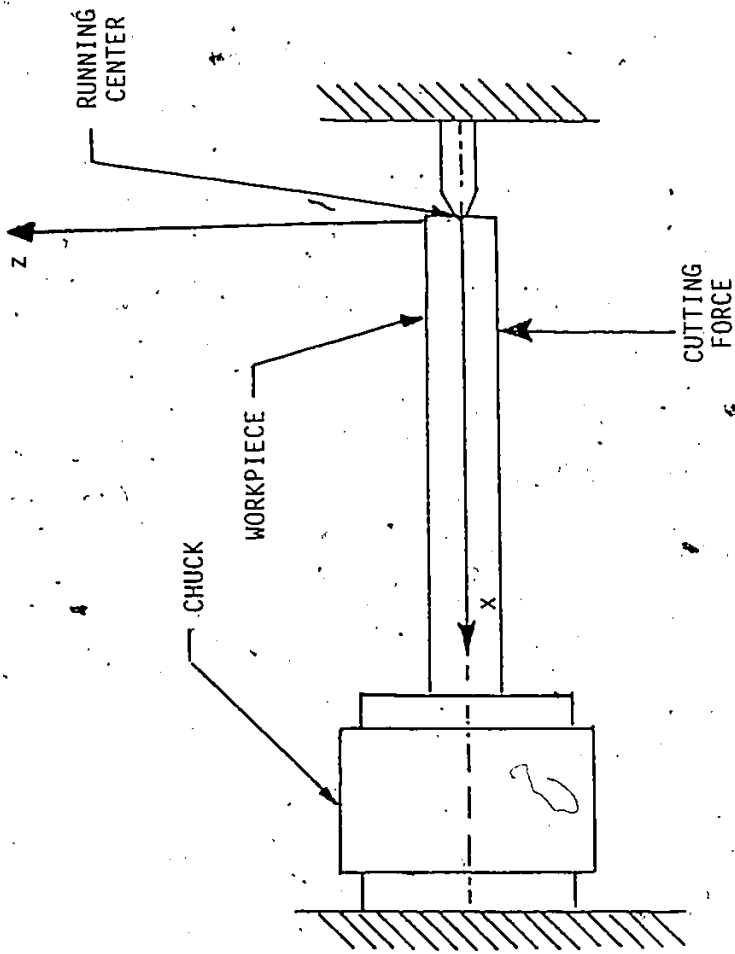


Fig. 4.1: The Representation of a Chuck-Workpiece-Running Center System.

roughing operation. Since the cutting tool continuously travels along the workpiece, the excitation on the workpiece is essentially a non-stationary random process.

The effect of random moving loads on the dynamic response of a beam, using the correlation method, has been studied earlier by Fryba [55]. A similar method has also been used to tackle the problem of vibration of bridges caused by random loads generated by the moving vehicles [56]. In these investigations [55,56], the response at a particular location, such as at the mid-point of the bridge, was of particular interest. In the present problem of workpiece vibrations involving moving random cutting forces, the response at the instantaneous location of the moving tool is of primary concern, since the workpiece surface roughness directly depends on the workpiece dynamic response taking place at the particular cutting tool location, especially in finish machining.

It has been shown earlier [41], that the finish machining forces are basically broad band in nature and therefore, for mathematical simplification, they can be approximated by a white noise process. Also, an equivalent viscous damping is assumed in this analysis for the workpiece, to account for the structural damping in the workpiece material. The mathematical model for the system then is a Bernoulli-Euler beam with the chuck end taken as fixed and the end at the running center considered hinged. The mathematical representation and the stochastic analysis for the response are presented in the following sections.

#### 4.2.1 The Mathematical Model and Analysis

Representing the workpiece as a Bernoulli-Euler beam, the equation of motion is given by [57]

$$EI \frac{\partial^2 W(x,t)}{\partial x^4} + 2m(x)\beta \frac{\partial W(x,t)}{\partial t} + m(x) \frac{\partial^2 W(x,t)}{\partial t^2} = f(x,t) \quad (4.1)$$

where

$W(x,t)$  is the transverse deflection of the beam

$EI$  is the constant flexural rigidity

$\beta$  is the equivalent viscous damping

$m(x)$  is the mass per unit length of beam

and

$f(x,t)$  represents the random forces exerted by the cutting tool on the workpiece

The natural frequencies and the normal modes of the beam are obtained by solving for the undamped free vibration of the system and are given by the solution of

$$EI \frac{\partial^4 W(x,t)}{\partial x^4} + m(x) \frac{\partial^2 W(x,t)}{\partial t^2} = 0 \quad (4.2)$$

with appropriate boundary conditions. Assuming a harmonic solution, of the form  $W(x,t) = \phi(x) \exp(i\omega t)$ , the equation of motion (4.2) reduces to the characteristic equation

$$(\omega_m^2 - \omega^2) \phi_m(x) = 0 \quad \text{with } m = 1, 2, 3, \dots, \infty \quad (4.3)$$

where  $\omega_m$  are the natural frequencies and  $\phi_m(x)$  are the normal modes of the beam [57].

The transverse deflection  $W(x,t)$  and the excitation  $f(x,t)$  may be examined in terms of the normal modes  $\phi_m(x)$  as

$$W(x,t) = \sum_{m=1}^{\infty} \phi_m(x) q_m(t) \quad (4.4)$$

and

$$f(x,t) = \sum_{m=1}^{\infty} m(x) \phi_m(x) Q_m(t) \quad (4.5)$$

where  $q_m(t)$  are a set of generalized modal coordinates and  $Q_m(t)$  are generalized modal forces. Substitution of equations (4.4) and (4.5) into equation (4.1) yields

$$\frac{d^2 q_m(t)}{dt^2} + 2\beta \frac{dq_m(t)}{dt} + \omega_m^2 q_m(t) = Q_m(t) \quad (4.6)$$

The generalized forces  $Q_m(t)$  are obtained by multiplying both sides of the equation (4.5) by  $\phi_m(x)$  and integrating along the length  $l$  of the work-piece. Using the orthogonality principle for the normal modes, the following equations can be written:

$$Q_m(t) = \begin{cases} \frac{1}{M_m} \int_0^l f(x,t) \phi_m(x) dx & t > 0 \\ 0 & t < 0 \end{cases} \quad (4.7)$$

The generalized mass  $M_m$  of the beam, appearing in equation (4.7) is defined by

$$M_m = \int_0^l m(x) \phi_m^2(x) dx \quad (4.8)$$

The response of the system in the time domain can be obtained by considering the unit impulse response function which for the  $m$ -th mode of the system is given by [57]



$$h_m(t) = \frac{1}{\omega_m'} \exp(-\beta t) \sin \omega_m' t \quad t \geq 0$$

$$= 0 \quad t < 0$$
(4.9)

where  $\omega_m'$  is the  $m^{\text{th}}$  damped natural frequency and is

$$\omega_m'^2 = \omega_m^2 - \beta^2$$
(4.10)

Then the solution of equation (4.6) is expressed in the form

$$q_m(t) = \int_0^t h_m(t-\tau) Q_m(\tau) d\tau$$

$$= \int_0^t h_m(\tau) Q_m(t-\tau) d\tau$$

$$= \int_{-\infty}^{\infty} h_m(\tau) Q_m(t-\tau) d\tau$$
(4.11)

If the forces are purely deterministic, the response is directly obtained by combining equations (4.4), (4.9), and (4.11).

#### 4.2.2 Response Under Non-Stationary Random Cutting Forces

Expressing the non-stationary cutting forces  $f(x,t)$  in terms of a mean value  $\bar{F}(x,t)$  and a centered random value  $f'(x,t)$ , one can write

$$f(x,t) = \bar{F}(x,t) + f'(x,t)$$
(4.12)

The response of the workpiece to such a non-stationary force will also be a non-stationary process and similarly it can also be expressed in the form

$$W(x,t) = \bar{W}(x,t) + W'(x,t) \quad (4.13)$$

Therefore, by analogy,  $\bar{W}$  will be the response due to  $\bar{F}$  and  $W'$  will be the response corresponding to the component  $f'$ .

Once the functional form of the mean value of the excitation,  $\bar{F}(x,t)$ , is known, the response  $\bar{W}$  of the system can be obtained by (4.4) through (4.11) since  $\bar{F}(x,t)$  is deterministic. An approximate expression for the mean value of the response is given later for a particular form of the mean cutting force that is considered.

The covariance  $C_{f',f'}$  of the random component  $f'(x,t)$  of the excitation, can be expressed as [58]

$$C_{f',f'}(x_1, x_2, t_1, t_2) = E [f'(x_1, t_1) f'(x_2, t_2)] \quad (4.14)$$

where,  $E[ ]$  denotes ensemble averaging. Combining equations (4.7) and (4.14), the covariance function for the generalized force  $Q_m'$  is obtained as

$$C_{Q_m', Q_n'}(t_1, t_2) = \frac{1}{M_m M_n} \int_0^{\ell} \int_0^{\ell} \phi_m(x_1) \cdot \phi_n(x_2) C_f(x_1, x_2, t_1, t_2) \cdot dx_1 dx_2 \quad (4.15)$$

Representing the generalized displacements in the  $m$ -th mode due to the centered random excitation  $f'(x,t)$  as  $q_m'(t)$ , the covariance of the generalized deflection is written as

$$C_{q_m', q_n'}(t_1, t_2) = E [q_m'(t_1) q_n'(t_2)] \quad (4.16)$$

Substituting for  $q_m'(t_1)$  and  $q_n'(t_2)$  from equation (4.11) into equation (4.16) and reversing the order of integration and then averaging,

$$C_{q'_m q'_n} = \int_0^t \int_0^t h_m(t_1 - \tau_1) h_n(t_2 - \tau_2) C_{Q_m Q_n}(\tau_1, \tau_2) d\tau_1 d\tau_2 \quad (4.17)$$

Using equations (4.4) and (4.17), the covariance of the displacement can be written as

$$C_{W'W'}(x_1, x_2, t_1, t_2) = \sum_{m=1}^{\infty} \sum_{n=1}^{\infty} \phi_m(x_1) \phi_n(x_2) C_{q'_m q'_n}(t_1, t_2) \quad (4.18)$$

The centered mean square value or the variance of the deflection is obtained from equation (4.18) as

$$\sigma_{W'}^2(x, t) = C_{W'W'}(x, x, t, t) = \sum_{m=1}^{\infty} \sum_{n=1}^{\infty} \phi_m(x) \phi_n(x) C_{q'_m q'_n}(t, t) \quad (4.19)$$

It has been shown [59] that in the equation

$$\sum_{m=1}^{\infty} \phi_m^2(x) C_{q'_m q'_m}(t, t) \gg \sum_{m=1}^{\infty} \sum_{n=1, n \neq m}^{\infty} \phi_m(x) \phi_n(x) C_{q'_m q'_n}(t, t) \quad (4.20)$$

Therefore, the variance of the displacement can be written as

$$\sigma_{W'}^2(x, t) = \sum_{m=1}^{\infty} \phi_m^2(x) C_{q'_m q'_m}(t, t) \quad (4.21)$$

#### 4.2.3 Characterization of the Moving Cutting Force

The metal cutting forces vary randomly in time and in addition they move along the workpiece with a constant tool velocity  $v$ . Therefore, it can be described through the form,

$$f(x, t) = \delta(x - vt) [\bar{F}' + f'(t)] \quad (4.22)$$

where  $\delta(\ )$  defines the Dirac delta function and  $\bar{F}$  is the mean value of the cutting force which is moving at a constant rate  $v$  along the workpiece. The response of the workpiece due to the mean force  $\bar{F}$  can be written using the procedures given in [ 56 ], and Tables [60].

Further, covariance of the centered random excitation  $f'(x,t)$  is expressed by

$$C_{f',f'}(x_1, x_2, t_1, t_2) = \delta(x_1 - vt_1) \delta(x_2 - vt_2) C_{f',f'}(t_1, t_2) \quad (4.23)$$

As mentioned earlier, since the random part of the cutting force is essentially a wide band process, it is considered, in this chapter as a white noise process having a constant power spectral density,  $S_f$ , throughout the frequency region. Accordingly, the covariance of the cutting force is

$$C_{f',f'}(t_1, t_2) = S_f \delta(t_2 - t_1) \quad (4.24)$$

#### 4.2.4 The Mean and the Variance Response of the Workpiece at the Tool Location

The mean displacement response of the workpiece at the point of contact is obtained by combining equation (4.4) through (4.11) and (4.22) as,

$$\bar{w}(x,t) = \bar{F} \sum_{m=1}^{\infty} \frac{\phi_m(x)}{M_m \omega_m'} \int_0^t \exp[-\beta(t-\tau)] \phi_m(v\tau) \sin \omega_m'(t-\tau) d\tau \quad (4.25)$$

The response at the tool location is then expressed as

$$\bar{w}(z) = \bar{F} \sum_{m=1}^{\infty} \frac{\phi_m(z)}{M_m \omega_m'} \frac{z}{v} \int_0^z \exp[-\beta \frac{z}{v}(z-x_1)] \phi_m(x_1) \sin \omega_m' \frac{z}{v}(z-x) dx_1 \quad (4.26)$$

where  $z = \frac{vt}{l}$  and  $x_1 = \frac{vt}{l}$ .

The mean displacement is then normalized by dividing it by the midspan displacement  $W_0$  of the workpiece defined under the force  $\bar{F}$  when applied at the same location. Therefore, the expression for the normalized displacement may be written as

$$\frac{\bar{W}(z)}{W_0} = \frac{192}{7\lambda_1^4} \frac{\pi^2}{\alpha^2} \sum_{m=1}^{\infty} \frac{\phi_m(z)}{a_m} I_m \quad (4.27)$$

where  $\phi_m(z)$  is the mode shape function for hinged-fixed beam and is given by

$$\phi_m(z) = (1 - \theta_m) \sinh z + (1 + \theta_m) \sin z \quad (4.28)$$

with

$$\theta_m = (\sinh \lambda_m + \sin \lambda_m) / (\sinh \lambda_m - \sin \lambda_m) \quad (4.29)$$

and

$$I_m = (1 - \theta_m) I_{m_1} + (1 + \theta_m) I_{m_2} \quad (4.30)$$

$$\text{where } I_{m_1} = \frac{a \exp(bz) - \exp(-kz) \{a \cos az + (k+b) \sin az\}}{(k+b)^2 + a^2}$$

$$+ \frac{\exp(-kz) \{a \cos az + (k-b) \sin az\} - a \exp(-bz)}{(k-b)^2 + a^2}$$

$$I_{m_2} = \frac{k \cos bz + (b+a) \sin bz - \exp(-bz) \{k \cos az - (b+a) \sin az\}}{(b+a)^2 + k^2}$$

$$- \frac{k \cos bz + (b-a) \sin bz - \exp(-kz) \{k \cos az + (b-a) \sin az\}}{(b-a)^2 + k^2}$$

Further,

$$W_0 = \frac{7 \bar{F} l^3}{768 EI}$$

$$b_m = \lambda_m, \quad \alpha = \pi v / \omega_1 l,$$

$$\zeta = \beta / \omega_1, \quad \eta_m = \omega_m / \omega_1,$$

$$k = \pi \zeta / \alpha, \quad a_m = \pi (\eta_m^2 - \zeta^2)^{1/2} / \alpha,$$

In the expressions for  $I_{m_1}$  and  $I_{m_2}$ , the subscripts for  $b$ ,  $a$ , and  $\eta$  are dropped for the sake of convenience. When the feed rate  $v$  is zero, the mean load applied by the tool is just a static load. Therefore, it is meaningful to compare equation (4.27) when  $v$  is zero with the expression for deflection of a beam having the same boundary conditions as that of the workpiece, at the point of application of a static load, which is given by [61]

$$\frac{\bar{W}_{st}(z)}{W_0} = \frac{64}{7} z^2 (1-z)^3 (3+z) \quad (4.31)$$

The variance response of the workpiece at any location is obtained by combining the equations (4.15), (4.17), (4.21), and (4.24) and can be written as

$$\sigma_{W'}^2(x, t) = \sum_{m=1}^{\infty} \frac{S_f \phi_m^2(x)}{M_m^2} \int_0^t \int_0^t h_m(t-\tau_1) h_m(t-\tau_2) \cdot \phi_m(c\tau_1) \phi_m(c\tau_2) \cdot \delta(\tau_2 - \tau_1) d\tau_1 d\tau_2 \quad (4.32)$$

Defining the new variables  $x_1$  and  $x_2$  by the relations  $x_1 = v\tau_1/l$ , and  $x_2 = v\tau_2/l$  respectively, the equation (4.24) is rewritten as

$$C_{f'f'} \left( \frac{\ell x_1}{v}, \frac{\ell x_2}{v} \right) = \frac{v}{\ell} S_f \delta(x_2 - x_1) \quad (4.33)$$

Substituting equations (4.9) and (4.33) into (4.32), the variance of the displacement at the tool location can be expressed as

$$\sigma_{W'}^2(z) = S_f \sum_{m=1}^{\infty} \left[ \frac{\phi_m(z)}{M_m \omega_m'} \right]^2 \frac{\ell}{v} \int_0^z \exp \left[ -\left[ \frac{2\beta \ell}{v} (z - x_1) \right] \right. \\ \left. \sin^2 \left[ \omega_m' \frac{\ell}{v} (z - x_1) \right] \phi_m^2(x_1) dx_1 \right] \quad (4.34)$$

The normalized variance of the deflection at the tool location is given by

$$\frac{\sigma_{W'}^2(z)}{W_0} = C_f^2 \bar{W}^2(z) \quad (4.35)$$

where

$$C_f^2 = S_f \frac{\omega_1}{F^2} \quad (4.36)$$

$$\text{and } \bar{W}^2(z) = \left( \frac{384}{7} \right)^2 \frac{\pi^2}{\alpha^3 \lambda_1^8} \sum_{m=1}^{\infty} \frac{\phi_m^2(z)}{a_m^2} \cdot J_m \quad (4.37)$$

Here,

$$J_m = \frac{(1 - \theta_m')^2}{16} J_{m_1} + \frac{(1 + \theta_m')^2}{16} J_{m_2} - \frac{(1 - \theta_m')^2}{4} J_{m_3} \quad (4.38)$$

with

$$J_{m_1} = \exp(2bz) \left\{ \frac{1}{k+b} - \frac{(k+b)}{(k+b)^2 + a^2} \right\} + \exp(-2bz) \left\{ \frac{1}{k-b} - \frac{(k-b)}{(k-b)^2 + a^2} \right\} \\ - \left\{ \frac{2}{k} - \frac{2k}{k^2 + a^2} \right\} + \exp(-2kz) \left\{ \frac{(k+b) \cos 2az - a \sin 2az}{(k+b)^2 + a^2} \right. \\ \left. + \frac{(k-b) \cos 2az - a \sin 2az}{(k-b)^2 + a^2} - \frac{2(k \cos az - a \sin az)}{k^2 + a^2} - \frac{2b^2}{k(k^2 - b^2)} \right\}$$

$$J_{m_2} = \frac{k \cos 2bz + (b-a) \sin 2bz}{(b-a)^2 + k^2} + \frac{k \cos 2bz + (b+a) \sin 2bz}{(b+a)^2 + k^2}$$

$$- \frac{2(k \cos 2bz + b \sin 2bz)}{k^2 + b^2} + \frac{2a^2}{k(k^2 + a^2)}$$

$$- \exp(-2kz) \left\{ \frac{k \cos 2az + (b-a) \sin 2az}{(b-a)^2 + k^2} + \frac{k \cos 2az - (b-a) \sin 2az}{(b+a)^2 + k^2} \right.$$

$$\left. - \frac{2 \{k \cos 2az - a \sin 2az\}}{k^2 + a^2} + \frac{2b}{k(k^2 + b^2)} \right\}$$

$$J_{m_3} = \frac{\exp(bz) \{(2k+b) \sin bz + (2a-b) \cos bz\}}{(2k+b)^2 + (2a-b)^2}$$

$$+ \frac{\exp(bz) \{(2k-b) \sin bz - (2a+b) \cos bz\}}{(2k-b)^2 + (2a+b)^2}$$

$$- \frac{\exp(-bz) \{(2k-b) \sin bz + (2a-b) \cos bz\}}{(2k-b)^2 + (2a-b)^2}$$

$$- \frac{\exp(-bz) \{(2k-b) \sin bz - (2a+b) \cos bz\}}{(2k-b)^2 + (2a+b)^2}$$

$$+ \frac{2\exp(bz) \{b \cos bz - (2k+b) \sin bz\}}{(2k+b)^2 + b^2}$$

$$+ \frac{2\exp(-bz) \{(2k-b) \sin bz - b \cos bz\}}{(2k-b)^2 + b^2}$$



$$\begin{aligned}
 & - \exp(-2kz) \left[ \frac{(2k+b) \sin 2az + (2a-b) \cos 2az}{(2k+b)^2 + (2a-b)^2} \right. \\
 & - \left\{ \frac{(2a+b) \cos 2az + (2k+b) \sin 2az}{(2k+b)^2 + (2a+b)^2} \right\} \\
 & - \left\{ \frac{(2a-b) \cos 2az + (2k-b) \sin 2az}{(2k-b)^2 + (2a-b)^2} \right\} \\
 & + \frac{(2k-b) \sin 2az + (2a+b) \cos 2az}{(2k-b)^2 + (2a+b)^2} \\
 & \left. + \frac{2b}{(2k+b)^2 + b^2} - \frac{2b}{(2k-b)^2 + b^2} \right]
 \end{aligned}$$

When the feed rate  $v$  is zero, equation (4.37) corresponds to the response of the workpiece to a non-moving random load. Comparing this case with the response of a beam having the same end conditions as that of the workpiece, at the point of application of a non-moving stationary random load, which can be obtained much more simply, is relevant at this point. The expression for the response of such a beam to random load is given by [58]

$$\bar{W}_{st}^2(z) = \left(\frac{192}{7}\right)^2 \frac{1}{\lambda_1^8 \xi} \sum_{m=1}^{\infty} \frac{\phi_m^4(z)}{\eta_m^2} \quad (4.39)$$

#### 4.2.5 Results and Discussion

Numerical computations were carried out for the mean and the variance of the workpiece deflections. The mean value was calculated using expressions (4.27) and (4.31) and the variance was calculated using expressions (4.37) and (4.39) derived earlier. All of the

response calculations were carried out at the tool contact, and the results are illustrated in Figs. 4.2 and 4.3. In evaluating the responses, commonly employed tool speeds in the range of  $\alpha = 2 \times 10^{-5}$  to  $1 \times 10^{-4}$  was considered. These correspond to  $v = 0.36 \text{ mm/s}$  to  $1.8 \text{ mm/s}$  for a typical workpiece of 30 cm in length and having a fundamental natural frequency of 30 Hz. The first five modes are considered in the computations. The mean deflection of the workpiece at the tool contact was evaluated from equation (4.27) and its plot for different contact points along the workpiece, is given in Fig. 4.2. The computed response was essentially the same for different feed rates and different damping ratios. This clearly indicates that the feed rate and the damping do not influence the mean displacement response of the workpiece. Further, this suggests that the complicated analysis followed in arriving at equation (4.27) can be replaced with a simpler form, without including the parameters describing the effect of feed rate and damping. Such analysis would lead to the expression given in equation (4.31), which considers the response only due to a static load at the point of application. Therefore, equation (4.31) was also evaluated at each point along the workpiece and when compared, these points coincided closely on the curve obtained from equation (4.27), in which effects of feed rates and damping were included.

The variance of the displacement of the workpiece at the tool contact is evaluated from equation (4.37) and is plotted for different contact locations along the workpiece in Fig. 4.3. It is to be noted that for the feed rates considered here, it is possible to conclude that the feed rate does not have any significant influence in the variance of the displacement response.

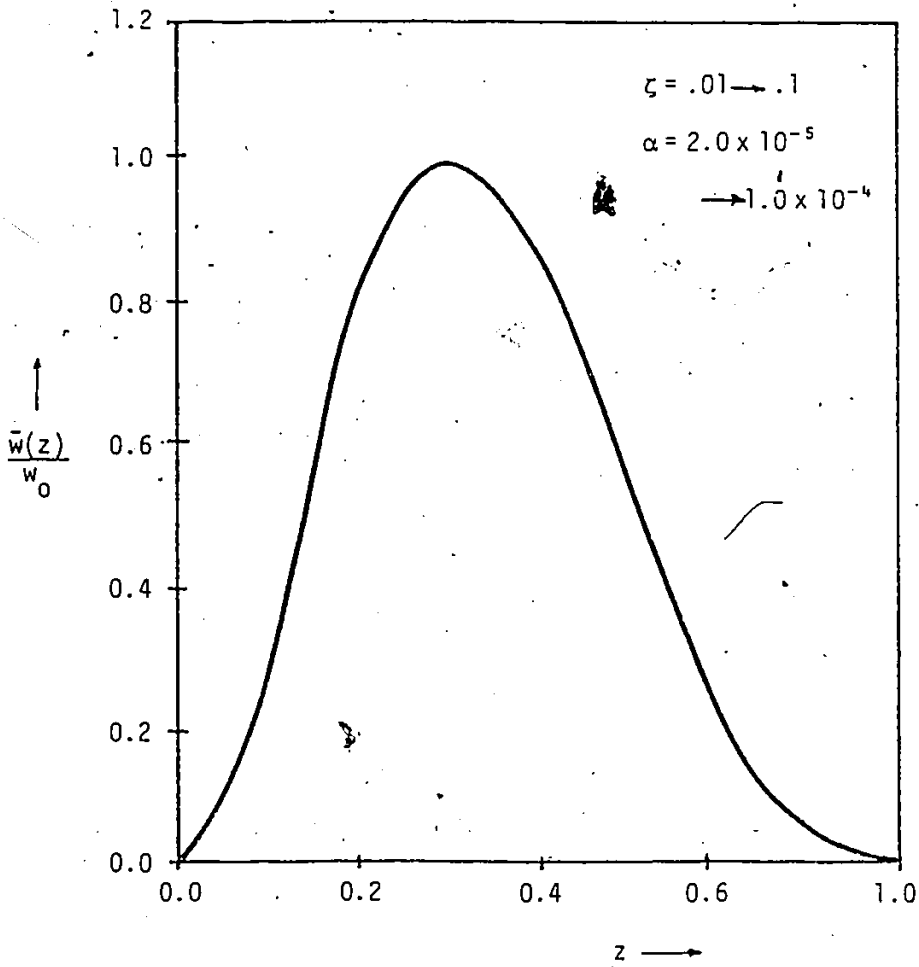


Fig. 4.2: Normalized Mean Displacement Response of the Workpiece Versus Tool Location.

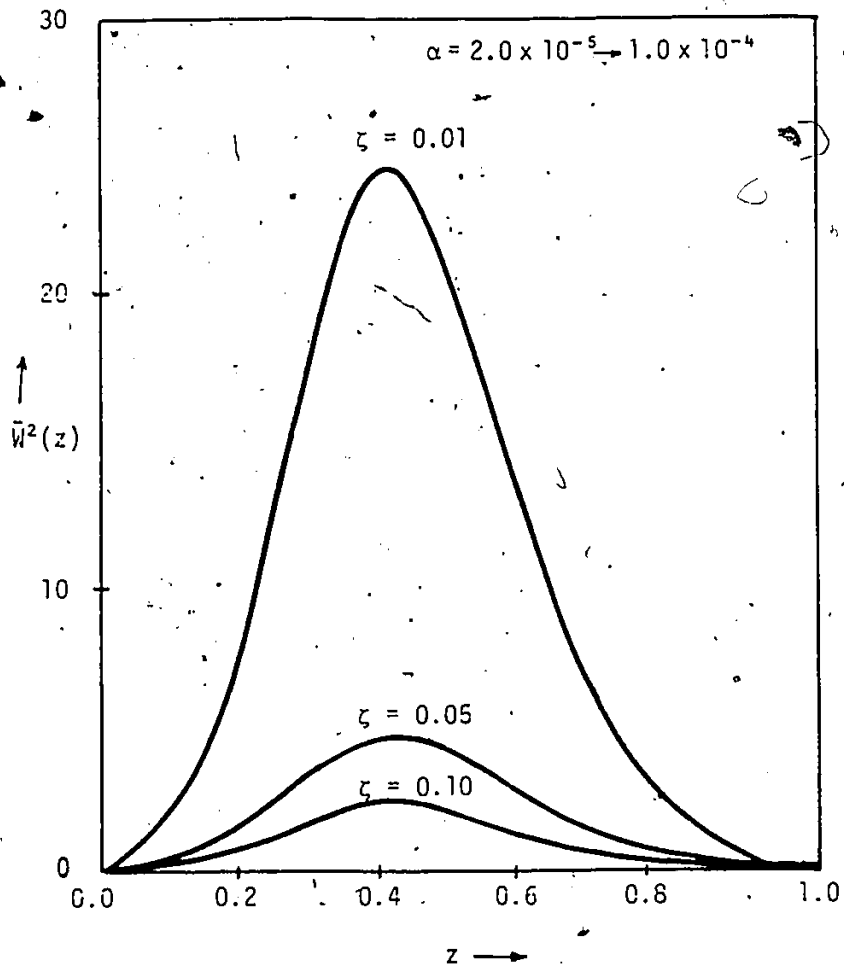


Fig. 4.3: Normalized Mean Displacement Response of Workpiece Against Tool Location.

In view of the above, it is possible to evaluate the variance of the displacement response by using a simpler expression such as the one shown in equation (4.39). In this equation, the values of the variance of the response at different points along the workpiece may be evaluated by substituting the corresponding values of  $z$ , as shown in Fig. 4.3. The effect of damping on the variance of the displacement response is also shown in Fig. 4.3 and as to be expected, increased value of damping reduces the variance response.

The above results indicate that for the range of feed rates normally used in finish turning operations, it is not necessary to consider the effect of feed rate in obtaining the mean and variance responses at the tool contact point. This is because the feed rates are very low compared to the flexural vibrational velocities in the workpiece material and so the transients die down sufficiently fast and hence do not influence the response at the succeeding tool locations as machining progresses. This result is very useful because much simpler expressions which do not consider the effect of the tool feed rate can be employed with success to compute the probabilistic responses of the workpiece.

#### 4.3 Spindle-Workpiece System Response Under Random Cutting Forces

As a first step in the investigation of dynamic response of the spindle-workpiece system, is to conduct actual tests to measure and record the metal cutting forces. The instrumentation set up organized for obtaining such information on the random cutting forces is shown in Fig. 4.4. The cutting forces were measured while a 0.051m (2 in) diameter,

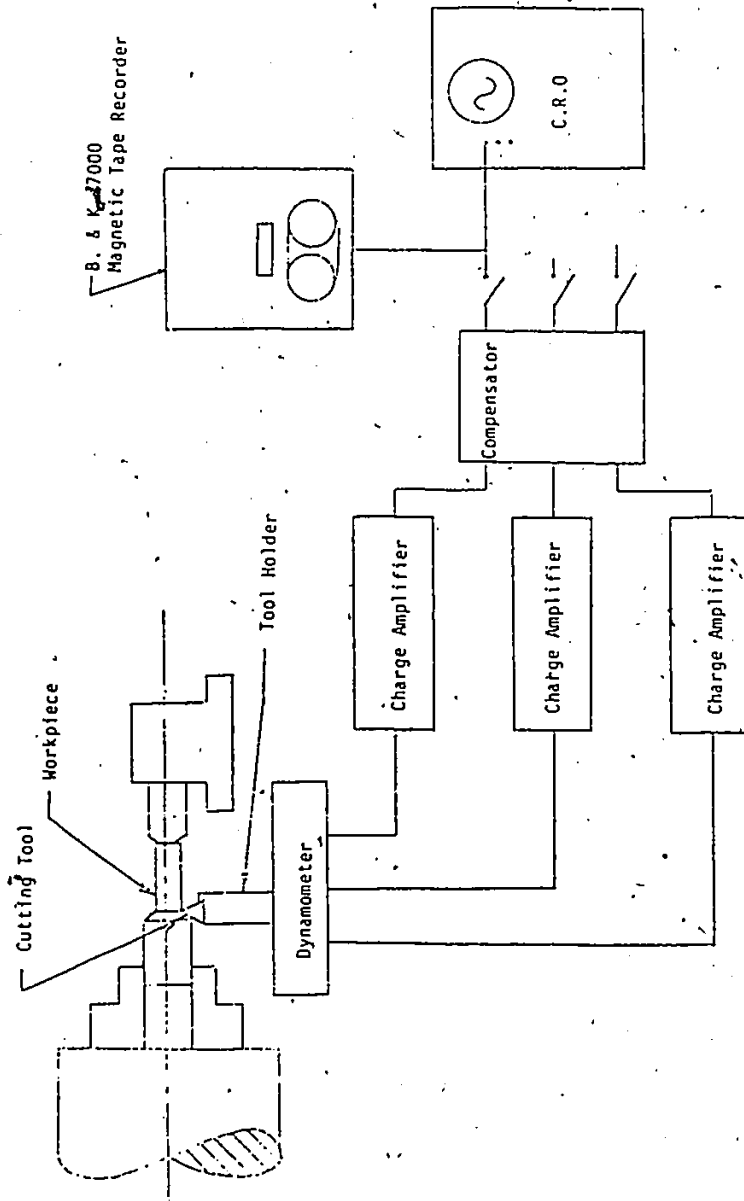
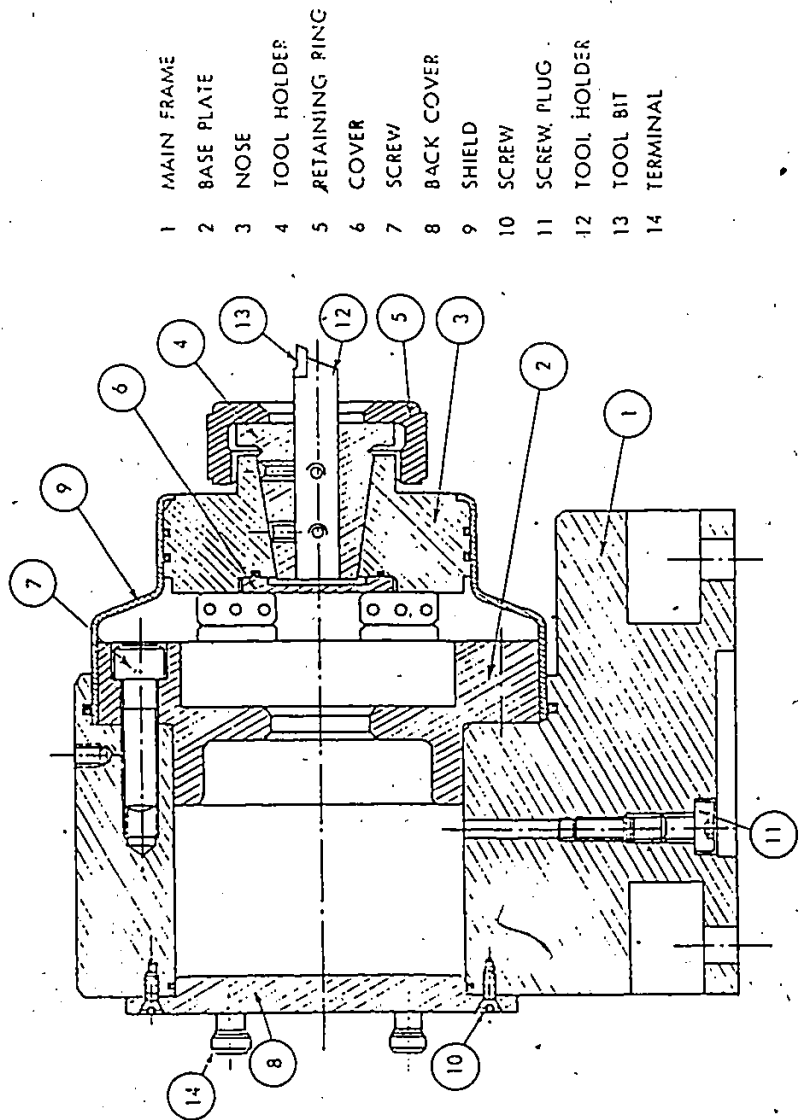


Fig. 4.4: The Schematic of the Instrumentation Used for the Cutting Force Measurement

AISI 1020 steel bar on a 12hp Demoor Lathe. To obtain the force signals and for recording the cutting forces, a special dynamometer was employed. This dynamometer had piezoelectric force transducers which were so arranged to measure the cutting forces in three mutually orthogonal directions. Three individual charge amplifiers were used corresponding to each of the three orthogonal force signals X-Y-Z compensator was employed to minimize the cross influence between these three signals. Each of these three cutting force signals, were then recorded using a B&K 7000 magnetic tape recorder on three separate channels. Also, these signals were observed on a cathode ray oscilloscope while being recorded.

#### 4.3.1 The Dynamometer

For an accurate measurement of the cutting forces, a special dynamometer which has quartz transducers as the sensing elements, was employed. These transducers have the property of converting the mechanical stress amplitudes into electrical charges. In the dynamometer that was used, the crystals are arranged in such a way that all the three components of the cutting forces can be measured independent of the point of application of the forces. This arrangement allows the cutting force magnitudes to be obtained accurately although their point of action is located at the interface between the tool and the chip. Figure 4.5 describes the cross-section of the dynamometer illustrating all the essential features such as the base plate, the tool holder, the bolts for preloading, the piezoelectric cells and the main frame. These components are designed in such a way that the dynamometer possesses a measurable response over a wide frequency range and also, possesses a



- 1 MAIN FRAME
- 2 BASE PLATE
- 3 NOSE
- 4 TOOL HOLDER
- 5 RETAINING RING
- 6 COVER
- 7 SCREW
- 8 BACK COVER
- 9 SHIELD
- 10 SCREW
- 11 SCREW PLUG
- 12 TOOL HOLDER
- 13 TOOL BIT
- 14 TERMINAL

Fig. 4.5: A Cross-Section of the Dynamometer (after Rakhit [4]).



high resolution.

The loading capacities of the dynamometer are specified as 2224N (500 lb<sub>f</sub>) in both the radial and the feed directions and 4448N (1000 lb<sub>f</sub>) in the direction of the main cutting force. The dynamometer has a natural frequency of 10 kHz in the feed and the main cutting force directions and along the radial direction its natural frequency is 13 kHz, which are sufficiently high in relation to the cutting force frequencies to be recorded.

#### 4.3.2 Static Calibration of the Dynamometer

The static calibration chart of a dynamometer is needed if it is to be mounted on a rigid base. In the present case where, the dynamometer was mounted on the cross slide of the lathe, the static calibration above is not sufficient. This is because the dynamic response of the machine tool also influences the dynamometer signals and thus the recorded signals may not represent only the cutting forces on a one-to-one basis. Therefore, static and the dynamic calibrations of the dynamometer employed, are essential.

The dynamometer was mounted on the lathe bed. The schematic arrangement of the various instrumentation is shown in Fig. 4.6. An external dead load was applied on the tool holder and this load was then increased gradually. The corresponding increase in the output voltage was observed on the oscilloscope screen. Figure 4.7 represents the calibration curve obtained. The ordinate represents the electric charge produced, and the abscissa represents the magnitude of the applied load, which was measured by a force transducer. This sensitivity was used later on to compute the magnitude of the actual cutting forces from their

T : CALIBRATED FORCE  
TRANSDUCER  
DYN. : DYNAMOMETER  
C.A. : CHARGE AMPLIFIER  
CRO : CATHODE RAY  
OSCILLOSCOPE  
COMP. : COMPENSATOR  
D.W. : DEAD WEIGHT

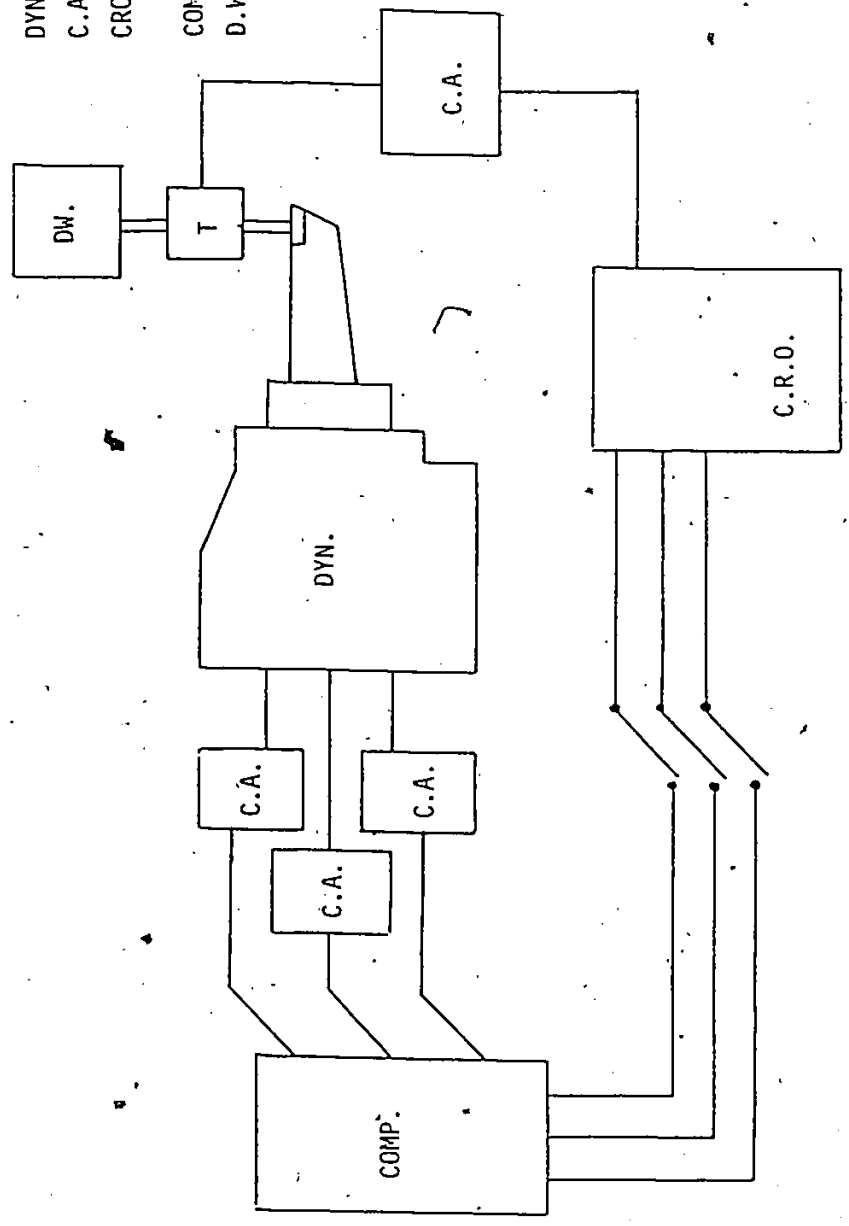


Fig. 4.6: A Schematic Diagram of the Set Up for Static Calibration of the Dynamometer.

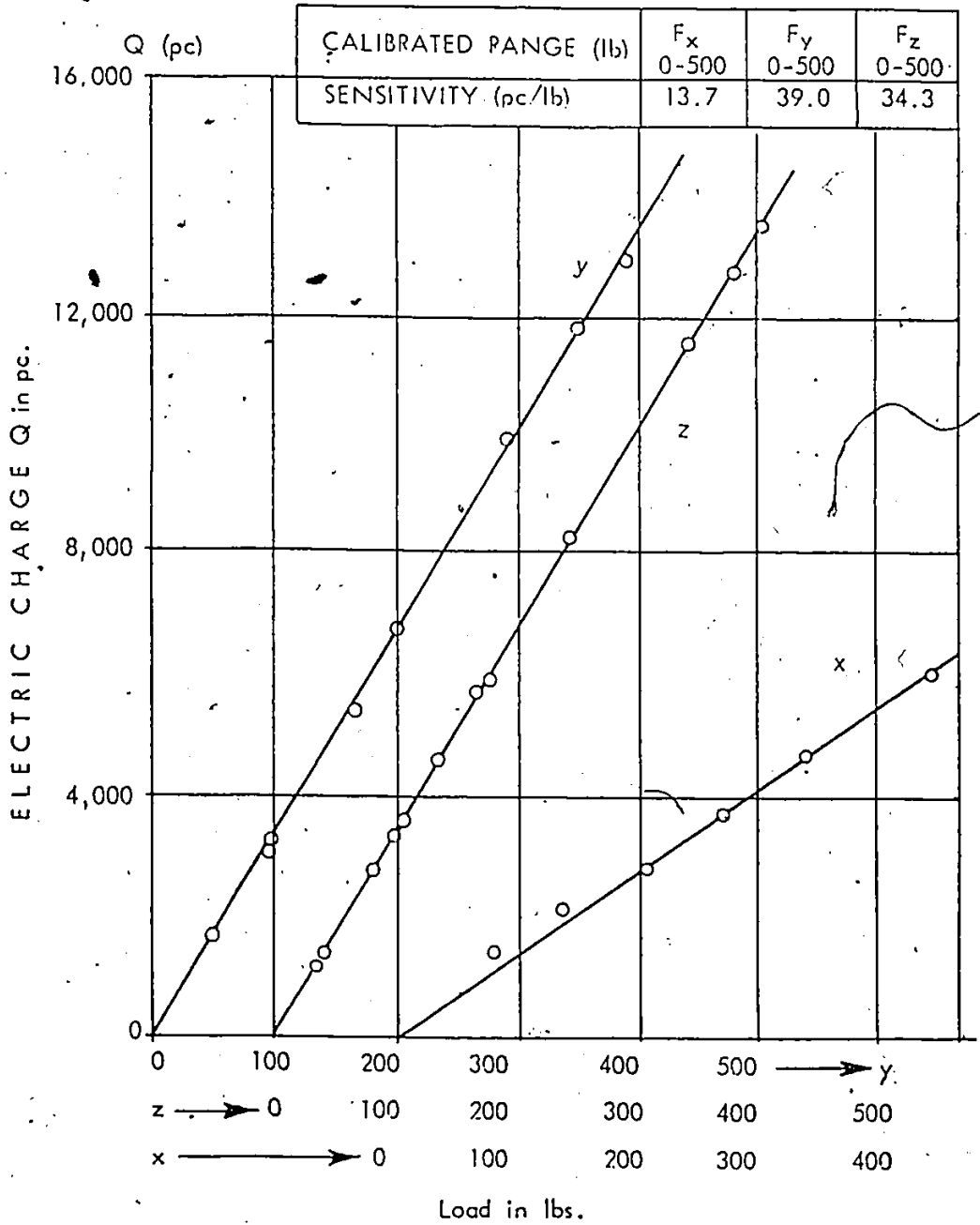


Fig. 4.7: Static Calibration Chart of the Dynamometer (after Rakhi [1]).

recorded signals, which were written  $\pm 1$  Volt on the tape.

#### 4.3.3 The Dynamic Calibration of the Dynamometer

The purpose of the dynamic calibration is to obtain a plot from which the actual force can be evaluated in the entire frequency range of interest. This is achieved by applying a known dynamic load and varying its frequency over the entire range of interest in this study.

To find the characteristics of the dynamometer, a dynamic load was applied at the tip of the tool and was kept constant by a feed back loop. It was found that the ratio of the output to the input forces was essentially unity up to 8 kHz. This confirmed that the static calibration curve was not distorted in the frequency range of interest.

#### 4.4 Cutting Force Measurements

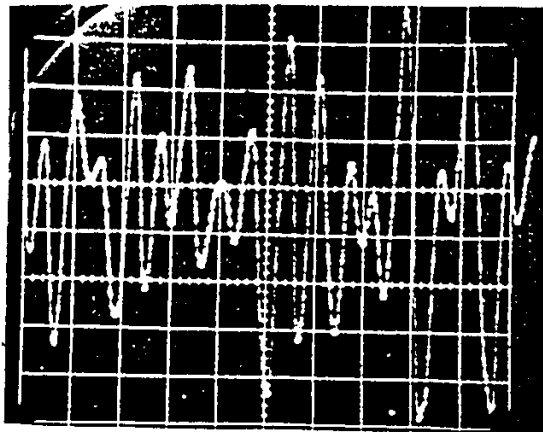
In order to measure the actual cutting forces, the dynamometer was mounted on the cross slide of the lathe. The output signal of the dynamometer was fed to three charge amplifiers corresponding to each of the three mutually orthogonal cutting force signals. An X-Y-Z compensator was employed to minimize the cross influence between these three orthogonal signals. A workpiece of  $0.051^{\circ}\text{m}$  ( $2^{\circ}$ ) diameter was machined using a  $0.0794 \mu\text{m}$  ( $1/32^{\circ}$ ) nose radius tool with a feed rate of  $0.0152 \mu\text{m}$  ( $0.006^{\circ}$ ) per revolution. The turning operation was performed with a spindle speed of 300 rpm. The sensitivities of the dynamometer along the x, y and z directions were set at 3.08, 8.77 and 7.71 pc/N respectively. The cutting force signals were visually observed on a cathode ray oscilloscope, and at the same time recorded on a B&K 7000 four channel F.M. magnetic tape recorder. The gain of these three charge amplifiers were selected as 22.241, 8.896, and 22.241 N/volts

respectively, in order that its output signals corresponding to the magnitude of the cutting forces were no more than within  $\pm 1$  volt at the input of the tape recorder. The signals were recorded on a B&K 7000, 4 channel tape recorder, at a tape speed of 0.381 m/sec (15"/sec). A typical signal record of the cutting force is shown in Fig. 4.8. The cutting force fluctuations as indicated in Fig. 4.8 may be seen to occur quite rapidly with time. Both Maragos [48], and Rakhit [41] studied the cutting force generated during roughing and finishing operations for various feed rates and depths of cut. A typical plot of these cutting forces and their spectral densities are shown in Fig. 4.9. They concluded that these cutting forces, for finishing operation, can be approximated by a stationary random process, and their probability density function can be taken as one of Gaussian distribution. With these approximations, the solution of the probabilistic differential equations for the variances of the response, becomes easier. This is because, for linear systems, as in the present case, if the excitation probability density has a Gaussian distribution then, the response probability density function is also Gaussian. For the processes having such a Normal distribution, mean and variance values are sufficient to characterize the process completely [51].

In the next section, the computation of the power spectral density of the measured cutting forces is discussed.

#### 4.5 Power Spectral Density (PSD) of the Cutting Force

The experimentally measured cutting force signals, such as the one shown in Fig. 4.8, have been recorded by setting the d.c. component or its mean equal to a zero value. This was achieved by setting the



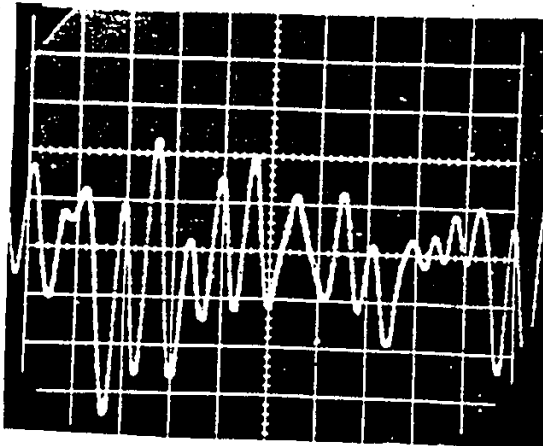
Main Cutting Force Component

$F_z$

Static Force = 200 lbs

10 lbs

1 m sec



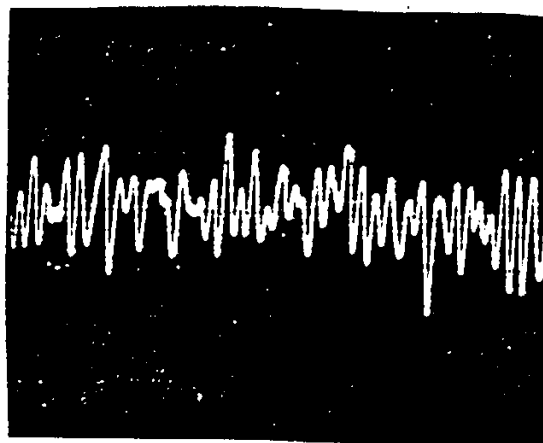
Feed Force Component

$F_y$

Static Force = 65 lbs

5 lbs

1 m sec



Radial Force Component

$F_x$

Static Force = 31.5 lbs

5 lbs

4 m sec

Fig. 4.8: A Typical Record of Cutting Forces (after Maragos [48]).

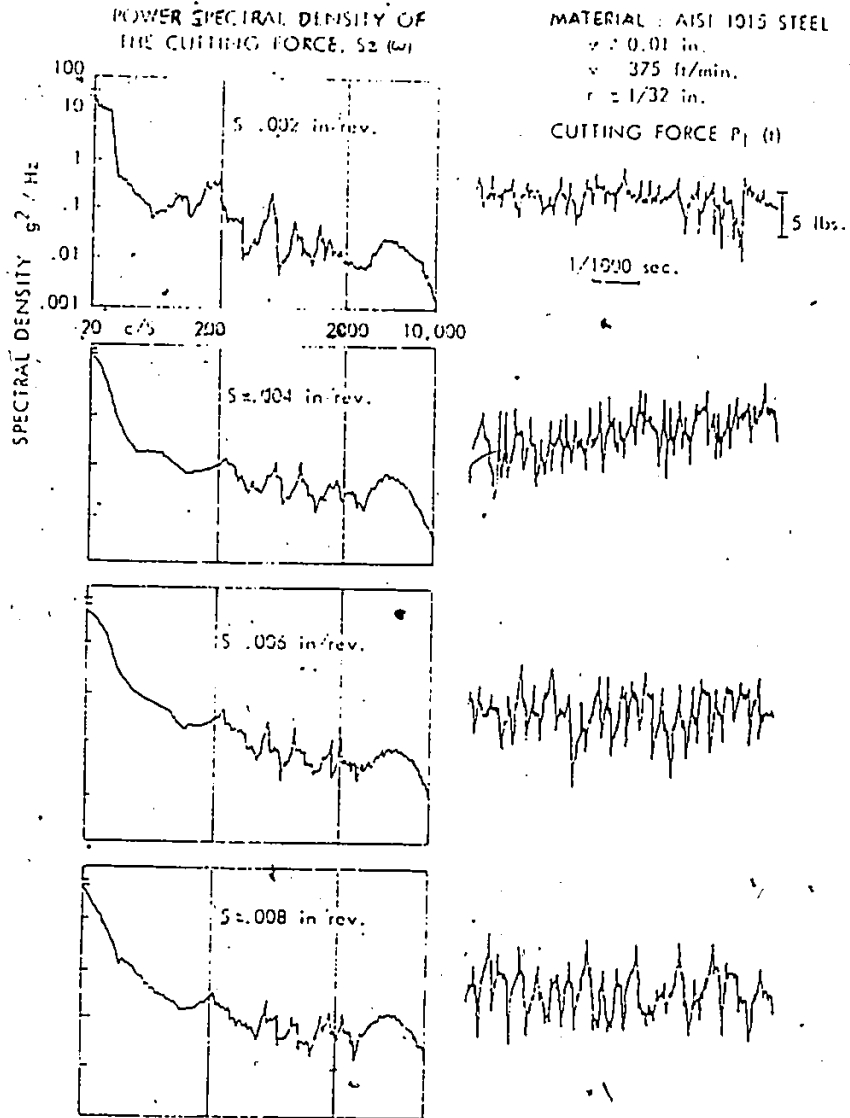


Fig. 4.9: Typical Spectral Density Plot of the Cutting Forces (after Rakhit [41])

time constant of the charge amplifier to a small value. Since cutting forces in a turning operation can be characterized by a normal probability density function, the response of the spindle-workpiece system modelled in chapter 2 under random cutting forces, would also be normally distributed with a zero mean, because of the linear behavior of the system. Hence, the mean square value is the only information that would be needed to characterize the response of the system. The mean square value of the response can be calculated using the cutting force signal in the time domain or in the frequency domain. In the time domain approach, the equation relating the mean square response and autocorrelation function of the excitation at zero time lag as shown below in equation (4.40) is utilized. That is,

$$E[\bar{W}^2] = R_W(0) = \int_{-\infty}^{\infty} \int_{-\infty}^{\infty} h(\lambda_1) h(\lambda_2) R_f(0) d\lambda_1 d\lambda_2 \quad (4.40)$$

where  $\lambda_1$  and  $\lambda_2$  are dummy variables,  $h(\lambda_1)$  is the impulse response function of the system. In the case of frequency domain analysis, the relationship between the mean square response and excitation Power Spectral Density (PSD) is given by the expression

$$E[\bar{W}^2] = \int_{-\infty}^{\infty} |H(j\omega)|^2 S_f(\omega) d\omega \quad (4.41)$$

where  $H(j\omega)$  is the frequency response function for the system under consideration, and  $S_f(\omega)$  is the Power Spectral Density (PSD) of the excitation. In this thesis, the frequency domain approach as given by equation (4.41) is employed to compute all the mean square responses. The PSD  $G_f(\omega)$  of the cutting force signals  $f'(t)$  is now needed in the



calculation of the mean square responses and is obtained by using the relationship [48]

$$G_{F_1}(\omega) = \lim_{T \rightarrow \infty} \frac{2}{T} \left| \int_{\frac{T}{2}}^{\frac{T}{2}} f'(t) e^{-i\omega t} dt \right|^2 \quad (4.42)$$

The recorded cutting force signals, which are in the analog form, are converted into the digital form by passing through an analog/digital converter. The digitized time series signals are then transformed by a Fourier Synthesis into the frequency domain. The Goodman-Enochson-Otnes (GEO) spectral window is applied to the raw Fourier transform quantities. Then the raw power estimates are computed using equation (4.42). These raw estimates are normalized and smooth estimates are obtained by an averaging process. The details of these procedures are provided in [48].

With the recent development of Fast Fourier Transform (FFT) algorithms, the power estimates can be calculated much more efficiently [62]. In the present work, a narrow band spectrum analyzer was used for the calculation of the Power Spectral Densities of the measured cutting forces, the frequency spectrum of the cutting forces were obtained using the set-up shown in Fig. 4.10.

The cutting force signals recorded were played back and analyzed on a B&K 2031 narrow band spectrum analyzer. This analyzer operates by a Fourier transformation of records of signal samples of the input into the frequency domain using a Fast Fourier algorithm. The frequency spectrum of the cutting forces are displayed on 400 channels in this analyzer.

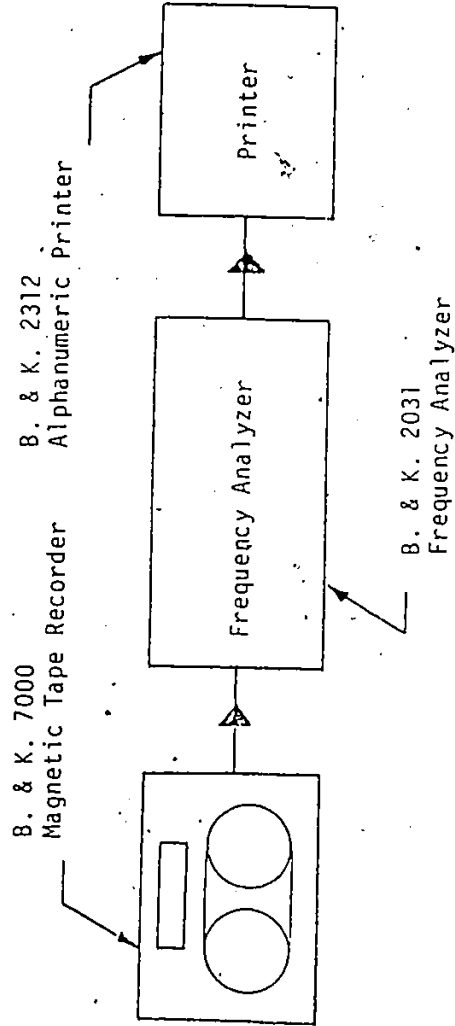


Fig. 4.10: The Schematic of the Instrumentation Used for the Frequency Analysis.

The calibration of the frequency analyzer was carried out by feeding a 1 volt signal at 1000 Hz from the tape recorder to the analyzer. Then the recorded cutting force signals were played back and exponentially averaged. An average of 32 spectra of the cutting forces were used to represent the stationary random excitation and the Hanning's window was used for the reduction of the frequency leakage. The highest frequency analyzed was 5 kHz using 1024 samples of the cutting force signals.

The output of this analyzer, which was the root mean square (RMS) value of the amplitude of the cutting forces, was further processed on a CDC Cyber 174 digital computer to obtain the power spectral density of the cutting forces. The power spectral density of an analyzed cutting force signal is shown in Fig. 4.11. In this figure, the experimental power spectral density varies quite significantly within the frequency range of 0-5000 Hz, and observing this figure one can clearly see that the spectrum is wide band in nature.

#### 4.6 The Mean Square Response of the Spindle-Workpiece System

In a finish turning process, there is a continuous relative displacement between the tool and the spindle-workpiece system. This continuous variation of this relative displacement takes place along the entire length of the system and is due to the variation in the compliance of the system. The compliance of the system continuously varies because the tool and the workpiece continuously change their relative position during machining. The cutting force varies because the depth of

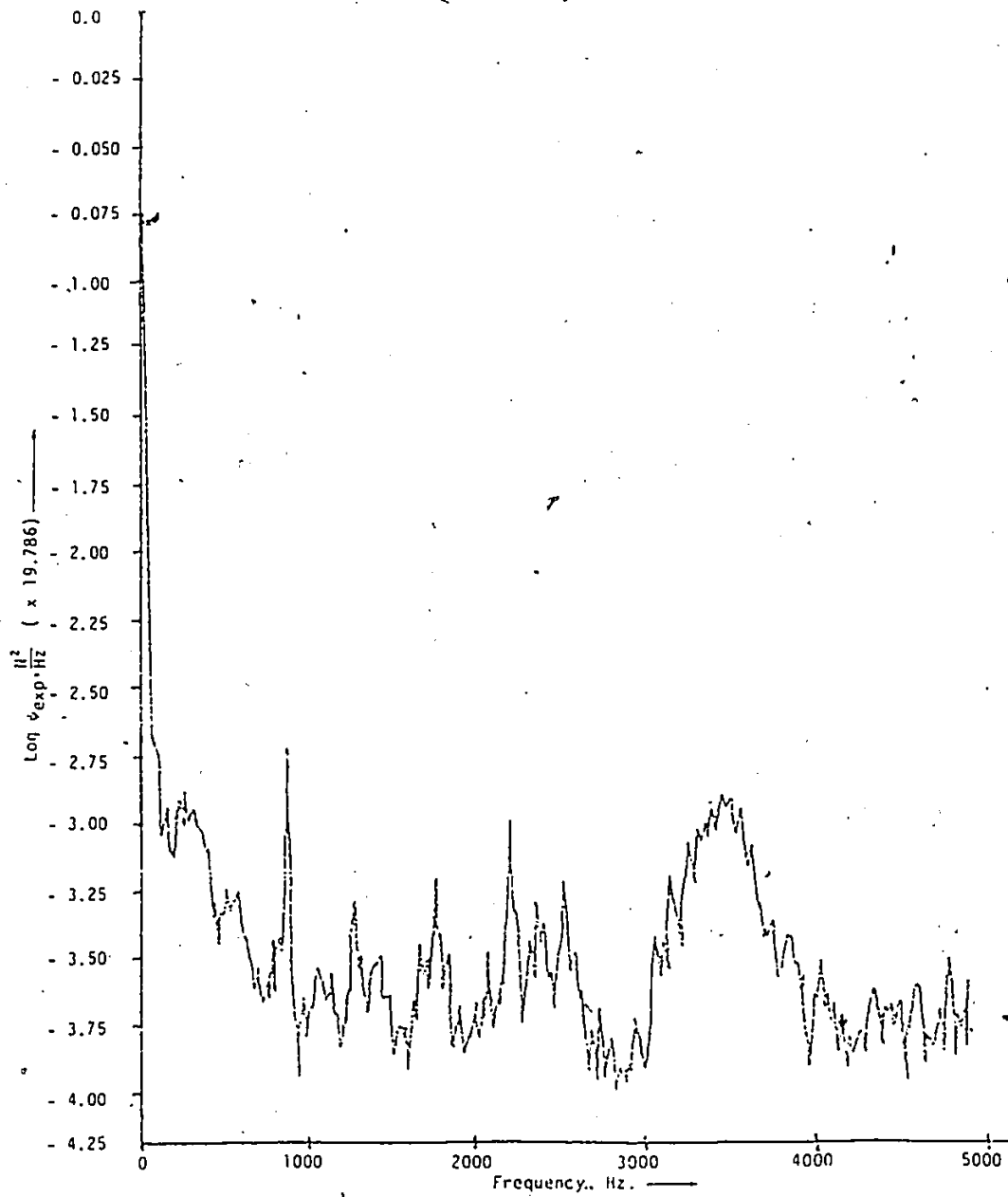


Fig. 4.11: The Experimental Power Spectral Density of the Cutting Forces

cut varies and this variation in the depth of cut is due to off-cylindrical shape of the workpiece at the beginning of the cutting process due to initial errors in the rough work.

A typical lathe spindle-workpiece system was described in Fig. 2.2 in chapter 2, where the spindle is divided into seven elements and the workpiece into five elements. The workpiece is held in a chuck on one end and supported by the running center on the other end. The boundary condition at the workpiece-running center interface has been established as hinged and the bearing properties are represented by a spring and a damper.

Based on conclusions drawn in section 4.2.5, that is, the variation of feed rates in a turning process has negligible influence on the response of the workpiece, the stochastic matrix differential equation of motion for the spindle-workpiece system can now be written as

$$\begin{matrix} [\bar{M}] & & & \\ 25 \times 25 & & & \end{matrix} \ddot{\{\bar{W}\}} + \begin{matrix} [\bar{C}] & & & \\ 25 \times 25 & & & \end{matrix} \dot{\{\bar{W}\}} + \begin{matrix} [\bar{K}] & & & \\ 25 \times 25 & & & \end{matrix} \{\bar{W}\} = \begin{matrix} \{\bar{F}\} \\ 25 \times 25 \end{matrix} \quad (4.42)$$

In equation (4.42)  $[\bar{M}]$ ,  $[\bar{C}]$ , and  $[\bar{K}]$ , are the mass, damping and the stiffness matrices respectively. The size of each of these matrices is 25 x 25 rather than 26 x 26 because it has already been established in chapter 3, that the workpiece-running center connection is better represented by a hinged end condition. This results in a constraint that the displacement at the joint number 1, which is the first component of the joint displacement vector  $\{\bar{W}\}$ , be zero for all times.

The relationship between the PSD of excitation  $[S_F(\omega)]$ , and the response  $[S_W(\omega)]$  for a linear system has been derived in Appendix B and also in [63,64]. This relationship can be written as

$$[S_{\bar{W}}(\omega)] = [A(j\omega)] [S_{\bar{F}}(\omega)] [A(j\omega)^*]^T \quad (4.43)$$

In the above equation  $[A(j\omega)]$  is the matrix of the transfer functions, and as derived in the Appendix B, can be evaluated by using the relationship

$$[A(j\omega)] = [\phi] [(j\omega) [M^*] + [K^*]]^{-1} [\phi]^T \quad (4.44)$$

where  $[\phi]$  has its columns as the eigen vectors of the modified version of matrix differential equation (4.42) obtained by using a state vector  $\begin{pmatrix} \dot{\bar{W}} \\ \bar{W} \end{pmatrix}$ , and the matrices  $[M^*]$  and  $[K^*]$  are given by the relationships

$$[M^*] = [\phi]^T \begin{bmatrix} [O] & [M] \\ [M] & [C] \end{bmatrix} [\phi] \quad (4.45)$$

and

$$[K^*] = [\phi]^T \begin{bmatrix} -[M] & [O] \\ [O] & [K] \end{bmatrix} [\phi] \quad (4.46)$$

Partitioning the matrix  $[S_{\bar{W}}(\omega)]$  is given in equation (4.43) into four equal submatrices, one can write

$$S_{\bar{W}}(\omega) = \begin{bmatrix} [S_{\bar{W}}(\omega)]_1 & [S_{\bar{W}}(\omega)]_2 \\ [S_{\bar{W}}(\omega)]_3 & [S_{\bar{W}}(\omega)]_4 \end{bmatrix} \quad (4.47)$$

The submatrices  $[S_{\bar{W}}(\omega)]_1$  and  $[S_{\bar{W}}(\omega)]_4$  represent the PSD of the velocities and the displacements respectively. Representing  $E[\bar{W}^2]$  as the mean square displacement (MSD) response, then

$$E[\bar{W}^2] = \int_{-\infty}^{\infty} S_{\bar{W}}(\omega) d\omega \quad (4.48)$$

#### 4.7 The Parameters of the Spindle-Workpiece System

In a spindle-workpiece system, parameters such as bearing stiffness, damping, bearing locations, cross-sectional area of the spindle, etc., exert considerable influence on the dynamic response of the system. In order to study their individual effects, a brief qualitative discussion on these parameters and their influence on the dynamic response are presented in the sections 4.7.1 through 4.7.4.

##### 4.7.1 The Bearing Stiffness

The static and the dynamic behavior of lathes are influenced significantly by the design of the spindle and its bearings. The factors which influence the static deflection of the spindle are: (i) the rigidity of the spindle; (ii) the stiffness of the bearings; and (iii) the location of the bearings. A spindle design based merely on static considerations is not sufficient because the dynamic cutting forces contain high frequency components. Thus the inertia and the damping forces also become important. Consequently, the bearing stiffness selection must include the effects due to all of the forces mentioned above.

##### 4.7.2 Bearing Location

The locations of the bearings exercise considerable influence on the effective stiffness of the spindle. A lathe spindle can be regarded as a beam on two flexible supports with damping and this beam has an overhanging end. Several researchers [42,45] have studied the effect of the bearing spacing on the overall rigidity of the spindle system. Terman [65] proposed two important static approaches for arriving at the optimum bearing spacing. In the first approach, a preliminary design of

a shaft may be completed in which the selection of shaft dimensions and bearing stiffness is based upon the boundary conditions. Then the bearing span is varied so that an optimum spacing is found. The optimum criterion was based on keeping the deflection at the point of application of the force a minimum. In the second approach, the various spindle cross-sectional areas are chosen in certain proportion and then the bearing spacing is varied until the optimum bearing span is arrived at.

The overall idea in all these approaches is to have a balanced design so that the stiffness of the bearings as well as that of the shaft is fully utilized. For a given cross-sectional area at the shaft and the bearing span, if the optimum bearing span is less than the starting span value, then it indicates that in the original design the full load capacity of the bearings are not fully utilized. Therefore by reducing the span, the loading on the bearings is increased at the same time as the flexibility of the shaft is reduced. This process is reversed if the optimum bearing spacing is found to be greater than the starting span dimension.

In the present work, both the presence of a workpiece and the dynamic cutting forces have been included in the mathematical model and a search for the optimal bearing span is based on the minimum of the maximum workpiece displacement response.

#### 4.7.3 Cross-Sectional Area of the Spindle

There are three important criteria in the design of shafts. These criteria can be based on one or a combination of the following:

- (1) least weight of the shaft,



- (2) minimum rotary inertia of the shaft, and
- (3) minimum response of the shaft.

The first criterion is very common in the design of shafts for aerospace applications where great care is taken to minimize the weight of the system. The second criterion is important in the design of machinery which has very high rotational speeds. Since the surface finish of a workpiece is directly related to the response, the third criterion has been used in work so as to obtain an optimal design of the spindle based on minimum workpiece response.

#### 4.7.4 Damping

There are several parameters which, if properly selected, can decrease the mean square displacement (MSD) at various locations of the spindle-workpiece system. Three of these parameters, have already been discussed in sections 4.7.1, 4.7.2 and 4.7.3. In this section, the effect of damping on the MSD along the spindle-workpiece system will be briefly explained.

In order to evaluate the effect of damping on the response of the spindle-workpiece system, the first step will be to estimate the actual amount of damping available in the system. An approximate idea of the overall damping of the spindle-workpiece system can be obtained by exciting the system with a shaker and measuring the viscous displacement amplitude as a function of the excitation frequency. This recorded plot is a form of the displacement transmissibility curve which when compared with a transmissibility curve of a single-degree-of-freedom system can provide the equivalent viscous damping of the overall system. Another method would be to use the logarithmic decrement method where the envelope curve

of the amplitudes of the decaying natural vibration is used [51].

After estimating the damping in the system, the effect of any externally applied damping and the location of such a damper on the displacement response can be studied. These studies should be carried out with an objective to find out, if there is any value of damping corresponding to which there is a minimum MSD response. Also, is there a best location of a damper for such a minimization.

In the next section, a parametric study for the optimal design of the lathe spindle has been carried out. The parameters used in the study are: (1) the bearing stiffness, (2) the bearing location, (3) flexural rigidity of the spindle, and (4) damping.

#### 4.8 Results and Discussion

##### 4.8.1 The Effect of Tool Location on the Mean Square Displacement (MSD) of the Workpiece

The MSD response at each of the joints was computed by combining equations (4.41) and (4.43). The size of each of the complex matrices in the equation (4.41) is 50 x 50. Referring to Fig. 4.10, the PSD of the cutting forces decreases as the frequency increases. Therefore, in this section, the computations were carried out by including the PSD of cutting forces up to 1200 Hz. This frequency range includes contributions of the first twelve free vibration modes [53].

To study the effect of tool location, the MSD response at various joints were calculated for different cutting tool locations, and the result obtained is shown in Table 4.1. It is to be noted that the displacement is always zero at the joint 1. The graphical representation of

TABLE 4.1

The Effect of Tool Location on MSD Response of the System

$$K_f = 1530.6 \times 10^6 \frac{N}{m} \quad c_r = 28.632 \times 10^3 \frac{N \cdot sec}{m} \quad L_B = 0.4699 \text{ m}$$

$$c_f = 22.328 \times 10^3 \frac{N \cdot sec}{m} \quad \frac{K_f}{K_r} = 3.190$$

| Tool Location<br>at Joint<br>Number | Mean Square Displacement at Joint Number<br>MSD x 1.355 x 10 <sup>-14</sup> , m <sup>2</sup> |       |       |       |       |       |       |       |       |       |       |       |  |
|-------------------------------------|--|-------|-------|-------|-------|-------|-------|-------|-------|-------|-------|-------|--|
|                                     | 2  | 3     | 4     | 5     | 6     | 7     | 8     | 9     | 10    | 11    | 12    | 13    |  |
| 2                                   | 0.118  | 0.222 | 0.145 | 0.038 | 0.010 | 0.003 | 0.002 | 0.004 | 0.005 | 0.005 | 0.011 | 0.028 |  |
| 3                                   | 0.222  | 0.503 | 0.365 | 0.109 | 0.030 | 0.011 | 0.006 | 0.010 | 0.013 | 0.014 | 0.031 | 0.071 |  |
| 4                                   | 0.145  | 0.365 | 0.342 | 0.138 | 0.044 | 0.017 | 0.007 | 0.008 | 0.014 | 0.022 | 0.042 | 0.079 |  |
| 5                                   | 0.038  | 0.109 | 0.138 | 0.100 | 0.044 | 0.019 | 0.007 | 0.006 | 0.012 | 0.023 | 0.039 | 0.063 |  |

the results presented in Table 4.1 is shown in Fig. 4.12. Referring to Fig. 4.12, the MSD response increases from zero at joint 1 to a maximum near the center of the workpiece and then reaches a minimum somewhere near the mid-span of the spindle. The MSD response at the free end is higher than at the mid-span of the spindle. It can also be seen that the maximum MSD occurs at the joint 3 for all tool locations (joints 2, 3, and 4) except for tool location at joint 5.

#### 4.8.2 The Effect of the Bearing Stiffness on the MSD of the Workpiece

The effect of the variation of bearing stiffness on the MSD of the workpiece is given in Table 4.2. Referring to Table 4.2, it can be seen that the maximum MSD occurs at joint 3 for all values of the bearing stiffness considered. Furthermore, it should be noted that all the MSD values in Table 4.2 correspond to a joint where cutting forces are also located. For increasing values of front bearing stiffness, the MSD decreases at first and then increases in the cases of joints 2 and 3, however at joints 4 and 5, the MSD decreases monotonically. This indicates that there exists an optimum bearing stiffness for which the maximum MSD of the workpiece is a minimum.

#### 4.8.3 The Effect of the Bearing Spacing on the Workpiece MSD

The effect of bearing spacing on the spindle response has been studied by several researchers [42,45,65]. In their study, using a deterministic model of the spindle-chuck system, the variation of the maximum deflection of the spindle was presented due to changes in the bearing spacing. However, in the present investigation, the location of the rear bearing was fixed and only the location of the front bearing

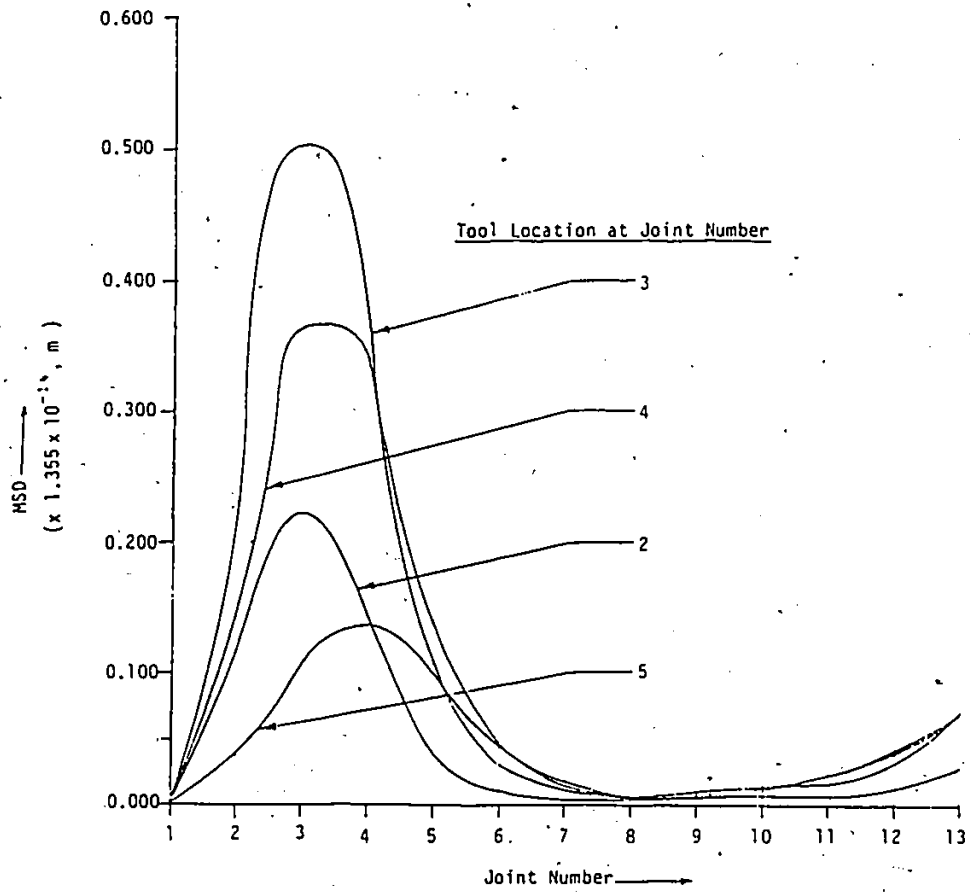


Fig. 4.12: The Effect of Tool Location on the MSD of the Spindle-Workpiece System.

TABLE 4.2

The Effect of the Bearing Stiffness on the  
MSD Response of the Workpiece

$$K_f = 1530.6 \times 10^6 \frac{N}{m}$$

$$c_f = 22.328 \times 10^3 \frac{N \text{ sec}}{m}$$

$$\frac{K_r}{K_f} = 0.3135$$

$$c_r = 28.632 \times 10^3 \frac{N \text{ sec}}{m}$$

$$L_B = 0.4699 \text{ m}$$

| Front Bearing Stiffness | Tool Location Mean Square Response<br>MSD x 1.355 x 10 <sup>-14</sup> , m <sup>2</sup> |              |          |          |
|-------------------------|--|--------------|----------|----------|
|                         | Joint #2   | Joint #3     | Joint #4 | Joint #5 |
| K <sub>f</sub>          | 0.118  | <u>0.503</u> | 0.342    | 0.100    |
| 2 K <sub>f</sub>        | 0.107  | <u>0.452</u> | 0.298    | 0.074    |
| 3 K <sub>f</sub>        | 0.104  | <u>0.434</u> | 0.288    | 0.070    |
| 4 K <sub>f</sub>        | 0.109  | <u>0.449</u> | 0.263    | 0.046    |

was varied. The results obtained are shown in Table 4.3. It can be seen from Table 4.3 that the MSD decreases and increases as the bearing spacing is increased. There are three local minima that can be identified with the the global minima occurring at higher values.

#### 4.8.4 The Effect of the Sectional Rigidity of the Spindle on the Mean Square Displacement (MSD) of the Workpiece

The spindle of the present system has been divided into 6 elements. The schematic of the stiffness distribution of the spindle-workpiece system is shown in Fig. 3.2.

In order to study the effect of sectional rigidity, the diameter\* of each of the elements can be varied one at a time within a range between the minimum and the maximum allowable values. From Figs. 2.2a and 2.2b, it can be seen that the bending moment at elements 7,8,9 and 10 is higher than at elements 11 and 12. Therefore higher elemental rigidity is required for the portion containing elements 7 to 10 to minimize the workpiece response. Hence in this study, the diameters of the elements 7 to 10 are kept constant at the maximum allowable value while the variations of individual sections are carried out independently one at a time.

The results obtained are presented in Table 4.4. The maximum cutting force frequency used in all these computations, was 187.5 Hz. This frequency range considered included the contributions of all the free vibration modes up to the sixth mode. Referring to this Table, it can be seen that for a given percentage change in the diameter of any of the elements, the greatest change in the MSD response is due to the variation in element 7. In other words, the change in diameter of element 7 has the greatest influence. This influence decreases as the

\*In this thesis, reference to diameter of an element represents its equivalent diameter.

TABLE 4.3

The Effect of Bearing Spacing on the Maximum  
MSD Response of the Workpiece

$$K_f = 1530.6 \times 10^6 \frac{N}{m} \quad c_f = 22.328 \times 10^3 \frac{N \text{ sec}}{m}$$
$$\frac{K_r}{K_f} = 0.3135 \quad c_r = 28.632 \times 10^3 \frac{N \text{ sec}}{m}$$

Tool Location at Joint 3

| Bearing Spacing<br>m | Maximum Workpiece Mean Square Response<br>MSD x 1.355 x 10 <sup>-14</sup> , m <sup>2</sup> |
|----------------------|--|
| 0.059                | 6.723  |
| 0.135                | 3.841  |
| 0.211                | 5.600  |
| 0.287                | 7.929  |
| 0.325                | 4.801  |
| 0.364                | 0.866  |
| 0.439                | 0.965  |
| 0.4699               | 0.503  |
| 0.508                | 0.925  |



TABLE 4.4  
The Effect of the Variation of the Spindle Diameter on the MSD Response

| Set Number | Equivalent Diameter of Element Number |                   |                   |                    |                    |                    | Tool Location Mean Square Response at Joint Number 3<br>MSD x 1.355 x 10 <sup>-14</sup> , m <sup>2</sup> | Maximum Variation in Mean Square Response |
|------------|---------------------------------------|-------------------|-------------------|--------------------|--------------------|--------------------|--|---|
|            | 7<br>x0.0254<br>m                     | 8<br>x0.0254<br>m | 9<br>x0.0254<br>m | 10<br>x0.0254<br>m | 11<br>x0.0254<br>m | 12<br>x0.0254<br>m |  |   |
| 1          | 10                                    | 10                | 10                | 10                 | 7.4                | 6.68               | 30.17  |   |
|            | 7.9                                   | 10                | 10                | 10                 | 7.4                | 6.68               |  |   |
|            | 5.0                                   | 10                | 10                | 10                 | 7.4                | 6.68               |  |   |
| 2          | 10                                    | 10                | 10                | 10                 | 7.4                | 6.68               | 16.57  |   |
|            | 10                                    | 7.9               | 10                | 10                 | 7.4                | 6.68               |  |   |
|            | 10                                    | 5.0               | 10                | 10                 | 7.4                | 6.68               |  |   |
| 3          | 10                                    | 10                | 10                | 10                 | 7.4                | 6.68               | 7.69   |   |
|            | 10                                    | 10                | 7.9               | 10                 | 7.4                | 6.68               |  |   |
|            | 10                                    | 10                | 5.0               | 10                 | 7.4                | 6.68               |  |   |
| 4          | 10                                    | 10                | 10                | 10                 | 7.4                | 6.68               | 2.37   |   |
|            | 10                                    | 10                | 10                | 7.9                | 7.4                | 6.68               |  |   |
|            | 10                                    | 10                | 10                | 5.0                | 7.4                | 6.68               |  |   |
| 5          | 10                                    | 10                | 10                | 10                 | 10                 | 6.68               | 0  |   |
|            | 10                                    | 10                | 10                | 10                 | 7.9                | 6.68               |  |   |
|            | 10                                    | 10                | 10                | 10                 | 5.0                | 6.68               |  |   |
| 6          | 10                                    | 10                | 10                | 10                 | 10                 | 10                 | 0  |   |
|            | 10                                    | 10                | 10                | 10                 | 10                 | 7.9                |  |   |
|            | 10                                    | 10                | 10                | 10                 | 10                 | 5.0                |  |   |

element number increases, that is, the farther the element is from the chuck, the lesser is its influence on the MSD of the workpiece. It may be noticed that elements 11 and 12 have little effect on the workpiece MSD response. This can be explained due to the fact that for the present system, the bending moments at these locations also decrease as the element number increases. Thus the elements at which the bending moments are small, the change in the diameters of those elements does not influence any significant changes in the workpiece MSD response. In view of the above, the elements, depending upon their influence on the workpiece MSD response, can be easily classified into two groups. Elements 7 to 10 can be grouped together as the first group, and elements 11 and 12 into the second group.

The first group of elements (element numbers 7 to 10) were varied in diameter between 75% to 125% of the existing design values. The corresponding variations in the MSD response are shown in Table 4.5. The results obtained indicate that there could be significant variation in the MSD response by varying the diameters of various elements in a group-wise manner. In fact, the minimum response as obtained in Tables 4.4 and 4.5 are quite close. Thus, an effective improvement in the spindle design can be brought about by adopting any one of the two ways mentioned above. In addition to this, the actual design modification would be based on other constraints such as intershaft distance, cost etc.

#### 4.8.5 Effect of Damping on the MSD of the Workpiece

The effect of damping on a lathe spindle has been studied by various authors [42,66,67]. The determination of damping coefficient for a spindle-workpiece system is a difficult task. An approximate

TABLE 4.5  
The Effect of Groupwise Variation of Diameter of Various  
Elements on the MSD Response

| Set Numbers | Group One                  |                    |                    |                     | Group Two                  |                     | Tool Location Mean Square Response at Joint Number 3<br>MSD x 1.355 x 10 <sup>-14</sup> m <sup>2</sup> |
|-------------|----------------------------|--------------------|--------------------|---------------------|----------------------------|---------------------|--|
|             | Diameter of Element Number |                    |                    |                     | Diameter of Element Number |                     |  |
|             | 7<br>x 0.0254<br>m         | 8<br>x 0.0254<br>m | 9<br>x 0.0254<br>m | 10<br>x 0.0254<br>m | 11<br>x 0.0254<br>m        | 12<br>x 0.0254<br>m |  |
| 1           | 11.238                     | 8.35               | 8.35               | 8.35                | 7.4                        | 6.68                | 0.170  |
|             | 7.9                        | 8.99               | 6.68               | 6.68                | 7.4                        | 6.68                | 0.180  |
|             | 6.743                      | 5.01               | 5.01               | 5.01                | 7.4                        | 6.68                | 0.213  |
| 2           | 7.9                        | 8.99               | 6.68               | 6.68                | 9.25                       | 8.35                | 0.180  |
|             | 7.9                        | 8.99               | 6.68               | 6.68                | 7.4                        | 6.68                | 0.180  |
|             | 7.9                        | 8.99               | 6.68               | 6.68                | 5.55                       | 5.01                | 0.180  |

method is to excite the system by a sinusoidal signal of constant amplitude and variable frequency  $\omega$  and to record the frequency response curve. By noting the response amplitude  $X$  over the frequency range, the damping ratio can be calculated by assuming a single degree-of-freedom system for the spindle [41]. From this experimentally calculated damping ratio, the equivalent viscous damping coefficient was calculated to a value of  $48.159 \times 10^3$  NS/m (275 lb<sub>f</sub> S./in.) [41]. Using this value as a guideline, the damping coefficients at the rear and front bearings were selected.

In order to study the influence of damping at the bearing locations on the MSD response, additional dampings were applied separately at these two locations and the results are presented in Tables 4.6 and 4.7. It can be seen from these two tables that the maximum MSD remained constant or decreased only slightly for any addition of damping in the bearings. Hence, it can be concluded that the effect of additional damping at the bearing locations, on the maximum MSD response is negligible.

In order to find the best possible location for applying external damping, an additional damping equal to 2.5% of  $C_c$  was applied at joints 8 to 13 separately and the results obtained are shown in Table 4.8. As can be seen from the table, the free end is the best possible location for applying external damping. There is an 11% reduction in the maximum MSD response if 2.5%  $C_c$  is applied at the free end of the spindle.

#### 4.9 Conclusions

In this chapter, the dynamic response of the spindle-workpiece system under random cutting forces is investigated. Since the cutting tool moves along the workpiece, the response of the workpiece is

TABLE 4.6

Additional Damping at the Front Bearing Location  
Versus MSD of the Workpiece

$$c_f = 22.328 \times 10^3 \frac{N \text{ sec}}{m} \quad K_f = 1530.6 \times 10^6 \frac{N}{m}$$

$$c_r = 28.632 \times 10^3 \frac{N \text{ sec}}{m} \quad \frac{K_r}{K_f} = 0.3135$$

$$c_a = 1.25\% c_c \quad c_c = 14.08 \times 10^5 \frac{N \text{ sec}}{m}$$

| Additional Damping at Front Bearing Location | Tool Location Mean Square Response at Joint Number<br>MSD x 1.355 x 10 <sup>-14</sup> , m <sup>2</sup> |              |       |              |
|--|--|--------------|-------|--------------|
|  | 2  | 3            | 4     | 5            |
| 0  | 0.118  | <u>0.503</u> | 0.342 | <u>0.100</u> |
| c <sub>a</sub>                               | 0.118  | <u>0.502</u> | 0.342 | 0.100        |
| 2 c <sub>a</sub>                             | 0.118  | <u>0.502</u> | 0.342 | 0.099        |
| 3 c <sub>a</sub>                             | 0.118  | <u>0.502</u> | 0.341 | 0.099        |

TABLE 4.7

The Effect of Additional Damping Applied at the  
Rear Bearing Location on the Maximum MSD Response  
of the Workpiece

$$c_f = 22.328 \times 10^3 \frac{\text{N sec}}{\text{m}} \quad K_f = 1530 \times 10^6 \frac{\text{N}}{\text{m}}$$

$$c_r = 28.632 \times 10^3 \frac{\text{N sec}}{\text{m}} \quad \frac{K_r}{K_f} = 0.3135$$

$$c_a = 1.25\% c_c \quad c_c = 14.08 \times 10^5 \frac{\text{N sec}}{\text{m}}$$

$$L_B = 0.4699 \text{ m}$$

| Additional Damping at Rear Bearing | Tool Location Mean Square Response at Joint Number |              |       |       |
|------------------------------------|--|--------------|-------|-------|
|                                    | MSD x 1.355 x 10 <sup>-14</sup> , m <sup>2</sup>   |              |       |       |
|                                    | 2  | 3            | 4     | 5     |
| 0                                  | 0.118  | <u>0.503</u> | 0.342 | 0.100 |
| c <sub>a</sub>                     | 0.118  | <u>0.501</u> | 0.340 | 0.098 |
| 2 c <sub>a</sub>                   | 0.118  | <u>0.500</u> | 0.338 | 0.096 |
| 3 c <sub>a</sub>                   | 0.117  | <u>0.498</u> | 0.335 | 0.094 |

TABLE 4.8

The Effect of Damping Location on the  
MSD Response of the Workpiece

$$c_f = 22.328 \times 10^3 \frac{N \text{ sec}}{m} \quad K_f = 1530.6 \times 10^6 \frac{N}{m}$$
$$c_r = 28.632 \times 10^3 \frac{N \text{ sec}}{m} \quad \frac{K_r}{K_f} = 0.3135$$
$$c_c = 14.08 \times 10^5 \frac{N \text{ sec}}{m}$$

| Addition Damping,<br>(2.5% $c_c$ ) Applied<br>at Joint Numbers | Maximum MSD Response<br>$\times 1.355 \times 10^{-14}, m^2$ |
|--|---|
| 8  | 0.502   |
| 9  | 0.501   |
| 10   | 0.501   |
| 11   | 0.501   |
| 12   | 0.498   |
| 13   | 0.480   |

essentially a non-stationary random process. Hence as a first step in the analysis, the dynamic response of the system in turning due to spatially moving random metal cutting forces (non-stationary random cutting forces) is carried out in detail. The workpiece was modeled as a Bernoulli-Euler beam with the chuck end assumed as fixed and the tailstock end as hinged at the running center. The mean and the variance response at the tool location, as a function of structural damping and the velocity of the tool, was calculated.

The results indicate that for the range of feed rates normally used in finish turning operations, it is not necessary to consider the effect of feed rate in obtaining the mean and variance responses at the tool contact. Since the feed rates are very low compared to the flexural wave velocities in the workpiece material, the transients die down fast enough and do not influence the response at the succeeding tool locations. This result is very useful since much simpler expressions without considering the effect of tool feed rate can be used to compute the responses of the workpiece.

The stochastic partial differential equation characterizing the behavior of the system was then solved using modal analysis. The actual cutting forces were measured while machining on a lathe using a special piezoelectric dynamometer. Then using a narrow band spectrum analyzer, B&K 2031, and a digital computer, the power spectral density of the cutting forces was determined. The PSD of the cutting forces were used to calculate the mean square response of the workpiece. For this purpose a new technique for the calculation of response spectral density for a linear multidegree-of-freedom system subjected to stationary random excitation has been developed. The method is based on modifying the



stochastic dynamic equations of the system by using a set of auxiliary variables. The response spectral density matrix obtained by using this approach contains the spectral densities and cross-spectral densities of the system generalized displacements and velocities. The new technique requires significantly less computation time as compared to the conventional method for calculating the response spectral densities.

A parametric study on the effect of bearing stiffness, bearing spacing, spindle sectional rigidity and damping on the mean square displacement of the workpiece was carried out. Based on this, the following conclusions are drawn:

(1) The MSD varies quite significantly along the spindle-workpiece system irrespective of the location of the tool.

(2) There exists an optimum bearing stiffness and span for which the maximum workpiece MSD is a minimum.

(3) The MSD along the spindle-workpiece system decreases with the increase in the sectional rigidity of the spindle.

(4) The MSD at the tool location decreases significantly as the damping at the free end of the spindle is increased.

In the next chapter, the optimal design of the lathe spindle is carried out. The parameters used in this optimization study are:

(1) the bearing stiffness, (2) the bearing locations, and (3) the sectional rigidity of the spindle.

## CHAPTER 5

### OPTIMIZATION OF THE LATHE SPINDLE-WORKPIECE SYSTEM UNDER STOCHASTIC CUTTING FORCES

#### 5.1 Introduction

In chapter 4, the effect of tool location, bearing stiffness and spacing, bearing damping, cross-sectional area, and that of additional damping at various joints on the MSD response of the workpiece was presented. It was also concluded that there exist optimum values of the bearing stiffness and the spacing for a minimum MSD response of the workpiece as either the bearing stiffness or the bearing spacing is varied. From Tables 4.6 and 4.7, it was concluded that a variation of the bearing damping individually has negligible influence on the maximum MSD response. Consequently it can be postulated that a set of optimal bearing stiffness and bearing spacing must exist for which the maximum MSD of the workpiece will be a minimum. In this chapter, this problem of finding an optimal set of bearing stiffness and spacing is carried out using a non-linear programming technique. The optimal results are compared with the existing design and conclusions are drawn.

#### 5.2 Formulation of the Problem

The present work deals with the problem of determining the optimal design parameters so as to minimize the maximum mean square displacement response of the workpiece. The first task is to select the design variables for the optimization scheme. In chapter 4, the effect of parameters, such as bearing stiffness and spacing, damping, diameters of the different elements which make up the spindle, on the

mean square displacement was presented. It was also shown that of all possible locations of the cutting tool, the tool located at joint number 3 yielded the maximum dynamic response of the work. Therefore, by this logic, the objective would be to minimize the response of the workpiece at the joint number 3 with the tool also located at the same joint. In the parametric study presented in chapter 4, the MSD response decreased monotonically as the damping increased. Therefore, it can be eliminated as one of the possible design variables for achieving an optimal design.

Since the MSD response was unaffected by any variation of diameters of elements 11 and 12, they are also eliminated as design variables for the optimization. Then the parameters remaining for the optimization are the diameters of elements of the first group, that is, element numbers 7,8,9 and 10; the bearing stiffness; and the bearing spacing.

Since the main objective of this investigation is to minimize the maximum mean square displacement of the workpiece, for any given set of design parameters, it is essential to solve the stochastic matrix differential equation outlined in chapter 4. This required a large computing time. When the search for the optimal design parameters are carried out using non-linear optimization techniques, the objective function evaluation has to be carried out several times and this obviously increases the computing time by several folds. In addition, the computer time increases proportionally with an increase in the number of design parameters.

Therefore, in order to reduce the computing time, only a limited set of important design parameters are to be considered for the optimization. Based on this logic, two separate optimal design schemes are carried out. In both schemes, the objective function remained the same, except that in

the first scheme only the bearing stiffnesses and bearing spacing are selected as design parameters, with all other parameters kept at their nominal values. In the second scheme, in addition to the bearing stiffnesses and spacing, the diameter of the element number 8 is included as a design variable. In chapter 4, it was shown that the mean square response of the system decreases when the diameters of the elements 7 to 10 are kept at their maximum allowable values for a constant set of bearing stiffnesses and spacing. However, in order to study the effect of variation in the diameter of elements, when the bearing stiffnesses and spacing are not kept a constant, a second optimization scheme is formulated wherein the diameter of element 8 has been selected also as a design variable. In this case, the upper bound values of the diameters of other elements 7,9 and 10 are considered.

Mathematically the objective function together with the constraints can be formulated in terms of two optimization schemes. They are:

### 5.2.1. First Optimization Scheme

$$\begin{array}{l} \text{minimize} \\ k_f, L_B \end{array} \quad [\max E(\bar{W}^2)] , \quad \text{the mean square displacement} \quad (5.1) \\ \text{of the workpiece}$$

$$\begin{array}{l} \text{Subject to:} \\ k_f^l \leq k_f \leq k_f^u \\ k_r^l \leq k_r \leq k_r^u \\ L_B^l \leq L_B \leq L_B^u \end{array} \quad (5.2)$$

$$k_r/k_f = 0.3135$$

where subscripts  $l$  and  $u$  represent the lower and the upper bound values of bearing stiffnesses and spacing.

### 5.2.2 Second Optimization Scheme

In addition to equations (5.1) and (5.2), a limit constraint on the diameter of element 8 is to be included. That is,

$$d_8^l \leq d_8 \leq d_8^u \quad (5.3)$$

In equation (5.1), in addition to  $k_f$  and  $L_B$ ,  $d_8$  will be included as the third design variable.

It should be noted that the ratio of the rear bearing stiffness to the front bearing stiffness is kept a constant. The selection of lower and upper bounds on bearing stiffnesses is based on the commercial availability of these bearings. For the selection of lower and upper bounds on the bearing spacing, the rear bearing was considered to be fixed at the mid-point of the element 11. Then the lower limit on the bearing spacing can be based on the distance between the rear bearing and the front bearing located at junction 11. Similarly, the upper limit on the bearing spacing is estimated on the basis of the distance between the rear bearing and the front bearing located at junction 7.

### 5.3 The Optimization Algorithm

The optimization procedure has been carried out by using the modified sequential simplex optimization method [68]. This method uses a flexible rather than a rigid geometric simplex of points. The basic idea in the sequential simplex method is to start with some arbitrary initial values for the parameters to be optimized. In a multi-parameter optimization with  $n$  variables, at least a set of  $n+1$  initial values should be arbitrarily selected. These  $(n+1)$  values will represent  $(n+1)$  points in the  $n$ -dimensional space and, if these points are connected by

straight lines, then a geometric figure will result. This geometric figure is known as simplex. For example, in two-dimensional optimization, a set of 3 initial values are selected and they form a triangle (Fig. 5.1). The objective function is evaluated at the points formed by the vertices of the geometric figure. One vertex is then rejected as being inferior in value to the others. The general direction of search may then be taken in a direction away from the worst point. It is chosen so that the movement passes through the center of gravity of the remaining points. A new point is then selected along the direction so as to preserve the geometric sense of the figure, and the function is evaluated ahead at this point. The method proceeds by this process of vertex rejection and regeneration until the figure "straddles" the optimum. The flow chart of this method is given in Fig. 5.2 and the steps involved in the optimization are given below:

$$(i) \text{ Minimize } F(\bar{x}), \{\bar{x}\} = \{x_1, x_2, \dots, x_n\} \quad (5.4)$$

where  $\{\bar{x}\}$  is a vector of variables  $x_1, x_2, \dots, x_n$  to be optimized subject to

$$a_i \leq x_i \leq b_i \quad ; \quad i = 1, 2, \dots, n$$
$$g_j(\bar{x}) \geq 0 \quad ; \quad j = 1, 2, \dots, q$$

(ii) The method requires the use of  $k \geq n+1$  vertices; each of which must satisfy all the imposed constraints. These vertices may be initially found by starting at a point that satisfied all the constraints. The remaining  $k-1$  points in the first complex are obtained by the use of pseudorandom numbers  $r_i$  in the relation

$$x_i = a_i + r_i (b_i - a_i) \quad ; \quad i = 1, 2, \dots, k \quad (5.5)$$

where  $r_i$  are uniformly distributed over the interval  $[0,1]$ . These points

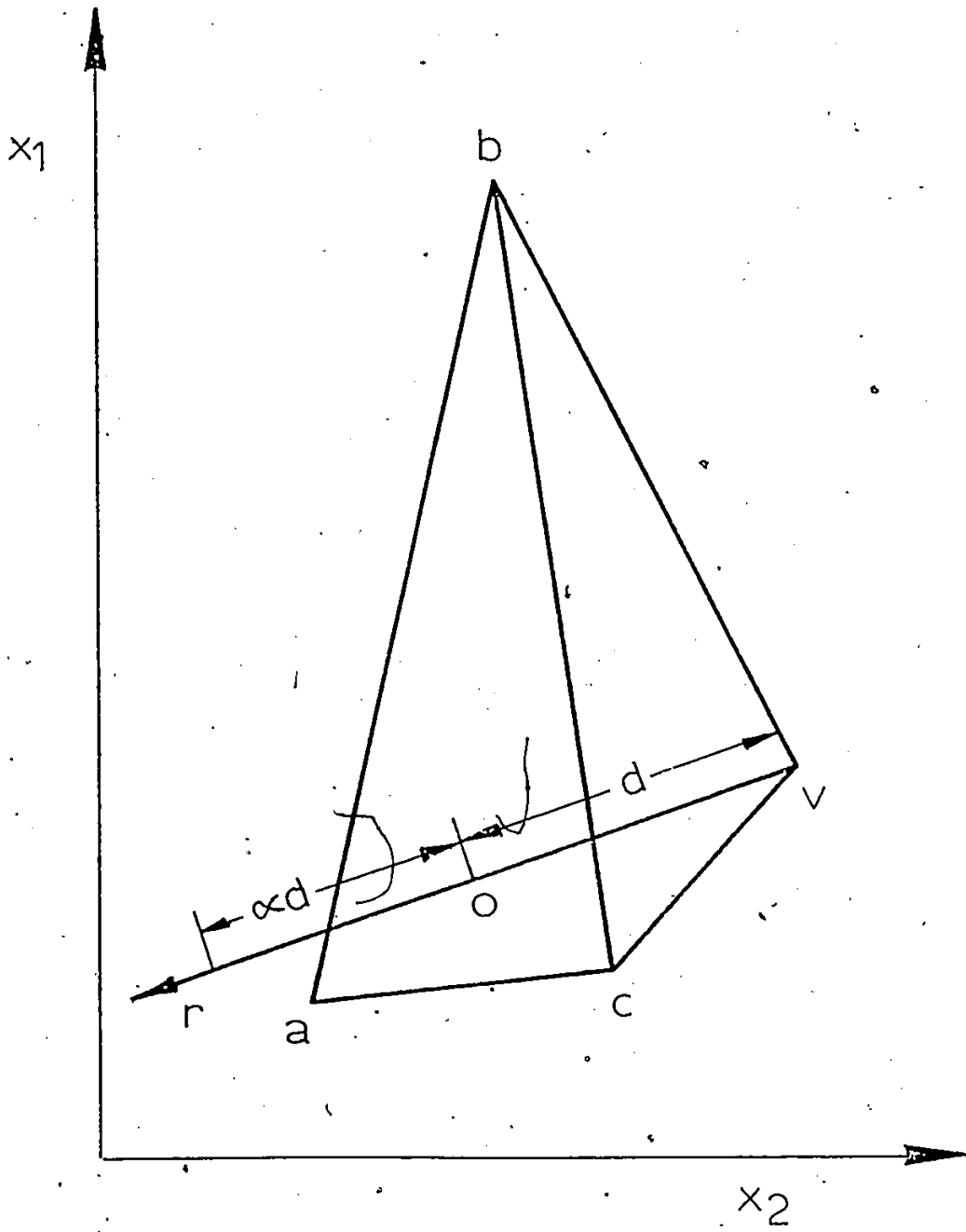


Fig. 5.1: Two-Dimensional Complex.

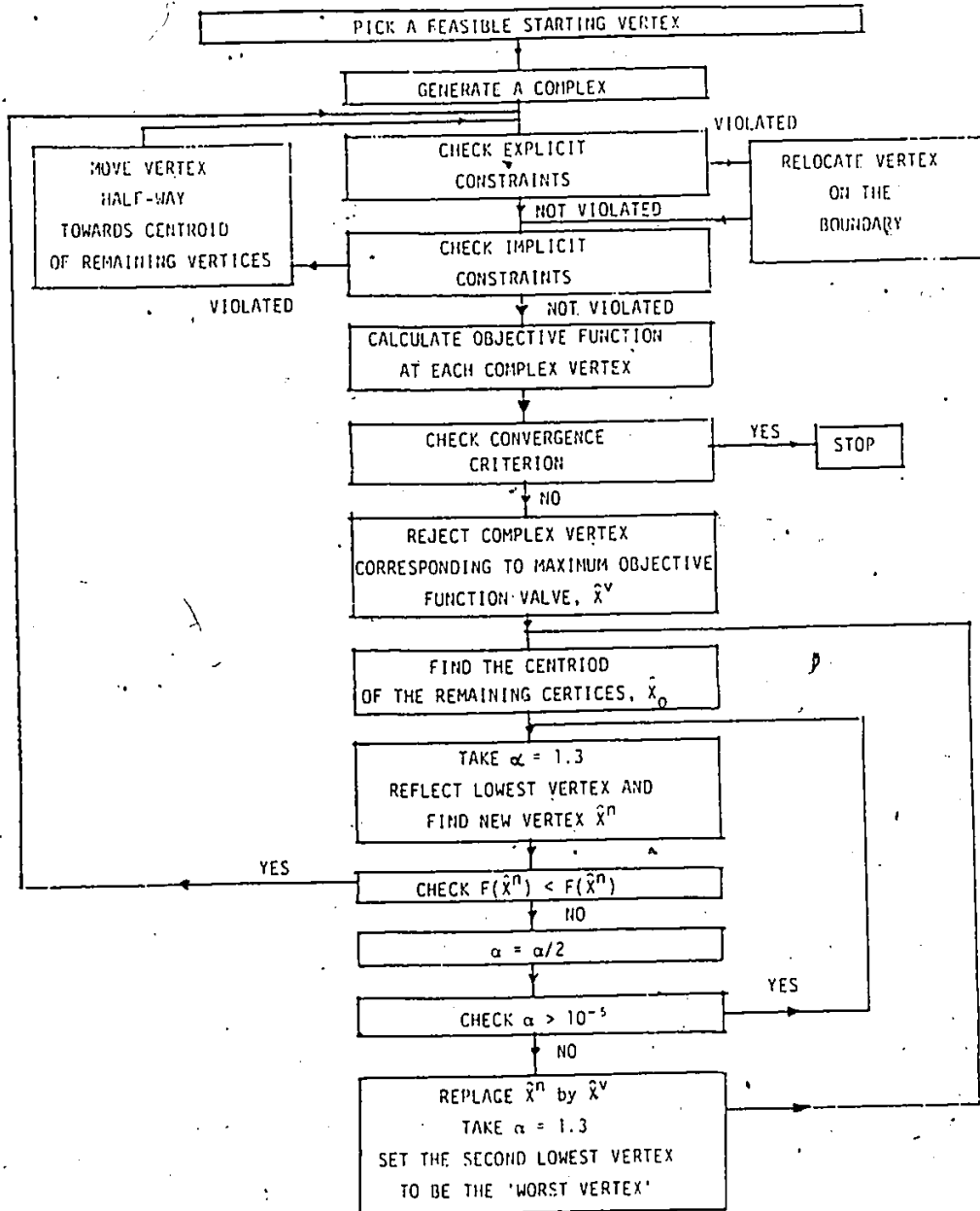


Fig. 5.2: Flow Chart of the Complex Optimization Method.



satisfy the lower and upper bound constraints. If some implicit constraints are violated, then the trial point is moved halfway toward the centroid of the already accepted points. The centroid  $\bar{x}_c$  is given by the expression

$$\bar{x}_c = \frac{1}{s} \sum_{k=1}^s x^k \quad (5.6)$$

where  $\bar{x}^1, \bar{x}^2, \dots, \bar{x}^s$  are available feasible vertices.

(iii) The objective function  $F(\bar{x})$  to be minimized is evaluated at each vertex and the vertex  $\bar{x}^v$  at which the function  $F(\bar{x})$  assumes the largest value is reflected by computing

$$\bar{x}^r = (1+\alpha)\bar{x}^0 - \bar{x}^v, \text{ with } \alpha \geq 1 \quad (5.7)$$

where  $\bar{x}^0$  is the centroid of the remaining vertices and is calculated from

$$\bar{x}^0 = \frac{1}{k-1} \sum_{\substack{i=1 \\ i \neq v}}^k x^i \quad (5.8)$$

(iv) If the function value  $F(\bar{x}^r) < F(\bar{x}^v)$  and  $\bar{x}^r$  is feasible, the point  $\bar{x}^v$  is replaced by  $\bar{x}^r$  and step (ii) is repeated. If  $F(\bar{x}^r) \geq F(\bar{x}^v)$ , the overreflection coefficient is reduced to  $\frac{\alpha}{2}$ , and new  $\bar{x}^r$  computed and tried. This is repeated until  $\alpha \leq \beta$  where  $\beta = 10^{-5}$  is a satisfactory value. If the relation  $F(\bar{x}^r) < F(\bar{x}^v)$  does not hold even for that small value of  $\alpha$ , then the projected point  $\bar{x}^r$  is replaced by the original value  $\bar{x}^v$  and the second worst vertex is reflected instead. This process keeps the complex moving toward the minimum unless the centroid is very close to it.

(v) For a nonconvex function, the centroid of all feasible

points may not itself be feasible. In this case all the points of the complex are discarded except  $\bar{x}^e$ , the point at which the objective function has the lowest value. Then the new complex is generated by using

$$x_i^k = x_i^e + r_i (x_i^0 - x_i^e) ; \quad i = 1, 2, \dots, n \quad (5.9)$$

where  $[\bar{x}^0 : x_1^0, x_2^0, \dots, x_n^0]$  is the previous infeasible centroid.

(vi) The process is terminated when the complex shrinks to an acceptably small size. Such a termination criterion can be expressed as

$$\frac{1}{k} \left\{ \sum_{i=1}^k [F(x^0) - F(x^k)]^2 \right\}^{\frac{1}{2}} \leq \epsilon \quad (5.10)$$

where  $\epsilon > 0$  is a predetermined, small convergence number.

#### 5.4 Results and Discussion on the Optimized System

The constrained optimization results of two and three parameters optimization schemes are shown in Tables 5.1 and 5.2 respectively. The results given in both tables indicate that the optimal bearing stiffness should be closer to its upper limit.

The optimal bearing spacing for the two optimization schemes have been found to be different, however, they are in the same proximity. Referring to Table 5.2, it can be concluded that the diameter of the element 8 should also be near the higher limit.

The results of the optimization indicate that the maximum mean square response of the workpiece can be reduced by about 23.33% if the optimal values of the bearing stiffness and the bearing spacing are used in place of the existing design values. A reduction of 28.39% in the

TABLE 5.1

Optimal Values for Two Parameter Optimization

$$\frac{K_r}{K_f} = 0.3135$$

$$c_f = 22.328 \times 10^3 \frac{N \text{ sec}}{m}$$

$$c_r = 28.632 \times 10^3 \frac{N \text{ sec}}{m}$$

Tool located at joint #3

Highest Frequency = 187.5 Hz

| Parameters             | Lower Limit                      | Upper Limit                      | Starting Valves                   | Optimum Valves                   | Values in the Existing Design    |
|------------------------|----------------------------------|----------------------------------|-----------------------------------|----------------------------------|----------------------------------|
| $K_f$                  | $76.526 \times 10^7 \frac{N}{m}$ | $535.71 \times 10^7 \frac{N}{m}$ | $408.345 \times 10^7 \frac{N}{m}$ | $533.22 \times 10^7 \frac{N}{m}$ | $153.06 \times 10^7 \frac{N}{m}$ |
| $L_B$                  | 0.0587 m                         | 0.531 m                          | 0.419 m                           | 0.415 m                          | 0.470 m                          |
| Max. $[E(\frac{W^2})]$ | —                                | —                                | $2.542 \times 10^{-15} m^2$       | $2.452 \times 10^{-15} m^2$      | $3.198 \times 10^{-15} m^2$      |

TABLE 5.2

Optimal Values for Three Parameter Optimization

Highest frequency = 187.5 Hz

$$c_f = 22.328 \times 10^3 \frac{\text{N sec}}{\text{m}}$$

Tool located at joint #3

$$c_r = 28.632 \times 10^3 \frac{\text{N sec}}{\text{m}}$$

$$D_7 = D_9 = D_{10} = 0.254 \text{ m}$$

$$D_{11} = 0.188 \text{ m}$$

$$\frac{K_f}{K_r} = 3.190$$

$$D_{12} = 0.170 \text{ m}$$

|                               | PARAMETERS                     |            |            |  |
|-------------------------------|--------------------------------|------------|------------|--|
|                               | $K_f$<br>N/m x 10 <sup>7</sup> | $L_B$<br>m | $D_0$<br>m | Max. $[E(\bar{W}^2)]$<br>x 10 <sup>-15</sup><br>m <sup>2</sup> |
| Lower Limit                   | 76.526                         | 0.0587     | 0.0762     | —  |
| Upper Limit                   | 535.71                         | 0.531      | 0.254      | —  |
| Values in the Existing Design | 153.06                         | 0.470      | 0.2283     | 3.198  |
| Optimum Values                | 532.56                         | 0.4200     | 0.2539     | 2.290  |

maximum MSD is possible if in addition to optimal bearing and spacing, the optimal diameter for element 8 is used. This shows that an additional reduction of approximately 5% is attributed to the selection of optimal diameter for element 8.

#### 5.5 Effect of Chuck Diameter on the Mean Square Response of the Optimized System

The chuck in a lathe is used for holding a workpiece and its size (diameter) is normally dictated by the size of the workpiece to be machined and by the swing of the lathe.

In this investigation, the lower and upper limit on the diameter of the chuck are fixed at 0.102m (4 inches) and 0.330m (13 inches) respectively. In order to study the effect of the chuck diameter on the mean square response of the system, the chuck diameter on the optimized system presented in chapter 4 was varied between the lower and upper limits and the MSD at the cutting tool location was calculated. The results are shown in Table 5.3. From this table, it can be seen that the maximum workpiece MSD decreased rapidly for increase in the chuck diameter from its lower limit. However, the MSD reached almost a constant minimum value for a chuck diameter greater than 0.203m (8 inches). Hence it can be concluded that the size of chuck in the existing design is itself near the optimal value for a minimum dynamic response.

#### 5.6 Effect of the Size of Workpiece on the Mean Square Response of the Optimal System

In order to study the effect of the various sizes of workpiece on the response of the system, workpieces of constant length but with different diameters were simulated on the optimized system and the MSD

TABLE 5.3

The Effect of the Diameter of Chuck on  
Workpiece Response

|  |  |
|--|--|
| $K_f = 532.558 \times 10^7 \frac{N}{m}$            | Tool at joint #3                             |
| $\frac{K_f}{K_r} = 3.190$                          | $D_7 = D_8 = D_9 = D_{10} = 0.254 \text{ m}$ |
| $c_f = 22.328 \times 10^3 \frac{N \text{ sec}}{m}$ | $D_{11} = 0.188 \text{ m}$                   |
| $c_r = 28.632 \times 10^3 \frac{N \text{ sec}}{m}$ | $D_{12} = 0.170 \text{ m}$                   |
|  | $L_B = 0.420 \text{ m}$                      |

Maximum cutting force frequency = 187.5 Hz

| Diameter of Chuck<br>m | Max. $[E(\bar{w}^2)]$<br>$\times 1.355 \times 10^{-14}$<br>$m^2$ |
|------------------------|--|
| 0.1016 (4 inches)      | 0.217  |
| 0.127 (5 inches)       | 0.187  |
| 0.1524 (6 inches)      | 0.177  |
| 0.1778 (7 inches)      | 0.173  |
| 0.2032 (8 inches)      | 0.170  |
| 0.2286 (9 inches)      | 0.169  |
| 0.254 (10 inches)      | 0.169  |
| 0.2794 (11 inches)     | 0.168  |
| 0.3048 (12 inches)     | 0.168  |
| 0.3302 (13 inches)     | 0.168  |

K7

at the cutting tool location were calculated. The results are presented in Table 5.4. It can be seen from the table that the maximum MSD decreased with an increase in the workpiece diameter or a decrease in the slenderness ratio. Based on this result it can be concluded that for dynamic considerations, a spindle-workpiece system should be designed for the smallest diameter of the workpiece which has its length equal to the maximum center to center distance of the lathe so that the maximum MSD is below the allowable limit.

### 5.7 Conclusions

In this chapter, the effect of the variation of parameters such as bearing stiffness, bearing spacing, and the diameter of the element 8, is discussed first, and then an optimization study, using these parameters as design variables is carried out. This study indicates that for the optimally designed spindle, bearing stiffness and the diameter of the element 8, should be at the upper limit, but the bearing spacing should be towards the higher limit. This study is followed by a study on the effect of the variation of the diameter of the chuck and the slenderness ratio of the workpiece on the maximum MSD response of the optimally designed spindle. This study shows that the maximum MSD response of the system decreases with the increase in the diameter of the chuck whereas it increases with the increase in the slenderness ratio of the workpiece.

Based on this study, the conclusions that can be drawn are:

The greater the diameter of the spindle, the lower would be the maximum MSD response of the workpiece.

There could be a significant decrease in the maximum MSD of the workpiece if the optimal design vector is used instead of the existing

TABLE 5.4

The Effect of Workpiece Slenderness Ratio  
on the Workpiece Response

$$K_f = 5.397 \times 10^9 \frac{N}{m} \quad \text{Tool at joint \# 3}$$

$$\frac{K_f}{K_f} = 3.190 \quad D_7 = D_8 = D_9 = D_{10} = 0.254 \text{ m}$$

$$c_f = 22.328 \times 10^3 \frac{N \text{ sec}}{m} \quad D_{11} = 0.188 \text{ m}$$

$$c_r = 28.632 \times 10^3 \frac{N \text{ sec}}{m} \quad D_{12} = 0.170 \text{ m}$$

$$L_B = 0.420 \text{ m}$$

Maximum cutting force frequency = 187.5 Hz

Length of the workpiece = 0.330 m (13 inches), a constant

| Diameter of Workpiece<br>x 0.0254, m | Slenderness Ratio | Max. Workpiece<br>MSD x $1.355 \times 10^{-14}$<br>$m^2$ |
|--------------------------------------|-------------------|--|
| 2.0                                  | 6.50              | 0.168  |
| 2.285                                | 5.688             | 0.062  |
| 2.666                                | 4.875             | 0.021  |
| 3.200                                | 4.063             | 0.0064   |
| 4.000                                | 3.250             | 0.0018   |
| 5.332                                | 2.438             | 0.00043  |
| 8.000                                | 1.635             | 0.000049   |



design vector.

At first, the MSD response decreases as the diameter of the chuck increases then it reaches a constant value above 0.203m (8 inches) diameter of the chuck.

The maximum MSD response decreases with the decrease in the slenderness ratio.

In the next chapter, additional design considerations such as stiffening of the spindle due to a third bearing and the design of a squeeze film damper, is discussed.

## CHAPTER 6

### EFFECT OF ADDITIONAL BEARING AND EXTERNAL DAMPER ON THE RESPONSE OF A SPINDLE-WORKPIECE SYSTEM

#### 6.1 Introduction

In chapter 4, the PSD of a spindle-workpiece system under different design parameters of the system are presented. The parameters considered are stiffness and damping of front and rear bearings, bearing spacing, workpiece slenderness ratio, cross-sectional area of the spindle, size of chuck, and additional damping in the spindle. In this chapter, the effect of incorporating a third bearing in the spindle on the PSD response of the system is presented. In addition, the effect of an external damper at the free end of the spindle is presented together with the design procedure for this damper.

#### 6.2 Effect of Introducing a Third Bearing in the System

The possibility of increasing the overall stiffness of the system by introducing a third bearing, was studied by Bollinger [42]. In this work the third bearing was incorporated between the front and the rear bearing. This resulted in the increase in the first natural frequency and decrease in the static deflection at the chuck.

In order to investigate the effect of a third bearing on the spindle-workpiece system, in the present investigation an optimized spindle-workpiece system presented in chapter 5 is selected. Then the parameters considered in the study would be (a) the magnitude of the stiffness of the third bearing, and (b) the spacing between the bearings. The results due to the variation of these parameters are shown in Table 6.1. Referring to this table, one can see that there is no significant

TABLE 6.1

Parametric Variations for the Third Bearing

$$W_0^* = \frac{\text{MSD Response at Joint \#3 with Third Bearing}}{\text{MSD Response of the Optimized System}}$$

Tool Located at Joint #3

$$K_f = 5.325 \times 10^6 \text{ KN/m}$$

$$\frac{K_f}{K_r} = 3.190$$

Highest cutting force frequency = 187.5 Hz

Spacing between the front and the rear bearing = 0.4200 m

MSD response of the three parameter optimized system without third bearing =  $2.29 \times 10^{-15}$ , m<sup>2</sup>

$$c_f = 22.328 \times 10^3 \frac{\text{N sec}}{\text{m}} \quad D_7 = D_8 = D_9 = D_{10} = 0.254 \text{ m}$$

$$c_r = 28.632 \times 10^3 \frac{\text{N sec}}{\text{m}} \quad D_{11} = 0.188 \text{ m}$$

$$D_{12} = 0.170 \text{ m}$$

| Third Bearing Stiffness<br>x 10 <sup>6</sup> , KN/m | W <sub>0</sub> <sup>*</sup> , Normalized MSD response at joint number 3 with the third bearing spacing (distance between rear and third bearing) equal to |            |            |            |            |
|---|---|------------|------------|------------|------------|
|   | 0.058<br>m  | 0.130<br>m | 0.202<br>m | 0.274<br>m | 0.347<br>m |
| 1.531   | 0.994   | 1.130      | 1.118      | 1.118      | 1.065      |
| 2.231   | 1.006   | 1.071      | 1.071      | 1.071      | 1.041      |
| 2.932   | 1.029   | 1.030      | 1.041      | 1.036      | 1.024      |
| 3.632   | 1.047   | 1.012      | 1.024      | 1.018      | 1.012      |
| 4.333   | 1.059   | 1.000      | 1.006      | 1.006      | 1.006      |
| 5.033   | 1.065   | 0.988      | 1.000      | 0.994      | 1.000      |

decrease in the MSD response due to either of the parametric variations. In fact, for the third bearing stiffness values  $2.231 \times 10^6$  KN/m- $4.332 \times 10^6$  KN/m, the presence of a third bearing increases the MSD response compared to an optimized system with only two bearings. It can be seen that slight improvement in the MSD response is possible by using either a very low or a very high value of bearing stiffness. In order to estimate the best combination of bearing stiffness and bearing spacing, an optimization was carried out. The results obtained by this optimization are shown in Table 6.2. Referring to this table, one can infer that there is only an improvement of 1.8% in the design of the system by incorporating a third bearing.

### 6.3 External Damping in the Spindle-Workpiece System

#### 6.3.1 Introduction

The influence of stiffness on the response of a lathe spindle-workpiece system has been studied extensively and presented in chapters 4 and 5. The purpose of this section is to provide detailed information on the influence of external damping on the spindle-workpiece system.

The static stiffness of a machine tool is defined as the ratio of the force to displacement. In the machine tool design, the consideration of the static stiffness only is not sufficient because the cutting forces, which are wide band in nature, act on the spindle-workpiece system. Therefore, due to the presence of high inertia forces, the dynamic stiffness also has to be considered. The dynamic stiffness can be mathematically written as

$$\frac{F}{X} = k - m\omega^2 + j\omega c \quad (6.1)$$

TABLE 6.2

Optimal Values for the Third Bearing

Maximum cutting force frequency = 187.5 Hz

MSD response of the three parameter optimized system without third bearing =  $2.29 \times 10^{-15}$ ,  $m^2$

$$K_f = 5.325 \times 10^6 \text{ KN/m}$$

$$\frac{K_f}{K_r} = 3.190$$

$$W_o^* = \frac{\text{MSD response of the optimized system with the third bearing}}{\text{MSD response of the optimized system without the third bearing}}$$

Distance between the front and the rear bearing = 0.4200 m (16.535 inches)

$$c_f = 22.328 \times 10^3 \frac{\text{N sec}}{\text{m}}$$

$$c_r = 28.632 \times 10^3 \frac{\text{N sec}}{\text{m}}$$

Tool located at joint #3

$$D_7 = D_8 = D_9 = D_{10} = 0.254 \text{ m}$$

$$D_{11} = 0.188 \text{ m}, D_{12} = 0.170 \text{ m}$$

|               | PARAMETERS                        |              |                               |
|---------------|-----------------------------------|--------------|-------------------------------|
|               | Stiffness<br>$\times 10^6$ , KN/m | Spacing<br>m | Objective Function<br>$W_o^*$ |
| Lower Limit   | 0.765                             | 0.058        | —                             |
| Upper Limit   | 5.357                             | 4.064        | —                             |
| Optimum Value | 5.357                             | 0.1667       | 0.982                         |

The equation (6.1) has been based on the fact that a machine tool is a single-degree-of-freedom system and that the various modes can be uncoupled whereby the system response can be analyzed on a mode to mode basis.

Similarly, the dynamic impedance can be mathematically written as

$$\frac{F}{V} = \frac{F}{\dot{x}} = c + j(\omega m - \frac{k}{\omega}) \quad (6.2)$$

In equation (6.1), if  $\omega = 0$ , then  $F = kx$  i.e., the existing force is balanced by the elastic restoring force. On the other hand, when  $\omega = \omega_n$ , i.e. the natural frequency of the system, then the restoring elastic force and the inertia force are in quadrature with the driving force and only the damping force is the only one to balance the driving force. This explains why just an increase in stiffness is not sufficient for controlling the vibrations in the range of resonance frequencies.

### 6.3.2 Dynamic Damped Vibration Absorbers

One of the ways of reducing the response of a spindle-workpiece system is to use an external damped vibration absorber. The principle behind an absorber design is to attach a secondary mass, spring and a damper to the main mass or structure in such a way so that the receptance of the main mass or the structure is considerably reduced in a particular frequency range. For systems excited with a constant frequency disturbance, the problem of controlling the vibration is relatively easy to solve using an absorber which is tuned so as to shift the resonance peak of the main system. The disadvantage in using an absorber is that instead of one peak in the receptance versus frequency diagram, two peaks occur but both of these two new peaks are

far away from the original peak [51]. Thus the receptance can be suppressed only in a narrow frequency range. These absorbers could be passive or active with feedback control [69]. The electromagnetic based active absorbers are complex and expensive devices. Their practical applications is limited to simple machine tool systems and considerable difficulties arise dealing with multi-degree-of-freedom systems. In these cases, some of the modes become unstable. Some interesting results have been obtained by Umback [70] and Van Herck [71]. Figure 6.1 shows the effect of varying damping ratio on the dynamic amplitude of a two degree-of-freedom system. The damping ratio is shown along the abscissa and the ratio of the maximum displacement to the static displacement amplitude is shown along the ordinate. The ratio of the secondary to the primary mass is represented by  $\mu$ . The damping of the main system has been taken equal to zero. It can be seen from Fig. 6.1 that as the mass increases, the dynamic displacement of the main mass decreases and also there is a corresponding increase in the optimal damping ratio. This problem has also been solved graphically by Van Herck [71]. He used dynamic resistance, which is the ratio of the externally applied force amplitude to the velocity response amplitude, as the criterion for the optimization. The optimum parameters resulting from Van Herck's graphical solution were quite close to that of Umback's.

Stone and Andrew [72] designed a two dimensional vibration absorber for a horizontal milling machine and is shown in Fig. 6.2. This absorber incorporated a polymeric material as a damping element, and was very effective against chatter. The optimal design of this absorber was based on minimizing the maximum negative in-phase component of the chatter receptance. The chatter receptance of the milling machine

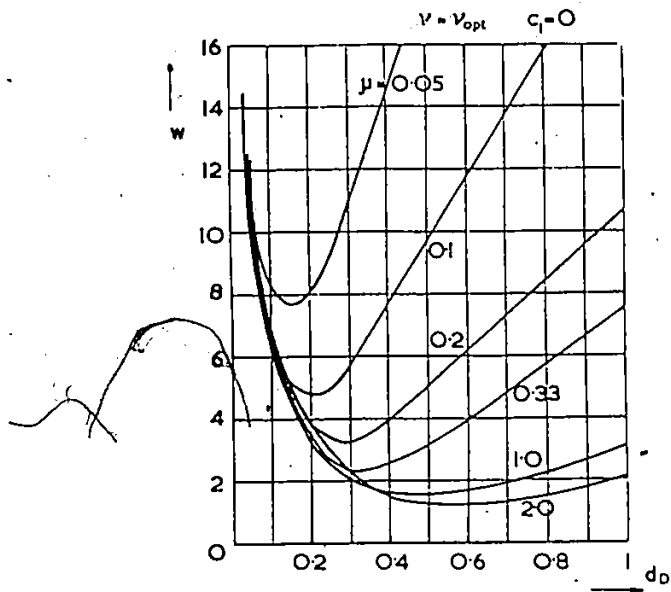


Fig. 6.1: Decrease of the Resonance Amplitude by Means of an Absorber in Relation to its Frequency and Damping (after Umback [70]).



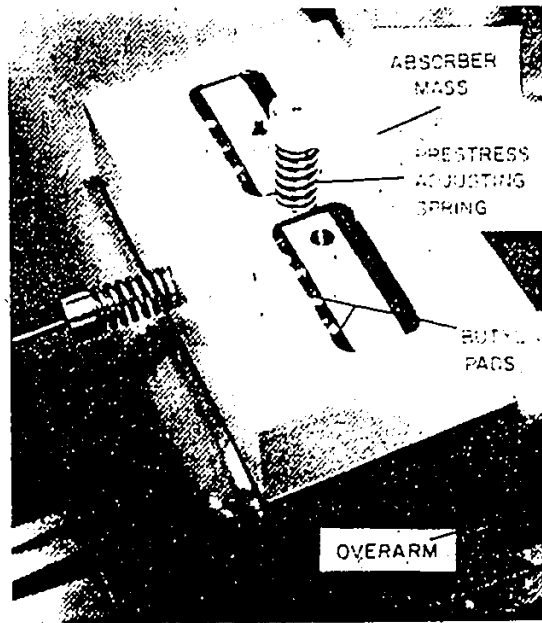


Fig. 6.2: Two-Dimensional Absorber for a Milling Machine (after Stone and Andrew [72]).

without and with the absorber are shown in Figs. 6.3 and 6.4 respectively. It can be seen from these two figures that the negative in-phase component can be reduced by a factor of six if this optimally designed absorber is used. The forced vibration behavior of the milling machine with and without the absorber is also shown in Fig. 6.5, which is a plot of modulus of forced vibration receptance versus frequency. It is evident from this figure that the absorber is very effective in reducing the receptance near the natural frequencies. The peak receptance is reduced by a factor of approximately three.

The vibration absorbers have not been very successfully applied in the case of lathe spindles because workpiece of various sizes are held by a chuck which is an integral part of the spindle. Therefore, the primary mass itself changes consequently, the tuning of the absorber is not possible unlike in the case of milling machines where the cutter, instead of the workpiece, is mounted on the spindle. The second unfavorable reason is that of the limitation of the size of the secondary mass which can be attached to the spindle. If this secondary mass is small then the effectiveness of the absorber is minimal and as a result, the tuning becomes difficult. Finally, the cutting forces in turning operations are wide band in nature, therefore, the absorbers are not very effective in controlling the vibrations over a wide frequency region. Thus, fluid dampers which are quite effective in such situations, have to be used, and a design of such a damper is discussed in the next section.

### 6.3.3 Fluid Damper

The principle of operation of a fluid damper is to squeeze a

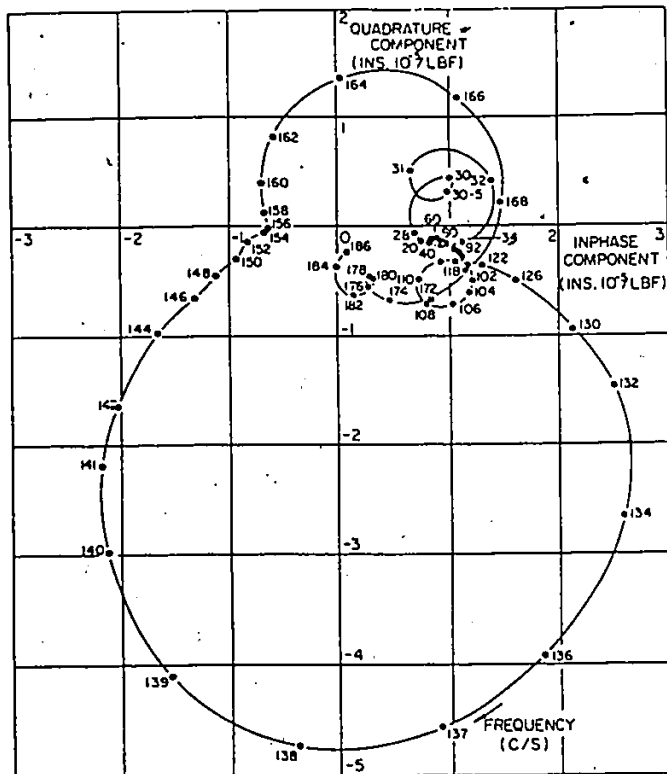


Fig. 6.3: Chatter Receptance of Machine Without Absorber (after Stone and Andrew [72]).

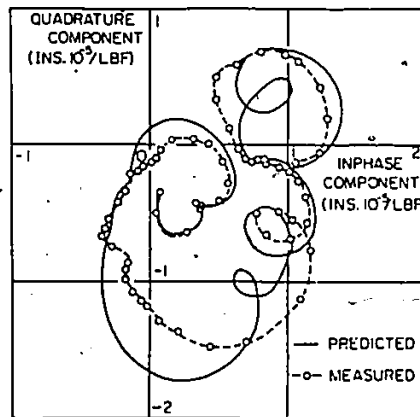


Fig. 6.4: Predicted and Measured Optimized Chatter Receptance With Two-Dimensional Absorber Added (after Stone and Andrews [72]).

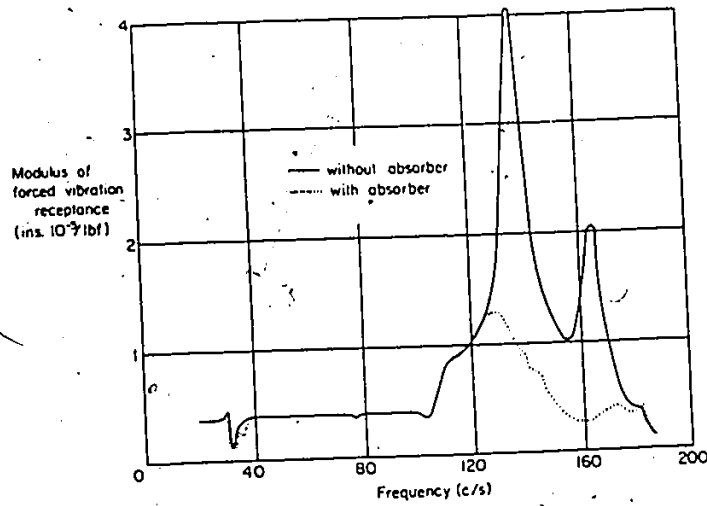


Fig. 6.5: Amplitude of Forced Vibration Receptance With and Without Absorber (after Stone and Andrew [72]).

a liquid film between two plates or in a cylindrical gap. There are certain requirements for these kind of dampers to be effective and they are [73]:

1. The fixed member should be rigid and not move with the element to be clamped. This is because the externally applied force is damped while being transmitted through a viscous medium and energy is dissipated due to the squeezing of a film of a liquid. If the fixed member moves, then the squeezing action does not take place.

2. The gap between the transmitting and the transmitted bodies should be wide enough to prevent their mutual contact. This can be explained by the fact that squeeze film effect would cease if the two bodies touch each other.

3. The damping constant must be adjustable from case to case. For too high a value of the damping constant, the fluid medium acts like a rigid body or support. Similarly if the damping constant is too low, then the transmissibility of the force will be high due to the light damping.

Figure 6.6 shows a fluid damper used by Peters [74], for a lathe spindle. In this damper the oil flows continuously, and the vibration of the spindle is damped due to the oil film squeezed between the spindle and the bushing.

#### 6.3.4 Theoretical Formulation of a Damper

The theoretical formulation of a damper can be obtained by using Newton's laminar flow theory.

For a rectangular liquid film with unidirectional flow (refer to Fig. 6.7), the expression for the force required to move the fluid with

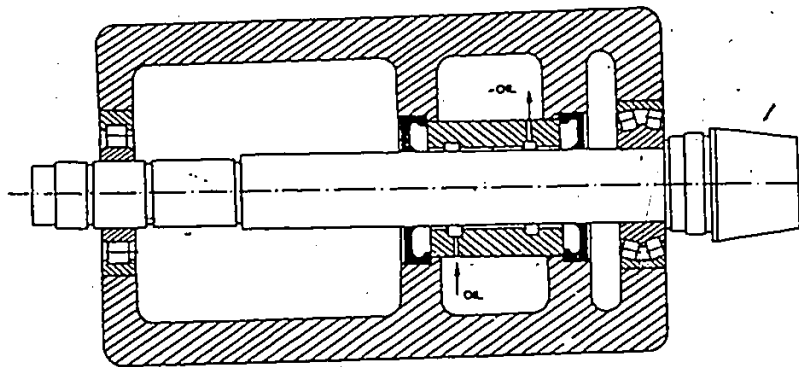


Fig. 6.6: Relative Viscous Damper of Spindle of a Lathe  
(after Peters [74]):

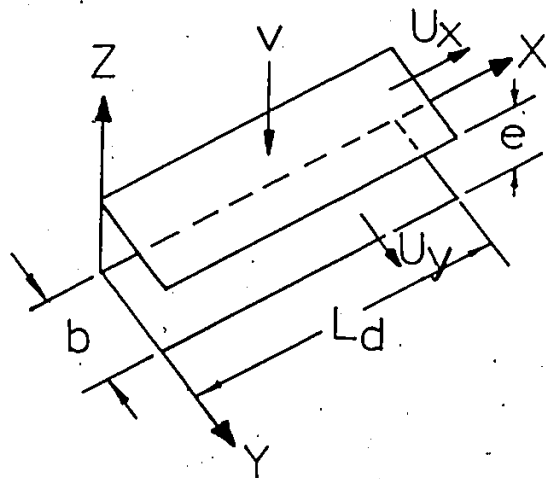


Fig. 6.7: Flat Liquid Film Damper.



a velocity  $v_d$  can be given by Peters [73]:

$$F_d = -v_d \left( \frac{L_d b^3}{12} \right) \left( \frac{12 \eta_d}{e^3} + \frac{j\omega \rho_d}{e} \right) \quad (6.3)$$

where,

$F_d$  is the force,

$v_d$  is the velocity,

$L_d$  is the length of plates,

$b$  is the width of plates,

$\eta_d$  is the dynamic viscosity coefficient of the fluid,

$e$  is the gap between the plates,

$\rho_d$  is the specific mass of the fluid,

$\omega$  is the frequency.

For rectangular liquid film with free flow in two directions:

$$F_d = -v_d \left( \frac{12 \eta_d}{e^3} + \frac{j\omega \rho_d}{e} \right) \left( \frac{4 L_d b}{\pi^2} \right)^3 \quad (6.4)$$

$$\sum_{m=0}^{\infty} \sum_{n=0}^{\infty} \frac{1}{m^2 n^2 (b^2 m^2 + L_d^2 n^2)}$$

where  $m$ , and  $n$  are odd integers. For a circular liquid film damper:

$$F_d = -\frac{\pi R_d^4 v_d}{8} \left( \frac{12 \eta_d}{e^3} + \frac{j\omega \rho_d}{e} \right) \quad (6.5)$$

where,  $R_d$  is the radius of the circular plate.

For a cylindrical damper with tangential flow:

$$F_d = -\pi R_d^3 v_d L_d \left( \frac{12 \eta_d}{e^3} + \frac{j\omega \rho_d}{e} \right) \quad (6.6)$$

For a cylindrical damper with only axial flow:

$$F_d = - \frac{\pi L_d^3 R_d v_d}{12} \left( \frac{12 \eta_d}{e^3} + \frac{j\omega \rho_d}{e} \right) \quad (6.7)$$

For a cylindrical damper with axial and tangential flow:

$$F_d = 2v_d \left( \frac{12 \eta_d}{e^3} + \frac{j \rho_d \omega}{e} \right) R_d^3 \pi \left[ R \frac{e^{L_d/2R_d} - 1}{1 + e^{-L_d/R_d}} - R_d \frac{e^{L_d/2R_d} - 1}{1 + e^{-L_d/R_d}} - \frac{L_d}{2} \right] \quad (6.8)$$

All of these equations have a common form and can be expressed as

$$F = v_d C_d + j\omega v_d M_d = v_d C_d + a_d M_d \quad (6.9)$$

In equation (6.9) one can see that the force needed to move the film has two components: one in phase with the velocity and one in phase with the acceleration.

In all of these equations, the term containing  $v_d$  gives the component of the force to overcome viscous resistance. This force is proportional to the viscosity of the fluid and is inversely proportional to the cube of the gap-width. The coefficient  $C_d$  in the equation (6.9) has the dimensions of damping coefficient. The second term in all these equations contains  $\rho$  and the corresponding force is in phase with the acceleration. This component of the force is directly proportional to the frequency and the specific mass. Surprisingly, it is also a function of the gap-width and is inversely proportional to it. The coefficient  $M_d$  has a dimension of a mass and it is, in reality, the equivalent mass of

the moving fluid. Separating the real and the imaginary parts in equation (6.8) we can write

$$C_d = \frac{\text{Real}(F_d)}{v_d}, \text{ and} \quad (6.10)$$

$$M_d = \frac{\text{Imaginary}(F_d)}{a_d} \quad (6.11)$$

Finally, the expressions for  $C_d$  and  $M_d$  can be written in a unified way as:

$$C_d = H_d \eta_d \frac{b^4}{e^3}, \text{ and} \quad (6.12)$$

$$M_d = H_d \eta_d \frac{b^4}{12e}, \quad (6.13)$$

where,  $H_d$  is a coefficient which depends upon the shape of a damper. Depending upon the geometry,  $H_d$  can be evaluated by using the following expressions:

For flat dampers:

(i) For circular cross-section damper:

$$H_d = \frac{3\pi}{32} = 0.29453 \quad (6.14a)$$

(ii) For rectangular damper with unidirectional flow in the b direction:

$$H_d = \frac{L_d}{b} \quad (6.14b)$$

(iii) For rectangular damper with free flow:

$$H_d = 6.7988 \left(\frac{L_d}{b}\right)^3 \sum_{m=0}^{\infty} \sum_{n=0}^{\infty} \frac{1}{m^2 n^2 [m^2 + (L_d/b)^2 n^2]} \quad (6.14c)$$

For cylindrical dampers:

(i) For pure axial flow:

$$H_d = \frac{\pi}{2} (L_d/b)^3 \quad (6.15a)$$

(ii) For pure tangential flow:

$$H_d = \frac{3\pi}{2} (L_d/b) \quad (6.15b)$$

(iii) For free flows in the axial as well as tangential directions:

$$H_d = \frac{3\pi}{2} \left( \frac{L_d}{b} - \tanh \frac{L_d}{b} \right) \quad (6.15c)$$

#### 6.3.5 Location of the Fluid Damper

The location of the fluid damper has been studied by Van Herck [75] and the results obtained are presented in Fig. 6.8. In Fig. 6.8, the ratio of the static deflection at the chuck to the resonant amplitude at the chuck has been plotted against the damper location. From Fig. 6.8 one can conclude that the best effect of an external damper can be achieved if it has high damping coefficient  $C_d$  and located near the front bearing. The author however recommended that the damper be located in the middle of the bearings where the effect of damper is insensitive to the frequency changes of the stiffness of the bearings and of the frequency. Similar studies were carried out by Bollinger [42] who found that the best results are obtained if the damper is located at the free end. The studies in chapter 4 also confirmed that the free end is the most effective location for the external damper. Therefore the damper

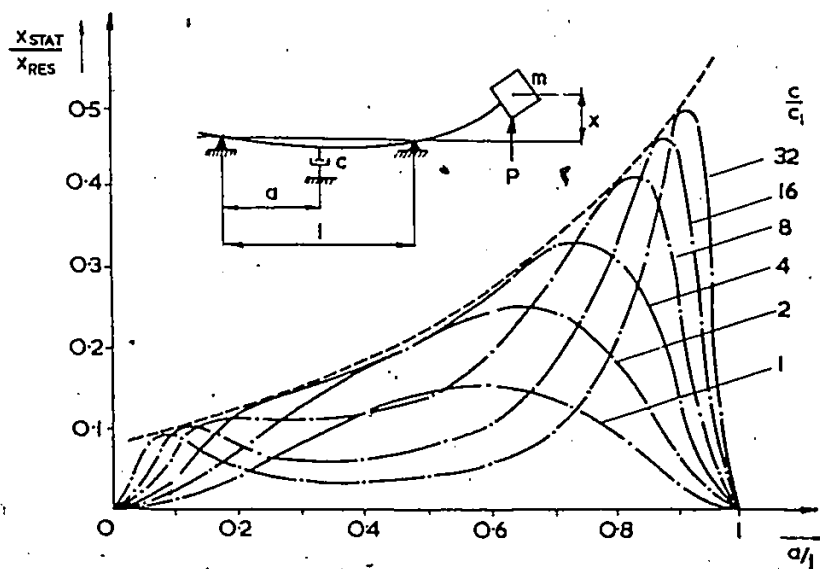


Fig. 6.8: Influence of Location of Damper (after Peters [74]).

design is based upon locating the damper at the free end.

### 6.3.6 Design of a Squeeze Film Damper for the Spindle-Workpiece System

The external damper would be of cylindrical shape as shown in Fig. 6.9. The design of the damper is based on the following set of formula [73]:

$$C_d = H_d \eta_d \frac{b^4}{e^3}, \quad (6.16)$$

$$M_d = H_d \rho_d \frac{b^4}{12e}, \quad \text{and} \quad (6.17)$$

$$H_d = \frac{3\pi}{2} \left( \frac{L_d}{b} - \tanh \frac{L_d}{b} \right) \quad (6.18)$$

where,

$b$  = diameter for cylindrical sleeves,

$e$  = width of the damper gap,

$\eta_d$  = dynamic viscosity,

$\rho_d$  = specific mass,

$H_d$  = a coefficient depending upon the shape of the damper,

$L_d$  = length of the cylindrical damper,

$C_d$  = damping constant, and

$M_d$  = equivalent mass of the oil.

The damper design is based on minimizing the dynamic amplification at the first mode. The following numerical values for the various parameters of the damper are selected:

$$L_d = 7.62 \times 10^{-2} \text{m (3")}$$

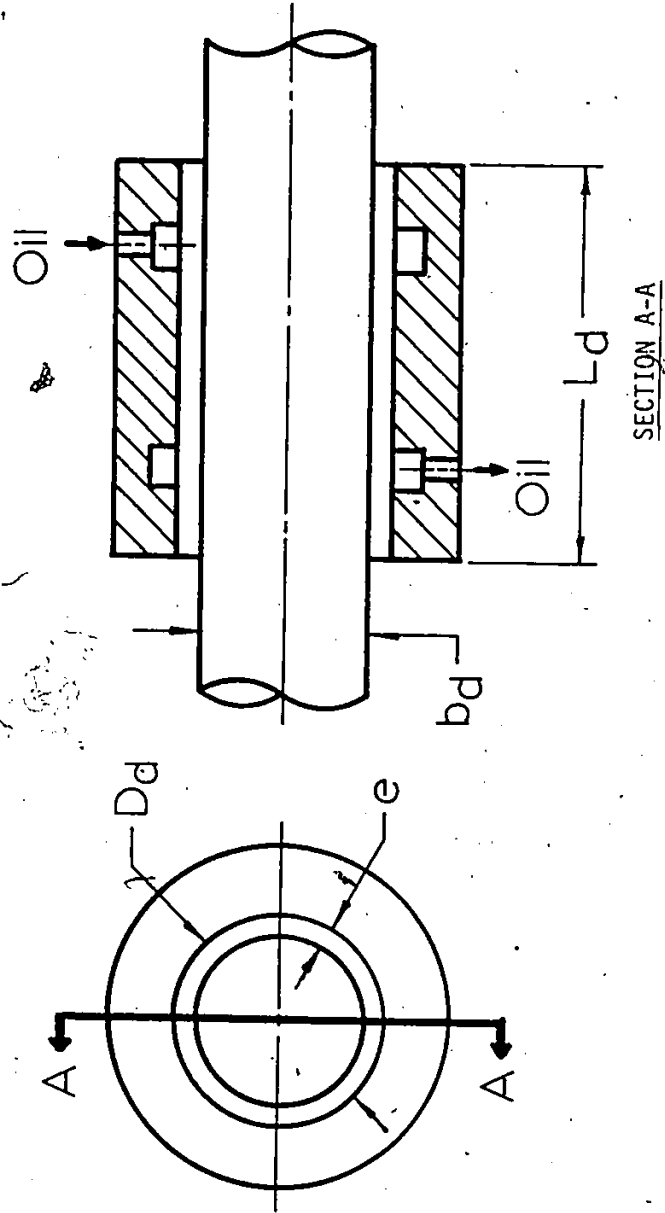


Fig. 6.9: Designed Fluid Dampèr

$$b = 0.169672\text{m (6.68")}$$

$$\eta_d = 0.563 \text{ Nm}^{-2} \text{ sec}$$

$$\rho_d = 890 \text{ kg/m}^3$$

$0.5 \times C_c$ , half of the critical damping constant =  $19.185 \times 10^5 \text{ N sec/m}$

Using the afore mentioned values of the parameters in equation (6.15), the value of  $H_d$  can be found as 0.130358. Substituting this value of  $H_d$  in equation (6.16), one obtains  $e = 0.000317\text{m}$ .

Peters [72], in order to reduce the discrepancy in the computed natural frequency and the experimentally obtained natural frequency when a squeeze film damper as outlined in this chapter was used, suggested a modification to equations (6.16), (6.17), and (6.18). He used a new parameter  $b_m$ , in place of  $b$  in all these equations. The relationship between  $b_m$  and  $b$  is given as

$$b_m = b + 2e \quad (6.19)$$

This modification as suggested by Peters was due to the addition of boundary effects in the damper design. Now, combining the equations (6.16) and (6.18), and (6.19) one can write

$$C_d = \frac{3\pi}{2} \left( \frac{L_d}{b+2e} - \tanh \frac{L_d}{b+2e} \right) \eta_d \frac{b+2e}{e^3} \quad (6.20)$$

Substituting the numerical values of all the parameters as before, the equation (6.20) was solved for  $e$ , by an iterative procedure. The new value of  $e_{\text{new}}$  obtained, was equal to 0.000318m.

Thus, all the parameters necessary to design a squeeze film damper have been calculated and the necessary details of this damper are



shown in Fig. 6.9.

In order to estimate the order of magnitude of improvement in the mean square response of the spindle-workpiece system when a fluid damper of different damping coefficient is incorporated at the free end. The normalized maximum mean square response on an optimized spindle, (optimal bearing stiffness and spacing, and diameter of the spindle) is shown in Table 6.3. This table shows that there could be 36.8% reduction in the maximum MSD response if the designed fluid damper is used. Figure 6.9 shows the various dimensions of this damper.

#### 6.4 Conclusions

In this chapter, the effect of a third bearing as a means of stiffening the spindle-workpiece system is studied. As a first step, a parametric study involving its stiffness and its location is carried out and followed by an optimization study. The study indicates that there is no significant improvement in the performance of the system by incorporating a third bearing on an optimally designed spindle (optimal bearing stiffness and spacing of a two bearing spindle-workpiece system).

Introduction of additional damping, as another means of improving the system performance is studied next. The effect of vibration absorbers and fluid dampers on the response of the spindle-workpiece system is also studied. It is concluded that the fluid damper is the most suitable candidate for improving the system response. The equations for the design of the damper are discussed and the geometric configuration of the damper is computed. Finally, the effect of an external damper located at the free end on the MSD response of an optimal system is discussed.

TABLE 6.3

The Effect of Additional Damping Applied at the  
Free-End on the MSD Response of the Three  
Parameter Optimized System

$$K_f = 5.325 \times 10^9 \text{ N/m}$$

$$\frac{K_f}{K_r} = 3.190$$

Highest cutting force frequency = 1250 Hz

Spacing between the bearings = 0.4200

$$c_f = 22.328 \times 10^3 \frac{\text{N sec}}{\text{m}}$$

$$c_r = 28.632 \times 10^3 \frac{\text{N sec}}{\text{m}}$$

$$D_7 = D_8 = D_9 = D_{10} = 0.254 \text{ m}$$

$$D_{11} = 0.188 \text{ m}$$

$$D_{12} = 0.170 \text{ m}$$

Normalizing value for the Max. MSD response =  $6.030 \times 10^{-15}, \text{m}^2$

$$c_c = 38.371 \times 10^5 \frac{\text{N sec}}{\text{m}}$$

| Damping Applied at the Free End of the Spindle (% $c_c$ ) | Normalized Max. MSD Response |
|---|------------------------------|
| 0   | 1.0                          |
| 0.25  | 0.782                        |
| 0.30  | 0.739                        |
| 0.35  | 0.703                        |
| 0.40  | .674                         |
| 0.45  | .649                         |
| 0.50  | .632                         |

Based on these studies, the following conclusions are drawn:

Inclusion of the third bearing does not lead to any significant stiffening of the spindle-workpiece system.

It is possible to design a fluid film damper which can significantly decrease the maximum MSD response of the system.

## CHAPTER 7

### CONCLUSIONS AND RECOMMENDATIONS

This is a computer based analytical investigation of a design of lathe spindles. In designing lathe spindles, there are several important factors which have to be taken into account. Some of these factors are, for example, location of the bearings, stiffness of the bearings, sectional rigidity of the spindle, possibility of using an external damper etc. The various parameters should be selected in such a manner so that the maximum displacement response of the workpiece-spindle system, be as small as possible.

A mathematical model of the spindle-workpiece system acted upon by random cutting forces have been formulated using finite element analysis. The theoretically obtained natural frequencies have been compared with the experimentally obtained natural frequencies in order to establish the boundary condition at the workpiece-running center interface. The variation of the natural frequencies and the undamped mode shapes as a function of the bearing stiffness have also been analyzed.

The forced vibration behavior of the system has been analyzed using modal analysis. The dynamic displacement response of the system has been studied by varying the parameters such as tool feed rate, bearing stiffness, bearing spacing, structural damping and the sectional rigidity of the spindle. The optimal design of the system has been obtained by simultaneously varying parameters such as bearing stiffness, bearing spacing, and the sectional rigidity of the spindle.

Finally, the possibility of using a third bearing has been analyzed and the design of an external fluid damper has also been

discussed.

## 7.1 Major Highlights

### 7.1.1 The Mathematical Model of the System Response Acted Upon by Random Excitations of Arbitrarily Varying Power Spectral Density

A new method for the calculation of the response power spectral density of a linear multi-degree-of-freedom system has been proposed. The method is based on modifying the governing equations of motion of the system with a set of auxiliary variables. As a first step in the calculation of the response, power spectral density matrix, the natural frequencies, and the modal matrix of the modified system were obtained. These matrices were then used to obtain the transfer function of the modified system. This procedure completely eliminates any matrix inversion corresponding to the system transfer function and it requires significantly less computation time for the computer of the response as compared to the conventional method. Two numerical examples have been used to demonstrate the usefulness of this technique.

### 7.1.2 Workpiece Response due to Spatially Moving Random Cutting Forces

The dynamic response of the spindle-workpiece at the moving tool location due to random cutting forces has been obtained. The ensemble of the random cutting forces have been taken to form a white noise process. An equivalent viscous damping to account for the structural damping in the method of the workpiece has been assumed. The investigation indicates that for the range of feed rates normally used in finishing operations, it is not necessary to consider the effect of feed rate in obtaining the

the mean and the variance responses at the tool contact.

### 7.1.3 Dynamic Behavior of Lathe Spindles with Elastic Supports Including Damping

The free vibration behavior of a lathe spindle-workpiece system using finite element analysis has been presented. The investigation has been carried out in three parts, which are: (1) the classification of the end condition at the running center, (2) the determination of the undamped natural frequencies and the mode shapes, and (3) the effect of bearing stiffness on the natural frequencies and the mode shapes. The results show that the workpiece support at the running center can be better represented by hinged condition as compared to the clamped condition; the first four natural frequencies, and the corresponding mode shapes are quite sensitive to any changes in the bearing stiffness.

### 7.1.4 Dynamic Analysis and Optimal Selection of Parameters of a Lathe Spindle Under Random Cutting Forces

The dynamic analysis of an elastically supported lathe spindle-workpiece system subjected to stochastic cutting forces has been presented. The stochastic partial differential equation characterizing the behavior of the system was formulated from the Euler-Bernoulli beam equations. A finite element technique in conjunction with the modal analysis technique, were used to calculate the mean square displacement of the workpiece. The experimentally calculated power spectral density of the cutting forces was used as the input excitation to the mathematical model. The effect of bearing stiffness, bearing location, sectional rigidity of the spindle, and damping on the mean square displacement were studied. Two-parameter (bearing stiffness and bearing spacing), and three-parameter (bearing

stiffness, bearing spacing, and flexural rigidity) optimization have been carried out. The results indicate that if the spindle is designed based on optimal parameters then, there could be a reduction of 23.33% and 28.39% in the maximum mean square response corresponding to the two-parameter and three-parameter optimization, respectively. The results also indicate that an additional third bearing does not significantly stiffen the optimally designed spindle and that an external fluid film damper mounted at the free end of the spindle can be effectively used to reduce the maximum mean square displacement response of the work-piece.

A step-by-step procedure for designing squeeze film damped is also outlined.

#### 7.1.5 Other Applications

The technique adopted in this investigation is fairly general. The technique can be extended to other machine tool spindles without any change in the methodology.

Based on these studies, the following conclusions can be drawn:

- 1) A comprehensive mathematical model of the spindle-workpiece system is developed which utilizes finite element technique in conjunction with modal analysis.
- 2) The end condition of the workpiece-running center connection is better represented by hinged end condition as compared to the clamped end condition.
- 3) The first natural frequency is sensitive to any changes in the low bearing stiffness at lower range but reaches a constant value at

higher bearing stiffness range.

4) The second, the third and the fourth natural frequencies are very sensitive to any changes in the bearing stiffness.

5) The fifth and the higher natural frequencies are insensitive to any changes in the bearing stiffness.

6) For the range of feed rates normally used in machining operations, it is not necessary to consider the effect of feed rate in obtaining the mean and mean square response of the work-piece system.

7) The mean square response of the workpiece decreases with the increase in the structural damping of the workpiece material.

8) The mean square response varies quite significantly along the spindle-workpiece system irrespective of the location of the tool.

9) The free end of the spindle is the most effective location for the reduction of the workpiece mean square response.

10) The MSD decreases with increase in the externally applied damping.

11) There exists an optimum bearing span and bearing stiffness for which the maximum MSD is a minimum.

12) The maximum MSD decreases as the sectional rigidity of the spindle increases.

13) There is insignificant decrease in the maximum MSD of an optimally designed spindle-workpiece system due to an optimally selected and located third bearing.

14) The maximum MSD of the workpiece decreases with the decrease



in the slenderness ratio of the workpiece.

15) An external fluid damper can be designed and very effectively used to reduce the workpiece maximum mean square response by mounting it at the free end of the spindle.

## 7.2 Limitations of the Investigation

The approach used in the present investigation in optimally designing a spindle, has the following limitations:

1) The stochastic excitations process have been treated as a stationary process, and described through their power spectral density variation in the frequency domain.

2) The spindle-workpiece system has been assumed to exhibit a linear behavior.

3) The bearing stiffness and damping values have been assumed to be independent of frequency.

4) The effect of shear deformation and rotary inertia have been assumed to be negligible.

## 7.3 Recommendations for Future Work

The basic purpose of this investigation was to study the flexural response of the spindle-workpiece system due to the cutting forces in a finish turning operation. The system was assumed to be linear. This work can be extended into several areas which are listed below.

1) The bearings can have non-linear stiffness characteristics.

2) The damping of the bearings can be a function of frequency.

3) The mathematical model can be refined to include the effects

shear deformation and rotary inertia.

4) The mathematical model of the spindle-workpiece system can be formulated to include all the nonlinearities and the dynamic analysis further carried out on a linearized model based on the statistical linearization approach.

5) The cutting force spectrum of different materials can be analyzed with a possibility of correlating machinability and some of the statistical parameters of the stochastic cutting forces.

6) The cutting forces, for various depths of cut, feeds and speeds, can be used as the random inputs and using finite element analysis, the life and reliability of the cutting tools can be determined.

7) An approach similar to this thesis can be used to study the spindle dynamics of other machine tools such as hobbing, milling, shaping, etc.

REFERENCES

1. Taylor, S., and Tobias, S.A., "Lumped Constants Method for the Prediction of the Vibrational Characteristics of Machine Tool Structures", Int. M.T.D.R. Conference, 1964.
2. Taylor, S., "A Computer Analysis of an Openside Planing Machine", Int. M.T.D.R. Conference, 1965.
3. Taylor, S., "The Design of Machine Tool Structures Using a Digital Computer", Int. M.T.D.R., 1966.
4. Knight, W.A., and Tobias, S.A., "Torsional Vibrations and Machine Tool Stability", Int. M.T.D.R. Conference, 1969.
5. Cuppan, B.C., and Bollinger, J.G., "Simulation of a Machine Tool Drive and Structure of an Analog Computer", Int. M.T.D.R. Conference, 1966.
6. Tlustý, J., "Die Berechnung des Rahmens der Werkzeugmaschine", Schwerindustrie der Tschechoslowakei, Vol. 1, No. 1, 1955, p. 8.
7. Ernst, H., and Merchant, M.E., "Chip Formation, Friction and High Quality Machined Surface", from "Surface Treatment of Metals", Trans. ASME, Vol. 29, 1941, pp. 299-328.
8. Merchant, M.E., "Basic Mechanics of the Cutting Process", Journal of Applied Mechanics, Vol. 11, 1944, pp. 168-175.
9. Merchant, M.E., "Mechanics of Metal Cutting Process", Journal of Applied Physics, Parts I and II, Vol. 16, 1945, pp. 267-275 and 318-324.

10. Lee, E.H., and Shaffer, B.W., "The Theory of Plasticity Applied to a Problem of Machining", Journal of Applied Mechanics, Vol. 18, Trans. ASME, Vol. 73, 1951, pp. 405-413.
11. Sabberwall, A.J.P., "Chip Section and Cutting Force During Milling Operations", C.I.R.P., 1961.
12. Sabberwall, A.J.P., "Cutting Forces in Down Milling", Int. J. Mach. Tool Des. Res., No. 1, 1962.
13. Wallace, P.W., and Boothroyd, G., "Tool Forces and Tool Chip Friction in Orthogonal Machining", J. Mech. Eng. Sci., Vol. 6, No. 1, 1964, pp. 74-87.
14. Koenigsberger, F., "Design of Metal Cutting Machine Tools", The MacMillan Co., 1964.
15. Wu, S.M., and Dalal, J.G., "Stochastic Model for Machining Process-Optimal Decision-Making and Control", Trans. ASME, J. of Eng. for Industry, Vol. 93, Series B, No. 2, 1971, p. 593.
16. Kwiatkowski, A.W., and Bennett, F.E., "Application of Random Force Excitation to the Determination of Receptances of Machine Tool Structures", Proceedings of the International Machine Tool Design and Research Conference, Sept. 1965.
17. Peklenik, J., and Kwiatkowski, W., "New Concepts in Investigating the Manufacturing Systems by Means of Random Process Analysis", Advances in Machine Tool Design and Research, 1966, p. 683.
18. Bickel, E., "Die Wechselnden Kräfte bei der Spanbildung", C.I.R.P. Annalen, 12(4), 1966, p. 206.

19. Field, C.F., "Cross-Correlation and Milling Machine Dynamics - A Case Study", International Journal of Machine Tool Design and Research, Vol. 9, 1969, p. 81.
20. Tobias, S.A., and Fishwick, W., "Theory of Regenerative Machine Tool Chatter", Engineer, London, Vol. 205, 1958, p. 199.
21. Cook, N.H., "Self-Excited Vibrations in Metal Cutting", Journal of Engineering for Industry, Trans. of the ASME, Series B, Vol. 81, 1959, p. 183.
22. Gurney, J.P., and Tobias, S.A., "A Graphical Analysis of Regenerative Machine Tool Instability", Journal of Engineering for Industry, Trans. of ASME, Vol. 84, No. 1, 1962, p. 103.
23. Tlustý, J., and Špacek, L., "Self-Excited Vibrations in Machine Tools", Czech. Nakladatelství CSAV Prague, 1954.
24. Sweeney, G., and Tobias, S.A., "An Algebraic Method for the Determination of the Dynamic Stability of Machine Tools", Proceedings of the International Journal of Research in Production Engineering, Pittsburgh, 1963, p. 475.
25. Merritt, H.E., "Theory of Self-Excited Machine Tool Chatter", Journal of Engineering for Industry, Trans. of the ASME, Series B, 1965, p. 447.
26. Kimball, A.L., "Vibration Damping Including the Case of Solid Damping", Trans. ASME, Vol. 51, 1929, p. 227.
27. Kimball, A.L., and Lovell, D.E., "Internal Friction in Solids", Trans. of the ASME, Vol. 48, 1926, p. 479.

28. Lacañ, B.J., "Damping of Materials and Members in Structural Mechanics", Pergamon Press, 1968.
29. Bert, C.W., "Material Damping: An Introductory Review of Mathematical Models, Measures and Experimental Techniques", J. Sound and Vibration, Vol. 29, No. 2, 1973, pp. 129-153.
30. Ruzicka, J.E., Editor, "Structural Damping", ASME, Colloquium, 1959.
31. Zener, C., "Elasticity and Anelasticity of Metals", University of Chicago Press, 1948.
32. "Internal Friction, Damping and Cyclic Plasticity", ASTM Special Technical Publication No. 378, 1965.
33. Crandall, S.H., "The Role of Damping in Vibration Theory", J. Sound and Vibration, Vol. 11, 1970, pp. 3-18.
34. Reed, R.R., "Analysis of Structural Response with Different Forms of Damping", NASA TN-D-3861, 1967.
35. Johnson, D.C., "Free Vibration of a Rotating Elastic Body", Aircraft Engineering, Vol. 24, 1952, p. 234.
36. Bishop, R.E.D., "The Vibration of Rotating Shafts", Journal of Mechanical Engineering Sciences, Vol. 1, No. 1, 1959.
37. Kimball, A.L., and Newkirk, B.L., "Internal Friction Theory of Shaft Whirling", General Electric Co., Review, Vol. 27, 1924.
38. Robertson, D., "The Whirling of Shafts", Engineer, London, Vol. 158, 1934, p. 228.

39. Bagci, C., "Torsional, Coupled Torsional and Lateral Vibrations of Shafts and Branched Systems on Non-Uniform Cross-Sections by Matrix-Displacement - Direct Element Method", Proceedings of the Third World Congress for the Theory of Machines and Mechanisms, Yugoslavia, Vol. 9, 1971.
40. Sankar, T.S., and Osman, M.O.M., "Flexural Stability of Machine Tool Spindles Under Randomly Fluctuating Cutting Forces", Proceedings of the Third World Congress for the Theory of Machines and Mechanisms, Yugoslavia, Vol. 9, Paper G-19, 1971, p. 269.
41. Rakhit, A.K., "The Influence of Random Metal Cutting Forces on the Formation of Surface Texture in Finish Turning", D.Eng. Thesis, Concordia University, Montreal, Quebec, 1974.
42. Bollinger, J.G. and Geiger, G., "Analysis of the Static and Dynamic Behavior of Lathe Spindles", Int. J. Mach. Tool Des. Res., Vol. 3, 1964, pp. 193-209.
43. Morse, I.E., Shapton, W.R., Brown, D.L., and Kuljanic, E., "Applications of Pulse Testing for Determining Dynamic Characteristics of Machine Tools", a paper presented at the Thirteenth International Machine Tool Design and Research Conference, University of Birminham, England, Sept. 1972.
44. Allemang, R.J., Thomas Graef, H., and Powell, C.D., "Dynamic Characteristics of Rotating and Nonrotating Machine Tool Spindles", a paper presented at the Design Engineering Technical Conference, Cincinnati, Ohio, Sept. 9-12, 1973.

45. Chomjakow, W.S., and Klepzig, W., "Dynamisch optimaler Lagerabstand zweifach gelagerter Arbeitsspindeln von Werkzeugmaschinen", Maschinenbäutechnik, 4, 1978, pp. 161-165.
46. Loewenfeld, K., "Zusatzdampfung von Werkzeugmaschinen durch Lamellenpakete", Der Maschinenmarkt, No. 19, 6, März, 1959.
47. Peters, J., "A Survey on the Methods for Increasing the Damping of Machine Tools", Report to the General Assembly of C.I.R.P., 1965.
48. Maragos, S.K., "Measurement and Modeling of Cutting Force Fluctuations During Machining", M.Eng. Thesis, Concordia University, Montreal, Quebec, 1973.
49. Tobias, S.A., "Machine Tool Vibration", Blackie & Son Ltd., Glasgow, U.K., 1965, p. 245.
50. Thomson, W.T., "Theory of Vibration with Applications", Prentice-Hall Inc., Englewood Cliffs, N.J., U.S.A., 1972, p. 272.
51. Meirovitch, L., "Elements of Vibration Analysis", McGraw-Hill Book Company, New York, N.Y., U.S.A., 1975, pp. 292-293, 311.
52. Burden, R.L., Faires, J.D., and Reynolds, A.C., "Numerical Analysis", Prindle, Weber & Schmidt, Boston, Mass., U.S.A., 1978, p. 541.
53. Sharan, A.M., Sankar, T.S., and Sankar, S., "Dynamic Behavior of Lathe Spindles with Elastic Supports Including Damping by Finite Element Analysis", The 51st Shock and Vibration Bulletin, 1980.



54. Bhat, R.B., Sharan, A.M., and Sankar, T.S., "Workpiece Response in Turning due to Spatially Moving Random Metal Cutting Forces", accepted for publication in the Journal of Mechanisms and Machine Theory.
55. Fryba, L., "Nonstationary Response of a Beam to a Moving Random Force", Journal of Sound and Vibration, 46, 1976, pp. 323-338.
56. Fryba, L., "Vibration of Solids and Structures Under Moving Loads", Noordhoff International Publishing, Groningen, 1972.
57. Timoshenko, S., Young, D.H., and Weaver, W., Jr., "Vibration Problems in Engineering", Fourth Edition, John Wiley & Sons, New York, 1974.
58. Lin, Y.K., "Probabilistic Theory of Structural Dynamics", McGraw-Hill, New York, 1967.
59. Bolotin, V.V., "Statistical Methods in Structural Mechanics", Holden Day, San Francisco, 1969.
60. Young, D., and Felgar, R.P., Jr., "Tables of Characteristic Functions Representing Normal Modes of Vibration of a Beam", The University of Texas Publications, No. 4913, 1949.
61. Shigley, J.E., "Mechanical Engineering Design", McGraw-Hill Book Company, New York, U.S.A., 1972.
62. Otnes, R.K., and Enochson, L., "Digital Time Series Analysis", John Wiley & Sons, Toronto, 1972, pp. 279-297.
63. Sharan, A.M., Sankar, S., and Sankar, T.S., "Response Spectral Density Calculations for a Stationary Multidegree-Freedom System- New Approach", accepted for publication in the Journal of Sound and Vibration.

64. Sharan, A.M., Sankar, S., and Sankar, T.S., "Dynamic Analysis and Optimal Selection of Parameters of a Finite Element Modeled Lathe Spindle Under Random Cutting Forces", accepted for publication in the Journal of Mechanical Design, Trans. ASME, 1981.
65. Terman, T., and Bollinger, J.G., "Graphical Method for Finding Optimum Bearing Span", Machine Design, 37, 159, May 27, 1965.
66. Koenigsberger, F., and Tlustý, J., "Machine Tool Structures", Vol. I, Pergamon Press, New York, 1970, p. 285.
67. Pitroff, H., and Rimrott, U.A., "Stiffness of Machine Tool Spindles", ASME, 77-WA/Prod. 42.
68. Beveridge, G.S.W., and Schecter, R.S., "Optimization: Theory and Practice", McGraw-Hill Book Company, N.Y., 1970, pp. 453-456.
69. De Ro. M., "The Magnetic Exciter as Applied to Active Damping of Machine Tools", Proc. 9th Int. M.T.D.R. Conference, Birmingham, 1968, Pergamon Press.
70. Umbach, R., "Verwendung von hochpolymerem Kautschuk für gedämpfte Hilfsmassensysteme an Werkzeugmaschinen", Industrie Anzeiger, No. 46, 1962.
71. Vanherck, P., "Optimisation de l'amortisseur dynamique pour machine-outil", CIRP Annalen XIII, 1964.
72. Stone, B.J., and Andrew, C., "Vibration Absorbers for Machine Tools", Proc. 9th Int. M.T.D.R. Conf., 1968, Birmingham, Pergamon Press.
73. Peters, J., and Vanherck, P., "Theory and Practice of Fluid Dampers in Machine Tools", Advances in Machine Tool Design and Research, Pergamon Press, 1969, pp. 57-70.

74. Peters, J., "What Can Vibration Research Contribute to Machine Tool Development", Prod. Eng. Res. Conference, ASME, Pittsburgh, 1963.
75. Van Herck, P., "L'amortissement des broches des machines outils par amortissement visqueux", CRIF-rue des Drapiers Bruxelles, 1964, CIRP. Annalen XIII, 3, 1966, pp. 177-181.
76. Roley, D.G., "Tractor Cab Suspension Modeling", Ph.D. Thesis, University of California, Davis, California, U.S.A., 1975, p. 16.

## APPENDIX A

MASS AND STIFFNESS MATRICES OF AN ELEMENT

In order to generate the mass and stiffness matrices of an element, the Lagrange's equation of motion for the element must be derived. For this purpose, the kinetic energy,  $T^*$  and the potential energy,  $V^*$  are derived as follows [51]:

Kinetic Energy

$$\begin{aligned}
 T^*(t) &= \frac{1}{2} \int_0^l m \left[ \frac{\partial W(x_1, t)}{\partial t} \right]^2 dx \\
 &= \frac{1}{2} \frac{m\ell}{420} \left[ 156 \dot{w}_1^2(t) + 4\ell^2 \dot{w}_2^2(t) + 156 \dot{w}_3^2(t) + \right. \\
 &\quad \left. 4\ell^2 \dot{w}_4^2(t) + 2 \times 22\ell \dot{w}_1(t) \dot{w}_2(t) \right. \\
 &\quad \left. + 2 \times 54 \dot{w}_1(t) \dot{w}_3(t) - 2 \times 13\ell \dot{w}_1(t) \dot{w}_4(t) \right. \\
 &\quad \left. - 2 \times 22\ell \dot{w}_3(t) \dot{w}_4(t) \right] \quad (A.1)
 \end{aligned}$$

Potential Energy

$$\begin{aligned}
 V^*(t) &= \frac{1}{2} \int_0^l EI \left[ \frac{\partial^2 W(x_1, t)}{\partial x^2} \right]^2 dx \\
 &= \frac{1}{2} \frac{EI}{\ell^3} \left[ 12 w_1^2(t) + 4\ell^2 w_2^2(t) + 12 w_3^2(t) - 4\ell^2 w_4^2(t) \right. \\
 &\quad \left. + 2 \times 6\ell w_1(t) w_2(t) - 2 \times 12 w_1(t) w_3(t) \right. \\
 &\quad \left. + 2 \times 6\ell w_1(t) w_4(t) - 2 \times 6\ell w_2(t) w_3(t) \right. \\
 &\quad \left. + 2 \times 2\ell^2 w_2(t) w_4(t) - 2 \times 6\ell w_3(t) w_4(t) \right] \quad (A.2)
 \end{aligned}$$

The Lagrange's equation of motion for this system can then be rewritten as:

$$\frac{d}{dt} \left( \frac{\partial L^*(t)}{\partial \dot{w}_j} \right) - \frac{\partial L^*}{\partial w_j} = Q_j \quad j = 1, 2, 3, 4 \quad (A.3)$$

where,

A.2

$$L^*(t) = T^*(t) - V^*(t)$$

Combining equations A.1, A.2, A.3, and A.4, one can write the matrix differential equation of motion as

$$[m] \begin{Bmatrix} \ddot{w}_1 \\ \ddot{w}_2 \\ \ddot{w}_3 \\ \ddot{w}_4 \end{Bmatrix} + [k] \begin{Bmatrix} w_1 \\ w_2 \\ w_3 \\ w_4 \end{Bmatrix} = 0$$

where,

$$[m] = \frac{m\ell}{420} \begin{bmatrix} 156 & 22\ell & 54 & -13\ell \\ & 4\ell^2 & 13\ell & -3\ell^2 \\ & \text{sym} & 156 & -22\ell \\ & & & 4\ell^2 \end{bmatrix}$$

is the mass matrix,

and

$$[k] = \frac{EI}{\ell^3} \begin{bmatrix} 12 & 6\ell & -12 & 6\ell \\ & 4\ell^2 & -6\ell & 2\ell^2 \\ & \text{sym} & 12 & -6\ell \\ & & & 4\ell^2 \end{bmatrix}$$

is the stiffness matrix.

## APPENDIX B

B.1 Introduction

For a  $n$  degree of freedom mechanical system, the governing dynamical equation can be written as

$$[m] \ddot{w}(t) + [c] \dot{w}(t) + [k] w(t) = f(t) \quad (B.1)$$

(nxn) (nx1) (nxn) (nx1) (nxn) (nx1) (nx1)

where  $[m]$ ,  $[c]$  and  $[k]$  are the mass, damping and stiffness matrices respectively,

and  $f(t)$  is the vector of random excitation forces.

If  $[\phi_f(\omega)]$  is the  $n \times n$  excitation spectral density matrix of the excitation force  $f(t)$ , then the response spectral density is given by

$$[\phi_w(\omega)] = [H(j\omega)][\phi_f(\omega)][H^*(j\omega)]^T \quad (B.2)$$

where  $[H(j\omega)]$  is a  $(n \times n)$  matrix of the transfer function of the system in equation (B.1),

$[H^*(j\omega)]^T$  is the transpose of the complex conjugate of  $[H(j\omega)]$

and  $[\phi_w(\omega)]$  is an  $n \times n$  response spectral matrix consisting of diagonal elements representing the spectral density of generalized displacement and off-diagonal elements representing cross-spectral density of generalized displacements.

$[H(j\omega)]$  can be found by calculating the Fourier Transform of equation (B.1) and can be represented as

$$[H(j\omega)] = [-\omega^2 [m] + j\omega [c] + [k]]^{-1} \quad (B.3)$$

## B.2

The calculation of the response spectral density  $[\phi_w(\omega)]$  in general is carried out over all frequencies of interest, and it involves matrix addition, multiplication and inversion. In particular during the calculation of  $[\phi_w(\omega)]$ , the matrix inversion is usually a time consuming operation in a computer. Further, if the degrees of freedom or the frequencies of interest are large in number, then the computer CPU time for the evaluation of  $[\phi_w(\omega)]$  also becomes large.

Here, a new method for the calculation of the response spectral density  $[\phi_w(\omega)]$  is introduced which eliminates any matrix inversion. Further this method provides in addition to  $[\phi_w(\omega)]$ , the response spectral densities  $[\phi_w^*(\omega)]$ ,  $[\phi_{ww}^*(\omega)]$  and  $[\phi_{ww}(\omega)]$  in a single calculation.

### B.2 Mathematical Formulation

Using a new set of variables,  $\dot{Y}(t)$  and  $Y(t)$ , equation (B.1) can be rewritten as

$$[M] \dot{Y}(t) + [K] Y(t) = F(t) \quad (B.4)$$

where

$$\begin{matrix} [M] \\ (2n \times 2n) \end{matrix} = \begin{bmatrix} [0] & [m] \\ [m] & [c] \end{bmatrix}$$

$$\begin{matrix} [K] \\ (2n \times 2n) \end{matrix} = \begin{bmatrix} [-m] & [0] \\ [0] & [k] \end{bmatrix}$$

$$\frac{Y(t)}{(2n \times 1)} = \begin{Bmatrix} \dot{w}(t) \\ w(t) \end{Bmatrix}, \quad \dot{Y}(t) = \begin{Bmatrix} \ddot{w}(t) \\ \dot{w}(t) \end{Bmatrix}$$

and

$$\frac{F(t)}{(2n \times 1)} = \begin{Bmatrix} 0 \\ f(t) \end{Bmatrix}$$

### B.3

Let  $[V]$  be the modal matrix ( $2n \times 2n$ ) consisting of the eigenvectors of equation (B.4).

$$\begin{aligned} \text{Defining } \underline{Y}(t) &= [V] \underline{Z}(t) , \\ \text{and } \dot{\underline{Y}}(t) &= [V] \dot{\underline{Z}}(t) , \end{aligned}$$

and premultiplying each term in equation (B.4) by  $[V]^T$  gives

$$[M^*] \dot{\underline{Z}}(t) + [K^*] \underline{Z}(t) = [V]^T \underline{F}(t) \quad (\text{B.5})$$

where

$$\begin{aligned} [M^*] &= [V]^T [M] [V] \\ \text{and } [K^*] &= [V]^T [K] [V] \end{aligned} \quad (\text{B.5a})$$

are diagonal matrices of size ( $2n \times 2n$ ).

Assuming the initial conditions are zero and taking the Laplace Transformation of equation (B.5) gives

$$\underline{Z}(s) = [s[M^*] + [K^*]]^{-1} [V]^T \underline{F}(s) \quad (\text{B.6})$$

Premultiplying by  $[V]$ , equation (B.6) becomes

$$\underline{Y}(s) = [A(s)] \underline{F}(s) \quad (\text{B.7})$$

$$\text{where } [A(s)] = [V][G^*(s)][V]^T \quad (\text{B.7a})$$

$$\text{and } [G^*(s)] = [s[M^*] + [K^*]]^{-1} \quad (\text{B.7b})$$

The matrix  $[G^*(s)]$  a diagonal matrix with its diagonal elements being the reciprocal of the diagonal elements of the matrix  $[s[M^*] + [K^*]]$ . From equation (B.7) it is evident that  $[A(s)]$  represents the transfer function of the system given in equation (B.4). Then the expression for response spectral density of the system (governed by equation (B.4) is given by



$$[\phi_Y(\omega)] = [A(j\omega)] [\phi_F(\omega)] [A^*(j\omega)]^T \quad (B.8)$$

(2nx2n)      (2nx2n) (2nx2n) (2nx2n)

where

$$[\phi_F(\omega)] = \begin{bmatrix} 0 & 0 \\ 0 & \phi_f(\omega) \end{bmatrix} \text{ is the excitation spectram matrix}$$

corresponding to the force vector  $\underline{F}(t)$

$[A^*(j\omega)]^T$  is the transpose of the complex conjugate of  $A(j\omega)$

and

$[\phi_Y(\omega)]$  is a 2nx2n response spectral matrix

If  $[\phi_Y(\omega)]$  is partitioned, then

$$[\phi_Y(\omega)] = \begin{bmatrix} \phi_W^*(\omega) & \phi_{WW}^*(\omega) \\ \phi_{WW}(\omega) & \phi_W(\omega) \end{bmatrix} \quad (B.9)$$

From equation (B.9) it is evident that the calculation of  $[\phi_Y(\omega)]$  provides response spectral matrices  $[\phi_W(\omega)]$ ,  $[\phi_W^*(\omega)]$ ,  $[\phi_{WW}^*(\omega)]$  and  $[\phi_{WW}(\omega)]$ . The procedure outlined in this section not only provides 4 times the information as compared to the solution obtained using equation (B.2) but also avoids the necessity of inverting the matrix corresponding to the system Transfer Function.

### B.3 Step-by-Step Procedure of the New Method

1) Formulate the modified governing equation of the system as shown in equation (B.4).

2) Obtain the modal matrix  $[V]$ , and the corresponding natural frequencies of the system represented by equation (B.4).

3) Calculate the diagonal matrices  $[M^*]$  and  $[K^*]$  given by the equation (B.5a).

4) Calculate the matrices  $[A(s)]$ , and  $[G^*(s)]$  given by the

equation (B.7a) and (B.7b) respectively.

5) Calculate the spectral density of response matrix  $[\phi_Y(\omega)]$  using the equation (B.8).

The required computations for each of the steps, starting from step 2, were done using a package written in FORTRAN language. The modal matrix  $[V]$  and the corresponding natural frequencies were obtained by using a sub-routine EIGCC from the IMS library of sub-routines.

#### B.4 Numerical Examples

##### B.4.1 The Inertia Matrix Diagonal, and the Stiffness and the Damping Matrices, Nondiagonal

The system chosen in Fig. B.1, and the details of the various parameters are given in Table B.1. In practice, for mechanical systems, the matrix  $[\phi_F(\omega)]$  can be determined experimentally.

Numerical computations were carried out with the parameter set as in Table B.1 to obtain, a) the matrix  $[\phi_W(\omega)]$  using equation (B.2), and b) the matrix  $[\phi_Y(\omega)]$  using equation (B.8) respectively. The calculations were repeated with the maximum frequency limit of 2000, 3000, and 4000 Hz. In all cases the lowest frequency was selected as 5 Hz with frequency step also chosen as 5 Hz. The computations were carried out on a CDC Cyber 174 digital computer. For a pre-selected maximum frequency limit, the matrix  $[\phi_W(\omega)]$  calculated using the conventional approach (equation (B.2)) was identical to that obtained using the method proposed in this paper (equation (B.8)). The computation time for each of the three sets mentioned above are given in Table B.2.

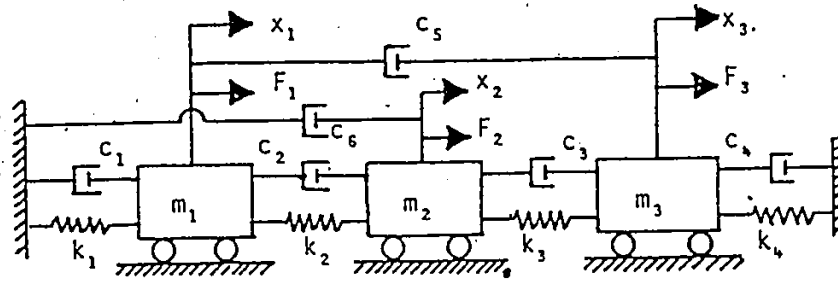


Fig. B.1: Three-degrees of freedom system.

TABLE B.1

Various Matrices of the Mechanical System

## 1. Inertia Matrix (kg)

$$[m] = \begin{bmatrix} 45.454 & 0 & 0 \\ 0 & 45.454 & 0 \\ 0 & 0 & 90.909 \end{bmatrix}$$

## 2. Stiffness Matrix (N/m)

$$[k] = 176.458 \times 10^6 \begin{bmatrix} 2 & -1 & 0 \\ -1 & 2 & -1 \\ 0 & -1 & 3 \end{bmatrix}$$

## 3. Damping Matrix (N.sec/m)

$$[c] = 1750.1 \begin{bmatrix} 3.3644 & -0.3747 & -0.0581 \\ -0.3747 & 3.3337 & -0.4079 \\ -0.0581 & -0.4079 & 6.3788 \end{bmatrix}$$

4. Excitation Spectral Density Matrix (N<sup>2</sup>/Hz)

$$[\phi_f(\omega)] = \begin{bmatrix} -10.0 \log \omega + 100 & 0 & 0 \\ 0 & -9.5 \log \omega + 100 & 0 \\ 0 & 0 & 9.0 \log \omega + 100 \end{bmatrix}$$

TABLE B.2  
 Computational Time for the Response Power Spectral Density Matrix  
 of the 3 Degrees of Freedom Mechanical System

| MATRIX                        | EQUATION S USED | COMPUTATION TIME (s)                 |                                      |                                      |
|-------------------------------|-----------------|--------------------------------------|--------------------------------------|--------------------------------------|
|                               |                 | CASE 1: MAX. FREQUENCY LIMIT 2000 Hz | CASE 2: MAX. FREQUENCY LIMIT 3000 Hz | CASE 3: MAX. FREQUENCY LIMIT 4000 Hz |
| $[\phi_w(\omega)]$<br>(3x3)   | B.2             | 8.821                                | 13.345                               | 19.960                               |
| $[\phi_w(\omega)]^*$<br>(3x3) | B.8<br>& B.9    | 3.501                                | 5.195                                | 7.005                                |
| $[\phi_Y(\omega)]^T$<br>(6x6) | B.8             | 11.488                               | 16.991                               | 22.550                               |

\*  $[\phi_w(\omega)]$  is obtained using equation (8) by calculating only the elements  $a_{n+1,n+1}$  to  $a_{2n,2n}$

#### B.4.2 The Inertia Matrix Nondiagonal, and the Stiffness and the Damping Matrices, Diagonal

The system under consideration is shown in Fig. B-2. This system represents an active suspension system of a tractor cab [76]. This problem involves the solution of a four degrees of freedom system. The four suspension units under each corner of the cab base plate, isolate the vibrations in the vertical, pitch and roll modes. The fifth suspension unit parallel to the cab base plate provides isolation in the side-to-side or the lateral direction. The forces are present along each of the coordinates  $x_1$ ,  $x_2$ ,  $x_3$ , and  $x_4$ . The system is subjected to the base excitation. This system can also be represented by the matrix differential equation (B.1) [76]. The details of the various parameters of this system are given in Table B.3. The response spectral density matrices  $[\phi_w(\omega)]$ , and  $[\phi_y(\omega)]$  mentioned in section B.4.1 were computed in a similar manner. Once again, there was no complex matrix inversion involved in the computation of the matrix  $[\phi_w(\omega)]$ . The details of the results of these computations are given in Table B.4. It should be noted that the elements of  $[\phi_w(\omega)]$  calculated using the conventional approach (equation (B.2)) was identical to that obtained using the proposed method.

#### B.5 Results and Discussion

Referring to Tables B.2 and B.4 it can be seen that there is a significant reduction in the computation time in obtaining the matrix  $[\phi_w(\omega)]$  if the new approach is used instead of using equation (B.2). Therefore, one can infer that the reduction in computer time realized in using the new approach would become large as the size of the matrix

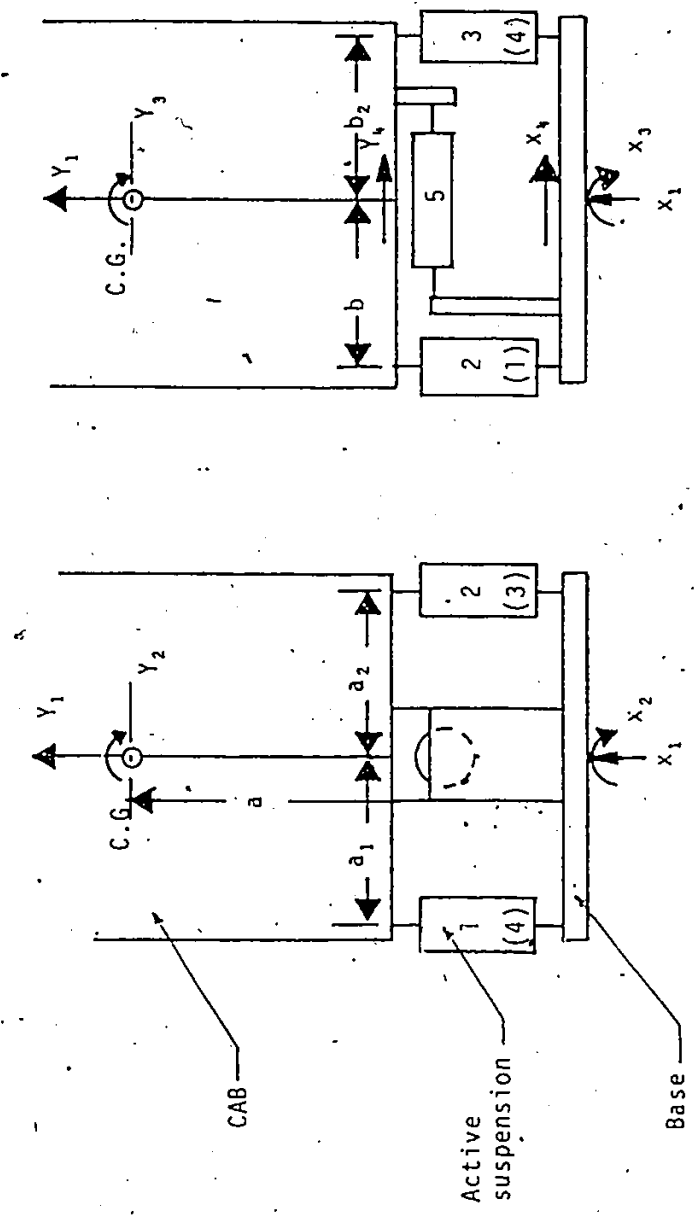


Fig. B.2: Geometric representation of the four degrees of freedom cab system.

TABLE B.3

Various Matrices of the Tractor Cab Suspension System [76]

## 1. Inertia Matrix (kg)

$$[m] = \begin{bmatrix} 681.82 & 0 & 0 & 0 \\ 0 & 736.67 & 0 & 0 \\ 0 & 0 & 395.9 & 519.5 \\ 0 & 0 & 519.5 & 681.82 \end{bmatrix}$$

## 2. Stiffness Matrix (N/m)

$$[k] = \begin{bmatrix} 26844 & 0 & 0 & 0 \\ 0 & 5606.37 & 0 & 0 \\ 0 & 0 & 5606.34 & 0 \\ 0 & 0 & 0 & 9843.0 \end{bmatrix}$$

## 3. Damping Matrix (N.sec/m)

$$[c] = \begin{bmatrix} 2042.8 & 0 & 0 & 0 \\ 0 & 426.63 & 0 & 0 \\ 0 & 0 & 426.63 & 0 \\ 0 & 0 & 0 & 729.51 \end{bmatrix}$$

4. Excitation Spectral Density Matrix (N<sup>2</sup>/Hz)  
(assumed)

$$[\phi_f(\omega)] = \begin{bmatrix} -10.0 \log \omega + 100 & 0 & 0 & 0 \\ 0 & -9.5 \log \omega + 100 & 0 & 0 \\ 0 & 0 & -9.0 \log \omega + 100 & 0 \\ 0 & 0 & 0 & -8.5 \log \omega + 100 \end{bmatrix}$$



TABLE B.4  
The Computation Time for the Response Power Spectral Density  
of the Cab Suspension System

| MATRIX                            | EQUATION S<br>USED | COMPUTATION TIME (s)                    |   |   |
|-----------------------------------|--------------------|---|---|---|
|                                   |                    | CASE 1: MAX. FREQUENCY<br>LIMIT 2000 Hz | CASE 2: MAX. FREQUENCY<br>LIMIT 3000 Hz | CASE 3: MAX. FREQUENCY<br>LIMIT 4000 Hz |
| $[\phi_w(\omega)]^{(1)}$<br>(4x4) | B.2                | 13.577                                  | 20.359                                  | 26.876                                  |
| $[\phi_w(\omega)]^{(2)}$<br>(4x4) | B.8<br>&<br>B.9    | 5.517                                   | 8.024                                   | 10.712                                  |
| $[\phi_y(\omega)]$<br>(8x8)       | B.8                | 23.958                                  | 35.370                                  | 47.338                                  |

The results of computation indicate that  $[\phi_w(\omega)]^{(1)}$  and  $[\phi_w(\omega)]^{(2)}$  were identical.

$[\phi_w(\omega)]$  increases. As a point of clarification it should be pointed out that the matrix  $[\phi_w(\omega)]$  in equation (B.9) has been computed without actually computing the matrix  $[\phi_y(\omega)]$ . This was possible by partitioning the matrices involved in the calculation.

In this new method when  $[\phi_w(\omega)]$  is calculated, the natural frequencies and the corresponding mode shapes of the system are automatically obtained as a by-product. In some vibrating systems such as the one in section B.4.2, the mode shapes and natural frequencies characterize the rigid body motion of the vehicle under consideration and thus provide very valuable information in the overall suspension design of the vehicle. In these situations using the method proposed here, one can obtain the vehicle response to random road surface undulations,  $[\phi_w(\omega)]$ , and vehicle natural frequencies and mode shapes in one single calculation. Further it is possible using this new method proposed to obtain spectral density  $[\phi_w^*]$ , and cross-spectral densities  $[\phi_{ww}^*]$  and  $[\phi_{ww}^*]$  without any added computational difficulty.